Alma Mater Studiorum – Università di Bologna

DOTTORATO DI RICERCA IN

Chimica

Ciclo XXXIII

Settore Concorsuale: 03/C2

Settore Scientifico Disciplinare: CHIM/04

STUDY OF NEW CATALYSTS FOR THE SELECTIVE OXIDATION OF *n*-BUTANE TO MALEIC ANHYDRIDE: THE ROLE OF CATALYST THERMAL TREATMENT

Presentata da: Laura Setti

Coordinatore Dottorato

Domenica Tonelli

Supervisore

Fabrizio Cavani

Co-Supervisore

Nikolaos Dimitratos

Tommaso Tabanelli

Stefania Albonetti

Esame finale anno 2021

Abstract

Maleic anhydride (MA) is a very versatile molecule, employed for many applications; indeed, with three functional groups (two carbonyl groups and one double bond C=C) it is an excellent joining and cross-linking material. Most commonly it is obtained through the selective oxidation of *n*-butane: the process is catalyzed by Vanadium/Phosphorous oxides (V/P/O), namely the vanadyl pyrophosphate (VPP), a compound with formula $(VO)_2P_2O_7$, responsible for the alkane activation via hydrogen extraction. The next oxygen insertions to obtain the desired product is achieved by a limited amount of $VOPO_4$ phase on the catalytic surface: a defined amount of V^{5+} is necessary to improve the catalytic performances, but an excess of oxidized species is detrimental for selectivity, leading to total combustion reactions. Even though the catalytic system has been largely studied over the years and it is normally used in the industrial production of maleic anhydride, the main open problem is to manage to completely control and understand its preparation and the effect of different parameters in order to obtain the optimal distribution of the phases, leading to an active and selective catalyst.

This thesis reports the effect of different preparation parameters employed during the calcination procedure for the transformation of VHP into the active catalyst. The thermal treatment is already known to be favoured when water was added in the inlet stream, hence the first study was on the role of different amount of water co-fed with air. The results demonstrate that it is important for the desorption and decomposition of organic species (through reactions such as reforming) derived from the synthesis of the precursor in organic medium and presents on the catalytic surface or trapped between the layer. The presence of water leads to obtain catalysts characterized by an higher crystallinity, but it is not the only parameter to control: the molar ratio of oxygen has also an important role in the development of the right phase, in order to obtain an active and selective catalyst. Some tests decreasing the "oxidizing power" of the mixture were carried out and it was observed a progressive development of VPP phase instead of oxidized V/P/O systems, in which the main phase was constituted of $VOPO_4$. Established the role of water and oxygen, the optimal conditions have been found when a ternary mixture composed of air, water and nitrogen was used for the calcination, in the molar ratio of 30:10:60% respectively. Also at the lower temperature tested, i.e. 400°C, the catalyst presents the higher conversion of *n*-butane and MA yield compared to all other samples. The important conclusion we have reached is that not higher amount of water is necessary to obtain the most performing catalyst, thus leading to economic savings. Moreover, performing the same experiments on two precursors characterized by different carbon content and P/V atomic ratio, give catalysts with different activity but the mixture previously descripted is always the one that leads to have the best performance.

1. Introduction

1.1. Maleic Anhydride

Maleic Anhydride (MA) is the anhydride of cis-butenedioic acid (maleic acid) with formula $C_4H_2O_3$. It is an organic compound constituted of an heteroatomic cyclic structure with four carbon atoms and three oxygen, as shown in Figure 1.

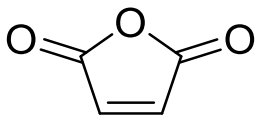

Figure 1. Maleic Anhydride structure

At room temperature, MA is a white crystalline solid with pungent odour; the most important physical and chemical characteristics are summarized in Table 1.

Table 1. Physical and chemical properties of MA

Molecular Weight (g/mol)	98.01
Melting Point (°C)	52.85
Boiling Point (°C)	202
Combustion heat (kJ/mol)	1391.2
Explosion limits (%)	Lower: 1.4 Upper: 7.1
Solubility in xylene (g/L at 30°C)	163.2
Solubility in water (g/L at 30°C)	572
Solubility in benzene (g/L at 35°C)	439.4

1.1.1. Maleic Anhydride uses

MA is a very versatile molecule, indeed with three active sites (two carboxylic group and one double bond C=C) it's an excellent material for several types of reaction, including alkylation, polycondensation, polyaddition and Diels-Alder reaction.

In particular, MA is an important monomer for the manufacturing of unsaturated polyester resins (that are used for the production of thermosetting plastics) and alkyd resins (used as ligands in the paint industry). Moreover, it is an intermediate molecule for the production of

fine chemicals: for instance, by selective hydrogenation, MA can be transformed into succinic anhydride, which is hydrolyzed to succinic acid, that is the starting material for the synthesis of γ-butyrolactone (GBL), tetrahydrofuran (THF) and 1,4-butandiol (BDO). MA also finds application in the food industries, as precursor of malic acid and fumaric acid, both used as additives to adjust the acid flavor. Finally, it is used for the production of aspartic acid from which is obtain aspartame.

The main products are summarized in Figure 2: more than 50% of MA is used to produce unsaturated polyester resins, approximately 20% for alkyd resins, the remaining part of the global maleic anhydride consumption is intended for other applications (i.e. chemicals)[1].

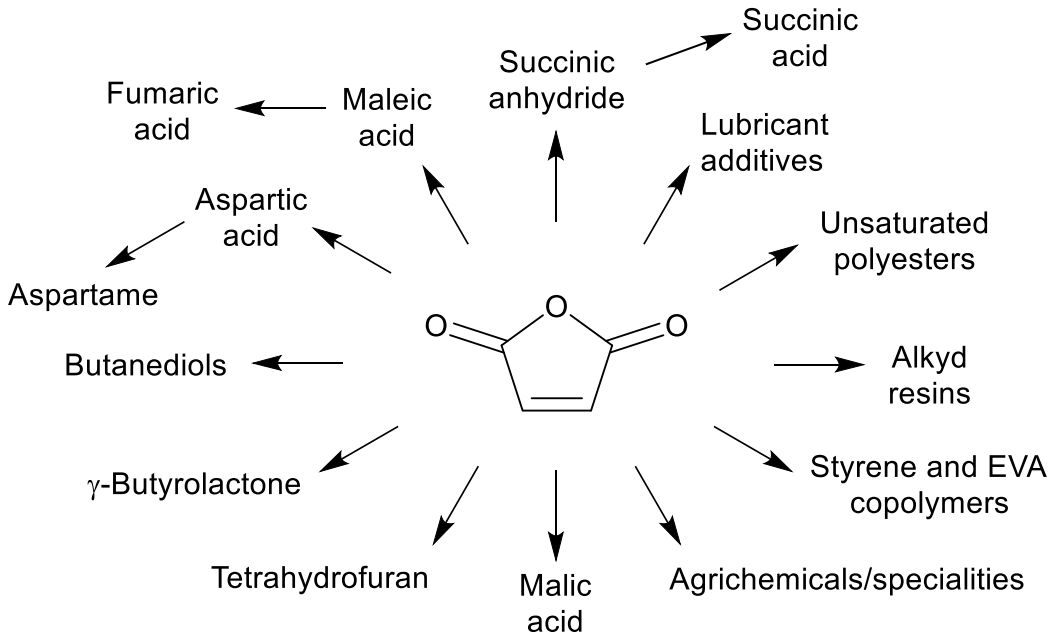

Figure 2. Main products obtained from Maleic anhydride.

1.1.2. Maleic Anhydride production: from the traditional to the most innovative process

The most important industrial production of maleic anhydride is located in the USA between the '80s and the 2000s, while in Europe MA production is dated around the '90s. In 2000, the annual production capacity in Western Europe was higher than in North America[2]. Nowadays the major global producer is China, from which the EU import about 100000 tons/year[1,3].

Considering the importance of MA as a *building block* in the industrial field, the optimization of its production represents an ongoing challenge.

The production of MA consists in a gas phase selective oxidation of petrochemical raw materials. It is an exothermic reaction, therefore they are required devices for the removal and recycling of the heat generated, in order to avoid *run away* events.

Until 1960, the industrial synthesis of maleic anhydride was based on the selective oxidation of benzene. Due to the carcinogenicity of reactant, this route has been gradually replaced with newest one, involving *n*-butane.

Gas phase selective oxidation of benzene (Figure 3) was carried out in a reactor with a fixed catalytic bed composed of a mixed oxide of vanadium (V_2O_5) and molybdenum (MoO_3) supported on an inert material. Usually, steatite was used for this purpose, because of its high thermal conductivity which helps to prevent *hot spots* on the catalytic surface that would lead to unselective total combustion reactions[4].

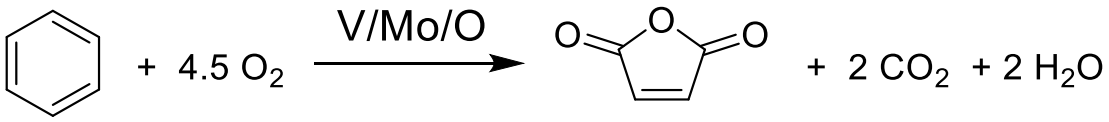

Figure 3. Selective oxidation of benzene to MA

Benzene and pre-heated air are mixed and fed into a multitubular fixed bed reactor, in the case of Polynt's process the so-called High-Load-Technology is used, which allows operation up to 180 g/h/tube of benzene (air/benzene=21). The reaction occurs in a temperature range between 400°C and 450°C and the pressure being adjusted to an optimum value of 0.15-0.25 MPa.

A considerable amount of heat is produced during the reaction ($\Delta H°$=-1875 kJ/mol), resulting in the presence of *hot spots* up to 500°C. The system is commonly cooled by molten salts. The reaction gases are cooled down by means of gas coolers and crude MA is partially recovered by condensation and partially as maleic acid in a water scrubber. Off gases leaving the scrubber are sent to a catalytic incinerator. Pure MA is obtained in a distillation column operated batch wise[5]. In these conditions the conversion of benzene reaches 97% with a MA selectivity of 75%; due to environmental regulations (limit of emission in atmosphere of 5 $\mu g/m^3$)[6,7] the small amount of unconverted benzene must be adsorbed and recycled or burned.

During the 70's the study and the development of new technologies for the production of maleic anhydride start to increase, because of the gradually (and successfully) substitution of benzene with *n*-butane. For this reason, nowadays, approximately 80% of MA is produced in the latter way.

A simplified reaction scheme is reported in Figure 4:

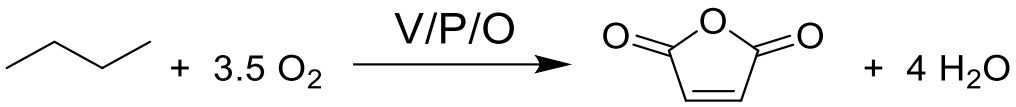

Figure 4. Selective oxidation of *n*-butane to MA.

The use of *n*-butane instead of benzene has some advantages:

- Lower costs of raw material: *n*-butane (450 €/ton) obtained from natural gas or steam cracking of oil so it is more available than benzene (850 €/ton);
- Higher atomic efficiency: *n*-butane has the same four C atoms of maleic anhydride, on the other hand, for benzene oxidation, two of the six carbon atoms are lost to form CO_2;
- Lower environmental impact: benzene is a proven carcinogenic compound;
- Lower exothermicity of the reaction ($\Delta H°$=-1250 kJ/mol instead of -1875 kJ/mol for benzene), with a reduction of heat removal costs;
- Lower costs of MA separation and purification, because of the production of heavy compounds such as phthalic anhydride or benzoquinone starting from benzene.

Currently, the synthesis of maleic anhydride through selective oxidation of *n*-butane in the most successful industrial example of the use of a paraffine as the reactant for the synthesis of a bulk chemical compound. The success of this reaction is due to the development of a high active and selective catalyst: the vanadyl pyrophosphate ($(VO)_2P_2O_7$).

Nevertheless, the reaction is still an oxidation, with all the problems related to it:

- By-production of high amount of total combustion products via parallel and consecutive reactions of *n*-butane and MA. CO and CO_2 are kinetically and thermodynamically favored at the reaction temperature, for this reason the alkane conversion must be maintained lower than 80%;
- *Run-away* risks related to the exothermicity of the reaction: the key factor is the control of the heat-removal;
- Process safety due to the possibility to form flammable mixture between the oxidant and a fuel: in each part of the plant the gas composition has to be far from explosion limits (except in the reactor).

Industrially, maleic anhydride is produced from *n*-butane mainly from three technologies: fixed-bed, fluidized bed and transported-bed reactor. The latter has been recently abandoned.

Fixed bed technology:

The reaction is carried out in a multitubular reactor cooled by molten salts, similar to the one used for benzene oxidation. 1.7% *n*-butane in air (under the lower explosion limit) is fed, working at 390-400°C and the catalyst is loaded in form of pellet packed into the reactor tubes. In these conditions the conversion in about 83% with MA yield of 60%.

The outlet stream from the reactor can be recovered in two different ways:

1) Absorption in water to form maleic acid which is dehydrated at temperature below 130°C, to minimize the isomerization to fumaric acid; finally, MA is purified by azeotropic distillation in o-xylene distillation (Denka-Scientific Design process);
2) Absorption in an organic solvent: in this way there is no formation of fumaric acid and almost 98% of MA produced is recovered by fractional distillation.

The main advantages of the fixed bed technology are the higher MA yield compared to the one obtained in fluidized bed, it's possible to build plants in parallel increasing the productivity and the old plant used for benzene route could be retrofitted.

Fluidized bed technology:

One of the most important advantage of the fluidized bed technology is the homogeneity in the thermal profile, without *hot-spots*, due to the fast mixing of the catalyst inside the reactor, this led to an efficient dissipation of the reaction heat. The second point is the higher productivity, thanks to the possibility to work in a higher butane concentration (inside the explosion limit), because the catalyst in fluidized bed configuration works as an efficient flame-trap.

This type of technologies has to be controlled and optimized because of *back-mixing* phenomena (resulting in a reduced selectivity in the desired product), more complex scale-up and higher mechanical stress and abrasion of the bulk catalyst. For the latter problem different solution might be employed:

- Impregnation of active phase on an inert support with good fluidization properties and high attrition resistance;
- Improve of mechanical resistance adding additives to the precursor;
- Encapsulation of the active phase in a silica structure.

One of the most advanced fluidized bed technology is the ALMA process, licensed by Polynt SpA. In this process the bulk catalyst is spray-dried with a low amount of additives to improve the mechanical resistance. 4% *n*-butane is mixed with air and fed to the reactor working at 400-430°C. Conversion is typically 80-85% with a molar yield to MA of 50% [8]. High-pressure

steam is generated by cooling coils inside the reactor. In the recovery section, an organic solvent is used to remove MA from the outlet stream through a conventional absorption/stripping scheme. Finally, MA is refined by distillation to separate solvent and undesired products synthetized during the reaction. The outlet gas of the separation process is sent to a burner that converts the residual hydrocarbon into energy for internal uses (e.g. extra steam)[5].

Transported bed technology:

The last reactor technology which can be applied is the circulating fluidized bed reactor (CFBR), developed by DuPont[9]. It worked from 1996 to 2004 for tetrahydrofuran (THF) production and in 2005 it was shutdown.

The process could be schematically divided into two parts:

- Step 1: *n*-butane is fed without air in the reactor; the catalyst transforms the hydrocarbon into MA, by exploiting the lattice oxygen, being itself consequently reduced. In this way oxygen and butane are fed separately so higher amount of the latter could be employed (20% of alkane). At this point the catalyst is recovered by a cyclone and transported to the regenerator reactor where air is fed in order to restore the oxidation state of the catalyst. MA is recovered by hydrolysis to maleic acid.
- Step 2: aqueous maleic acid is fed into a hydrogenation reactor and reduced to form THF.

With this technology the *n*-butane conversion is about 50% with a MA yield of 37%. VPP has to be coated with silica which gives a very high mechanical resistance, because of the complexity design of the reactor system.

In the last decades, the attention of research is moved on to processes that allow to obtain the most important *building block* from biomasses and their transformation into added value chemical compounds through sustainable processes. 1-Butanol used as a reactant for the bio-based synthesis of MA is an example of it; due to the availability and competitive cost makes it an interesting molecule in the field of *platform molecules* derived from biomasses.

A simplified scheme of the reaction is reported in Figure 5.

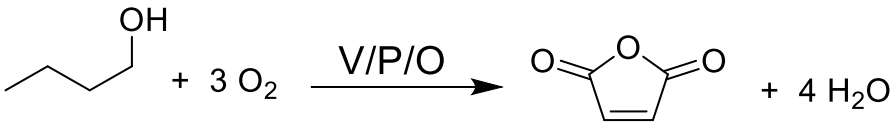

Figure 5. Selective oxidation of 1-butanol to Maleic Anhydride.

From biomass fermentation based on *Clostridium acetobutylicum*, it's possible to obtain an ABE mixture, made of acetone, butanol and ethanol starting from both five- and six-carbon atoms sugars[10].

Alternatively, 1-butanol can be obtained via: I) hydroformylation of propylene (oxo synthesis), II) Guerbet reaction starting from bio-ethanol, III) Reppe process with the direct hydroxycarbonylation of propylene, IV) Catalytic hydrogenation of CO from syngas.

The mechanism for the MA production starting from 1-butanol (reported in Figure 6) consists in a dehydration of alcohol to butenes followed by selective oxidation of butenes to MA. Therefore, two different catalytic properties are needed: acidic sites to promote the formation of olefinic intermediates and redox ones for the next oxygen insertion.

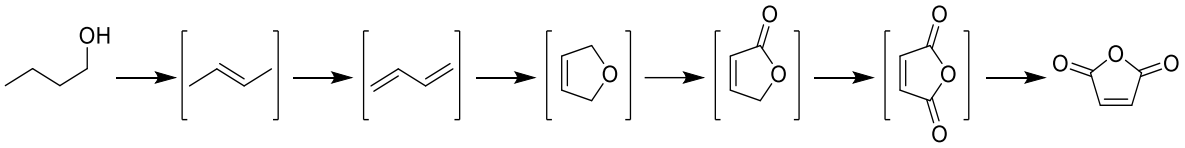

Figure 6. Reaction pathways for the oxidation of 1-Butanol to MA.

Three reactor configurations are possible since the reaction is formally divided in two steps:

a) Two reactors system (Figure 7-a): in the first reactor the dehydration of 1-butanol takes place with an acid catalyst and in the second one the oxidation step occurs using a redox catalyst. In this way it is possible to optimize each reactor both in terms of technology (dehydration is endothermic and the oxidation is exothermic), catalyst design and operative conditions in order to obtain the best catalytic performances in terms of selectivity of the desired product. This is the most versatile because two consecutive reactors are employed, however, high investment costs are required.

b) One reactor system (Figure 7-b): only one reactor is used in which two separate catalytic beds are arranged; the first one is the acid catalyst used for the dehydration of butanol, the second one is the redox catalyst that promotes the oxidation step of butenes. Promising catalysts with this dual functionality are Fe and Co molibdates-based material[11,12] and also VPP, catalyst for MA from *n*-butane[12,13]. Moreover, considering that the feed is composed of 1-butanol and air mixed together, the acid catalyst must be active also in presence of oxygen while the redox one receiving the products flow coming out from the first bed must be resistant to water poisoning (deriving from the dehydration) and it must not catalyze secondary reactions on unreacted 1-butanol. So,

in this configuration it is more difficult to manage the operative conditions for each step, but the investment costs are lower than the previous two-reactor systems.

c) One-pot reaction (Figure 7-c): in this case only one reactor is needed but bi-functional catalyst is required. The disadvantages are the same described in point b), but the investment costs are reduced and the plant management is simpler.

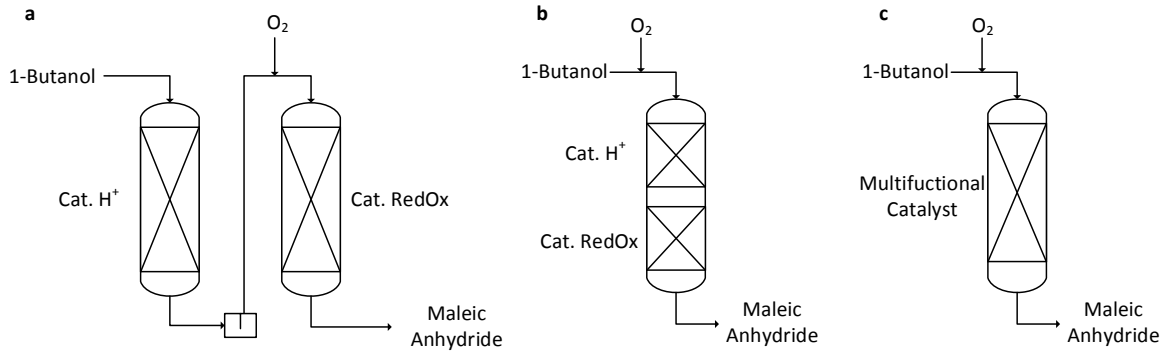

Figure 7. Reactor configurations for the selective oxidation of 1-butanol to MA.
a) two reactors system, b) one reactor system, c) one reactor and one-pot reaction.

1.2. The catalytic system

Vanadium/phosphorous oxides gained much attention in selective oxidation reactions; in particular, due to the capability of these elements to assume different oxidation states and exist as different species, it is possible to obtain different V/P mixed oxide with different structure and catalytic properties.

Vanadyl pyrophosphate ($(VO)_2P_2O_7$, VPP) is the V/P/O system which leads to the best performances in terms of conversion, selectivity and productivity for the synthesis of maleic anhydride from *n*-butane; it is a bifunctional bulk catalyst, characterized by both acidic (necessary for paraffine activation reactions) and redox (for the next oxidation of intermediates to MA) properties[8,14–16].

1.2.1. Synthesis of vanadyl pyrophosphate

VPP-based catalyst has been widely studied in terms of preparation method (mainly organic or inorganic medium used for the synthesis). There is a general consensus on the fact that the main steps are:

1. Synthesis of the precursor, i.e. vanadyl hydrogenphosphate hemihydrate ($VOHPO_4 \cdot 0.5H_2O$, VHP) starting from vanadium pentoxide V_2O_5 and phosphoric acid;

2. Thermal decomposition of the VHP precursor to form the active VPP-based catalyst, with total or partial loss of crystallization water: during this step vanadyl pyrophosphate phase is formed with suitable morphology and mechanical resistance and impurities deriving from the synthesis are eliminated;
3. Activation in reactive mixture to obtain stable catalytic performances.

Synthesis of the precursor: $VOHPO_4 \cdot 0.5H_2O$

The precursor used to generate the active catalyst for the selective oxidation of *n*-butane is the vanadyl hydrogenphosphate hemihydrate (VHP); it can be obtained by reduction of a V^{5+} compound (normally V_2O_5) followed by addition of phosphoric acid. In function of the reducing agent used, three kind of preparation methods can be distinguished: VPA, VPO and VPD routes[17].

The VPA method (schematized in Figure 8) is the oldest one and involve the reaction in water medium, using HCl as reducing agent. In strongly acid condition the reagent V_2O_5 is soluble in water, so firstly it is solubilized as $VOCl_3$, reduced to V_2O_4 with simultaneous release of Cl_2 and finally H_3PO_4 is added to form the so called $VOHPO_4 \cdot 0.5H_2O$ precursor. The solid precursor is obtained after crystallization process adding water (because the acidic conditions do not allow the precipitation) or by solvent evaporation together with an amorphous phase.

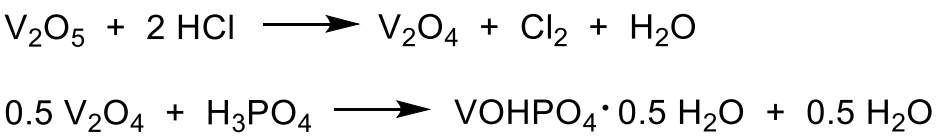

Figure 8. Scheme of VPA preparation method.

The most common preparation method is named VPO: an organic medium, i.e. a single alcohol (generally isobutanol) or a mixture of alcohols, acts both as a reducing agent and as a solvent. V_2O_5 is solubilized through the formation of vanadyl alcoholates, which are reduced by the organic solvent to V_2O_4. Thus, H_3PO_4 is added and it reacts with V^{4+} species leading to VHP at the liquid-solid interface. The catalyst is finally recovered after filtration, centrifugation, decantation or evaporation. The VPO route is schematically reported in Figure 9:

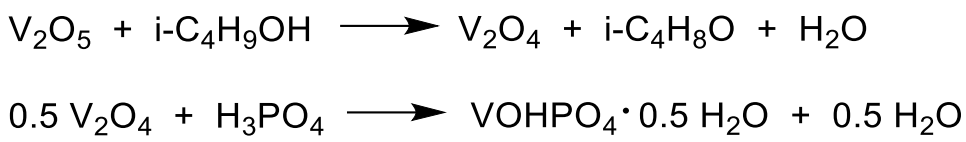

Figure 9. Scheme of VPO preparation method.

Lastly, the VPD route is composed by two steps reported in Figure 10: i) formation of vanadyl orthophosphate dihydrate ($VOPO_4 \cdot 2H_2O$) directly from V_2O_5 and H_3PO_4 in water; ii) reduction of dihydrate phase with isobutanol.

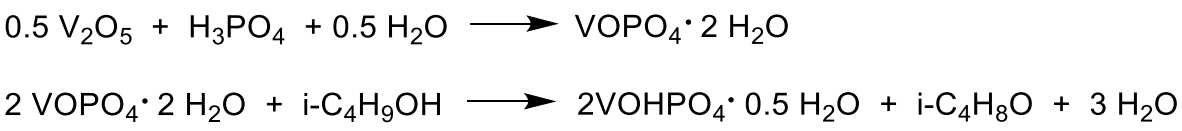

Figure 10. Scheme of VPD preparation method.

The synthesis of the precursor plays a fundamental role in the overall process because it strictly affects the morphology and surface area (consequently the catalytic behaviour) of the active phase VPP. In particular, the precursors obtained via VPA method presents the lower surface area (3-5 m^2/g) compared to that obtained with the VPO route (10 m^2/g). From X-rays diffraction analysis it has been observed that the latter presents lower crystallinity compared to the VPA one, due to alcohols molecules retained between the VHP layers (which has a lamellar morphology). These organic residues "intercalated" inside the crystalline structure create a defective structure that it is known to improve the catalytic performances. Moreover, the organic route leads to a preferential exposition of hemihydrate (001) planes, correspondent to (100) planes of vanadyl pyrophosphate, which possess the higher density of active sites.
The VPD route produces material characterized by the highest surface area (30 m^2/g) and a different morphology (so called "rosette"), but the dominance of unselective planes (220) make this route not suitable for the synthesis of active VPP catalyst.

Thermal treatment of the precursor

After the synthesis, the vanadyl hydrogenphosphate hemihydrate undergoes a calcination process: the crystalline structure is rearranged and the typical structure of vanadyl pyrophosphate is obtained, without changing the vanadium oxidation state. This transformation involves two steps and two water molecules are lost: firstly, an amorphous or microcrystalline compound with still the typical functional groups of the VHP is formed; the second step

involves the condensation of orthophosphate to form the pyrophosphate groups. The sequence of reactions are reported in Figure 11[18]:

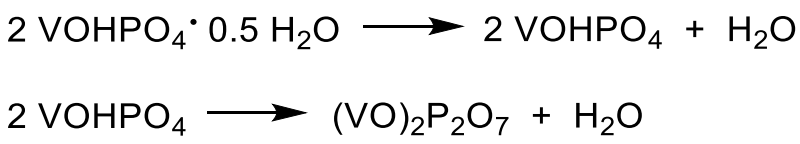

Figure 11. Synthesis of VPP starting from the precursor VHP.

The thermal treatment is carried out using a multi-step procedure:

- Drying at temperature lower than 300°C: the dehydration is avoided but chlorinated (in case of VPA route) or organic (in VPO synthetic method) compounds remained from the synthesis are released.
- Dehydration and calcination processes of the precursor to obtain the active phase (VPP). Several methods of dehydration are reported in literature, the most used treatments are: (i) *In-situ* dehydration inside the reactor starting from a relative low temperature (280°C) in reactive mixture (*n*-butane and air) at low contact time, increasing both contact time and temperature until reaching the common reaction conditions. After 24h the dehydration is usually completed. (ii) Dehydration in oxygen-free conditions at high temperature (> 400°C) followed by a treatment with *n*-butane/air mixture[19]. (iii) Calcination at high temperature (> 400°C) and then introduction of the reactive mixture[20,21] or feeding directly *n*-butane in air at ambient temperature and after that the increase of the temperature. (iv) Hydrothermal treatment which consists in a treatment at 280°C under air/water atmosphere and the second step in nitrogen at 390°C.

In the literature different hypothesis regarding the transformation of precursor into VPP are presents, since a great number of parameters may influence the entire process (e.g. temperature, time and atmosphere of treatment, precursor crystallinity and morphology, P/V ratio, presence of additives or structural defects). However all agree that vanadyl pyrophosphate retains the morphology of the precursor[22–24]: a topotactic transformation occurs, consisting in a structural conversion in which V-O and P-O bonds remain unaltered, while weak V-H_2O and P-H_2O are broken. After the dehydration of the precursor, the rearrangement of the structure takes place, and finally layers of precursor condense to obtain the structure of the vanadyl pyrophosphate.

VHP structure (reported in Figure 12) is composed of pairs of [VO_6] octahedra sharing a face, linked by hydrogen phosphate tetrahedral groups; the molecule of water is bridged-connected between two adjacent vanadium atoms, and O-H groups maintained in the *trans* position with

respect to the V=O bonds; in this way a layered structure is obtained[25]. The layers are kept together in the *c* direction thanks to strong hydrogen bonds between water molecules and the P-OH groups, thus reflected in the high temperature required for water loss in the precursor transformation. In the synthesis via VPO route, organic species between the layers are presents, this leads to a decrease in the distance between the planes, favoring the formation of crystals with higher exposure of the (100) plane, the selective one towards MA[26].

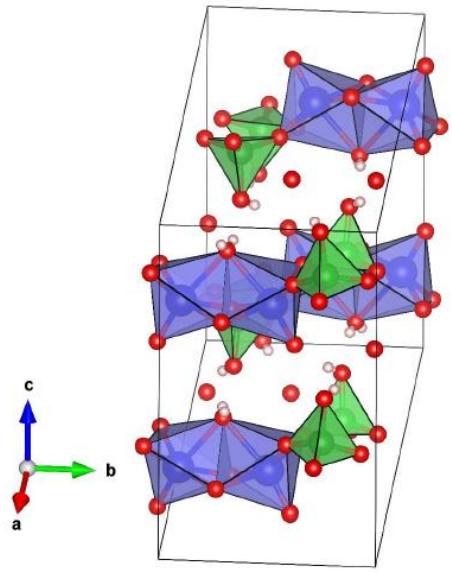

Figure 12. Crystal structure of $VOHPO_4 \cdot 0.5H_2O$ (VHP) precursor.
Violet octahedrals: [VO_6] and green tetrahedrals: [PO_4]

During the thermal treatment, the formation of breaks and voids leads to the transformation of VHP into VPP phase; in particular the loss of water molecules of the V octahedra induces the decreased of the layers distances. At the same time the face-shared octahedra are converted in edge-shared ones (arranged parallel to each other), resulting in a small expansion of the *a* axis. Proton transfer occurs from two vicinal P-OH groups and subsequently the second water molecule is lost. During this step the distance between the layers decreases favoring the bond between vanadium and the oxygen of two adjacent layers; moreover the inversion of the central P atom permits to obtain the pyrophosphate groups.

After the thermal treatment, vanadyl pyrophosphate structure is obtained: it is built of pairs of [VO_6] octahedra liked through a common edge, forming double chains of octahedral connected by the edge-oxygen in the *c* direction and by pyrophosphate groups with a P-bridge bond. Along the chain, single bond V-O and double bond V=O are alternate, respectively 1.60 Å and 2.30

Å. The structure of vanadyl pyrophosphate (with orthorhombic unit cells) is shown in Figure 13.

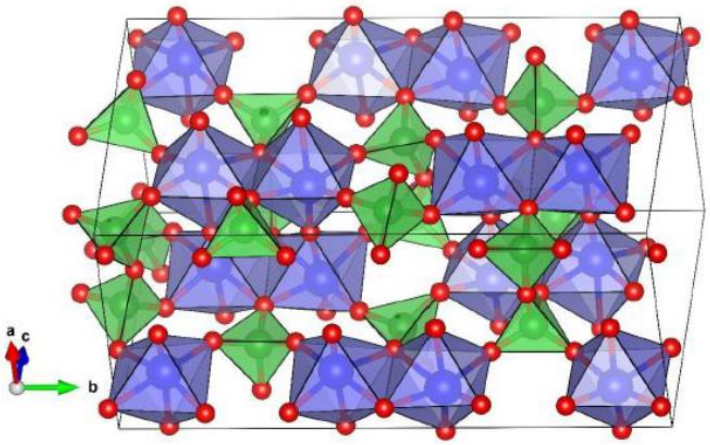

Figure 13. Structure of $(VO)_2P_2O_7$ (VPP).
Violet octahedrals: [VO_6] and green tetrahedrals: [PO_4]

Even though vanadium is present as V^{4+}, the V/P/O system obtained by thermal treatment of the crystalline VHP could contain crystalline and amorphous vanadium phosphate phase other than VPP[27,28]. In this regar, oxidized V^{5+} ($VOPO_4$) phases or even V^{3+} phase could coexists together with vanadyl pyrophosphate (V^{4+}). For this reason, in literature there are several hypotheses concerning the identification of the real active phase in the V/P/O based catalyst. It's generally accepted that an active catalyst is composed of a core of $(VO)_2P_2O_7$ with patches of $VOPO_4$ phases on the surface[29,30]. Other surface layers of V^{5+} phosphate may develop in the reaction environment, playing an active role in the catalytic cycle.

Activation under reaction mixture

The VPP obtained after the thermal treatment does not exhibit the best catalytic performance. For this reason, it is necessary an activation (or equilibration) process carried out in *n*-butane/air reaction mixture at 400°C for several hours: generally 100h are necessary to get stable conversion and yield/selectivity in the desired product.

The fresh (non-equilibrated) catalyst is more active than the equilibrated one because the V^{4+} easily oxidizes to V^{5+} in the final part of catalytic bed, in which the *n*-butane concentration is low but the oxygen is still relatively high: during the equilibration time on stream it's observed a decreases in *n*-butane conversion while the yield to MA increases due to the increase of selectivity. During this period the catalytic performances changes, as well as the chemical-physical features of the catalyst.

An "equilibrated" catalyst possess: (i) a preferential exposure of (100) planes, these are recognized to be the structure-sensitive planes for MA formation[15], (ii) stable V oxidation state, leading to a stable catalytic performances, in the range of 4.00-4.04, (iii) a surface area of 16-25 m^2/g and (iv) a slight excess of phosphorous compared to vanadium (P/V=1.05)[18].

1.2.2. Crystalline structure in V/P/O systems

As mentioned above different V/P mixed oxides can be obtained as function of the preparation method used to form the precursor, of the thermal treatment conditions and the P/V atomic ratio. In particular due to the two principal vanadium oxidation states, the active catalyst for the selective oxidation of *n*-butane to MA is constituted both of vanadyl pyrophosphate ($(VO)_2P_2O_7$, V^{4+}) and $VOPO_4$ (V^{5+}).

Some authors report that the vanadyl pyrophosphate can crystallize into different crystallographic forms. Bordes and Courtine first hypothesized that two crystalline forms at least may exist: γ- and β-VPP, which cannot undergo interconversion[31]. The first one was reported to be the structure usually formed in the transformation of the precursor to the catalyst when the dehydration is carried out in air or nitrogen; the structure is characterized by layered plates of (100) crystal planes of vanadyl pyrophosphate. This structure can be reversibly oxidized to γ-$VOPO_4$, involving only a small displacement of the atoms. The second form, the β-$(VO)_2P_2O_7$, was reported to be obtained by reduction of β-$VOPO_4$ at temperatures higher than 700°C. These two different forms have different activity in the reaction; the γ redox couple [γ-$(VO)_2P_2O_7$ ↔ γ-$VOPO_4$] is the one with higher activity[32]. Structurally, the β form is characterized by a lower exposure of the (100) crystallographic planes with respect to the γ form (which is referred to as a layered structure), while other cleavage planes, such as (010), (101) and (110) are exhibited. This justifies the superior catalytic performance claimed by the authors for the γ form, since the pairs of vanadium octahedra present at the surface of the (100) layers are the active sites, able to catalyze the first step in *n*-butane oxidation mechanism, that is the oxidehydrogenation to form olefins.

Matsuura and Yamazaki[33,34] hypothesized the existence of three different crystalline forms of VPP, namely α, γ, β. They differ in the intensity of the diffraction line referred to the crystallographic plane (200), which correspond to 2θ=23°: the β form shows a weak and broad reflection and resulting in the higher activity when tested in the selective oxidation of *n*-butane to MA (conversion of *n*-butane equal to 82% at 360°C). The α and γ (possessing very similar

XRD patterns) exhibit instead an intense and sharp reflection for the (200) plane; they possess higher selectivity to MA, compared to the one obtained with the β-VPP because of the higher exposure of the selective face, but a lower activity.

Regarding the oxidised phase several forms have been identified: α_I, α_{II}, β, δ, γ, ω and the hydrated phases $VOPO_4*nH_2O$[35–37].

In general $VOPO_4$ structures consist of $[VO_6]$ octahedra and $[PO_4]$ tetrahedra linked by V-O and hydrogen bonds, only connected through a corner (no edge-sharing as VPP): the different allotropic forms are distinguished by the arrangement of octahedra and tetrahedra inside the layer. It has been observed that δ-$VOPO_4$ and γ-$VOPO_4$ presents a low activity but a really positive effect in the selectivity to MA, probably due to the long V-O bond (3.1 Å) and high O=V-O angle (168°); on the other hand the α phases, together with the presence of VPP, presents a positive effect in the conversion of hydrocarbon but are un-selective in the desired product[35]. The ω-$VOPO_4$ structure is closely related to the one of δ-$VOPO_4$: it is obtained directly and quickly from the δ form at 400°C in air[38]. β-$VOPO_4$ is totally undesirable because is the most stable phase, so do not show any catalytic activity[31].

1.2.3. Critical factors for the catalytic properties in V/P/O systems

P/V ratio

Crucial for the catalytic and redox properties of the VPP-based catalysts is its chemical composition, in particular the content of phosphorous: several studies concerning the atomic ratio between the V and P sources used in the preparation of precursor are reported in literature[39–41].

The general agreement is that a slight excess of phosphorous compared to the stoichiometric in $(VO)_2P_2O_7$ limits the oxidation of V^{4+} to V^{5+}, so it is important to control this parameter in order to obtain stable catalytic performances with high selectivity to MA[42]: P/V ratio lower than 1.0 gives highly active catalyst, encouraging nevertheless the total combustion reactions, compared to samples with P/V>1. On the other hand, a catalyst with P/V ratio between 1.0 and 1.2 show a lower activity but an higher selectivity to MA[43]. However, too much P content leads to the formation of $VO(PO_3)_2$ which is detrimental for the catalytic activity[44].

The different catalytic behaviour observed as a function of the P/V ratio are due to the preferential formation of specific $VOPO_4$ over other phases: a ratio greater than 1.0 helps the formation of δ-$VOPO_4$ which is the most selective towards MA, but less active. A ratio lower

than 1 leads to the formation of α-phase which is more active but less selective for the oxidation of *n*-butane[45]. Approximately, P/V between 1.0-1.2 in the bulk is the optimum value; at the catalytic surface the concentration of phosphorous is higher (P/V=1.6-1.8) and it is considered the responsible of the selective oxidation to MA[17].

Vanadium oxidation state

The second key point in VPP-based catalyst is the vanadium oxidation state and this aspect has been discussed for several years. Indeed, many species of V^{3+} and V^{5+} could be formed both as amorphous or crystalline phosphate because the selective oxidation of *n*-butane to maleic anhydride is a redox reaction based on a Mars-Van Krevelen mechanism: the lattice oxygen of the catalyst structure oxides *n*-butane and V^{4+} is reduced to V^{3+}; in the second step the catalyst is re-oxidized by molecular O_2 co-fed with the hydrocarbon[46]. The thermal treatments adopted for the precursor transformation plays a fundamental role in determine the final ratio of these compounds.

Moreover, Mallada et al.[47] demonstrate that the different species of vanadium are also function of reaction conditions, i.e. the reducing and/or oxidizing gas phase atmosphere: in the first case (hydrocarbon-rich) V^{3+} species are formed together with a decreases in MA selectivity due to amounts of C deposits[48].

Volta et al. demonstrate that the optimal value of V^{5+}/V^{4+} has to be equal to 0.25[49]: in this condition only a defined and isolated amount of $VOPO_4$ over a core of VPP is presents and it should be the key factor for the success of these catalysts.

The presence of oxygen related to V^{5+} species is fundamental for the oxidation/reduction reactions involved in the reaction mechanism: Bordes and co-workers claim that the alkane activation is associated with V^{4+} species, while the insertion of oxygen to form MA is associated to V^{5+} species[32].

Abon et al.[50] report that an excess of V^{5+} in the form of $VOPO_4$ phases (or even if $VOPO_4$ is formed as a bulk phase[32]) is detrimental for the catalytic performances, indeed increasing V^{4+} instead of V^{5+} increases both the conversion of hydrocarbon and the selectivity in MA and, at the same time, CO and CO_2 decreases.

Regarding the V^{3+} species, their role is controversial: it is generally agrees about its negative effect on the selectivity, but a discrete amount in the lattice VPP is supposed to play a positive role on catalytic activity, due to its associated vacancies[51].

Acidity of the catalyst

Vanadyl pyrophosphate is a bifunctional catalyst due to the presence of redox (discussed above) and acidic properties. In particular, two types of acid sites are presents and plays a different role in the reaction mechanism:

- Lewis acid sites, related to V^{4+}=O ions, acts as a promoter for alkane activation and hydrogen extraction, leading to the formation of olefinic intermediate; in the catalyst prepared by organic route the Lewis acid sites are more active with respect to the one obtain in water medium:
- Brϕnsted acid sites identified in P-OH groups play a key role in the selective path to MA: it was supposed by Centi et al. that they stabilized the intermediates and the adsorbed oxygen species, favouring the oxygen insertion; they also facilitate maleic anhydride desorption, avoiding total oxidation[52]. They are involved in the selective oxidation to non-combustion products: this could be considered another explanation of the positive effect of P-enrichment (i.e. P/V>1) for promoting the desired product MA.

New catalytic systems: dopants and supported systems

The molar yield in MA obtained from selective oxidation of *n*-butane reaches the maximum value of 60% (70% if reactor is equipped with a recycling system)[53], because of the great number of side-reactions, e.g. parallel reactions of hydrocarbon combustion leading to oxidative degradation to acetic and acrylic acids and/or consecutive total combustion reactions to COx both favoured by the presence of hot-spots along the catalyst surface. The limits in MA yield has been also attributed to local catalysts overheating (hotspots), due to the high exothermicity of the reaction and the poor heat-transfer properties of the catalytic material. To overcome these problems dopants might be added to the catalytic system in order to increase the acid-base and redox properties, or the active phase could be supported over highly heat-conductive materials.

The dopant may enhance the catalytic performance in two ways:

- Contributing directly to the formation of MA or limiting the side-reactions;
- Forming solid solution with the catalyst $[(VO)_xM_{1-x}]_2P_2O_7$ (M is the promoter metal), causing defects on VPP lattice which can act as active sites for the *n*-butane oxidation or limiting the formation of un-selective phase on the surface.

The most used metals are Co, Fe, Bi, Ga[54–61] and Nb[62–64], which acts as a promoter for the reaction for different effects. For example, Co affects the redox properties of VPP, controlling

the V^{5+}/V^{4+} surface ratio, increasing the selectivity to MA; Fe increases the conversion of *n*-butane and Ga increases the surface area, leading to an highly active catalyst. Finally, Nb increase the surface acidity, promotes the desorption of MA, increasing the selectivity.

In the case of VPP-supported catalysts, the support may have good mechanical properties to improve attrition resistance of the catalyst, not very high specific surface area to avoid high residence time of reactant inside the pores and finally it has to be inert, avoiding changes in its morphology. The most studied supports are:

- TiO_2: the supported VPO showed activity and selectivity in *n*-butane oxidation at 100°C lower than commercial VPO catalysts, related to higher surface area, strong interaction of the VPO component with the titania support, different reducibility of VPO on TiO_2 and different average oxidation state of vanadium ions on the surface[65].
- SiO_2: the VPO component in the silica-supported catalysts was well dispersed but interacted weakly with the support surface as compared to the titania-supported system, leading to lower active (attributed to the non-reducible nature of silica support) but highly selective catalyst. However, the higher surface P/V ratios found in the silica-supported catalysts as compared to the titania-supported systems, may also be responsible for lower activity in *n*-butane oxidation and higher selectivity to maleic anhydride at high conversion in these catalysts[65].
- Al_2O_3: the high affinity between Al and P limited the dispersion of VPO phase on the support, leading to poor catalytic performances[66].
- $AlPO_4$: the most used type of $AlPO_4$ was trydimite; in this case the main VPO phase is present as vanadyl pyrophosphate. This system improves both catalytic performances and activation time of the catalyst. Very high conversion (90%) and MA selectivity (42%) are reached, and the activation time is lower (20h instead of the classical 100h, necessary for the bulk VPO)[67,68].

1.3. Reaction scheme and mechanism

The conversion of *n*-butane to maleic anhydride is a selective oxidation in which 14 electrons are transferred, 8 C-H bonds are broken and also the insertion of 3 oxygen atoms takes place, coproducing water. Therefore it is a demanding reaction.

During the reaction, according to the Mars-Van Krevelen mechanisms, the catalytic cycle can be divided in two steps: during the "reduction" step the lattice oxygen oxides the hydrocarbon and V ions are reduced; in this step the catalyst give 7 O^{2-} ions: four are used to co-produce

water, the remaining three are incorporated in the butane molecule to form MA. In the "oxidation" step the oxygen co-fed with *n*-butane re-oxides the catalyst and forms O^{2-} ions, which are incorporated in the structural vacancies generated during the reduction step. The catalytic cycle is summarized in Figure 14:

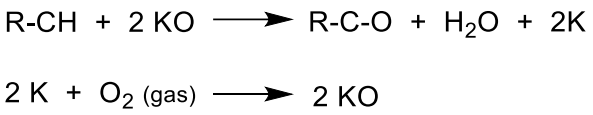

Figure 14. Mars-Van Krevelen mechanism for the catalytic oxidation of alkane. R-CH and R-C-O are the reactant and the product respectively and KO and K are the oxidized and reduced catalyst.

Due to the absence of by-products, the study of reaction scheme is quite difficult: the reaction intermediates are more reactive than *n*-butane, so they are quickly transformed in MA before desorption from the surface of catalyst. Several hypotheses have been evaluated over the years, however the most proposed scheme (reported in Figure 15) involves oxidative dehydrogenation and oxygen insertions sequential steps:

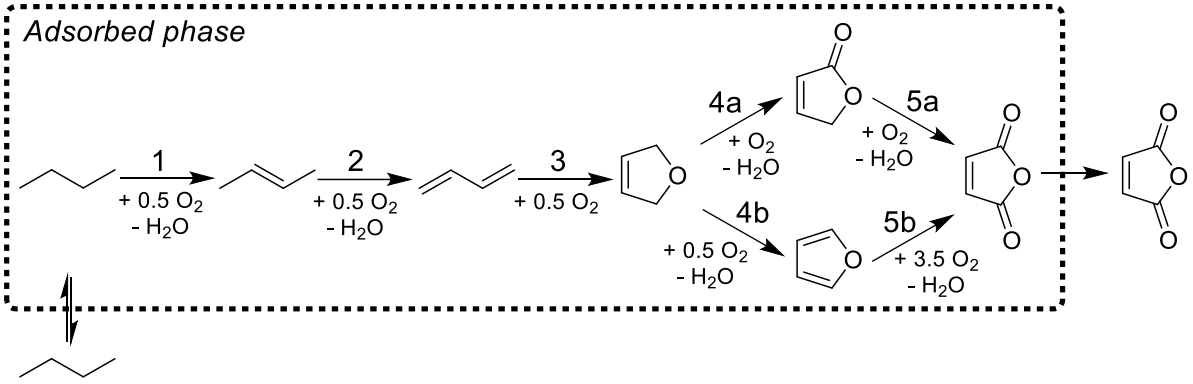

Figure 15. Reaction scheme for the selective oxidation of *n*-butane to MA.

1) Alkane activation via oxidative dehydrogenation, forming butenes;
2) Allylic H extraction to form 1,3-butadienes;
3) 1,4-oxygen insertion leads the formation of 2,5-dihydrofurane;

4a – 5a) MA is obtain directly through o-allylic insertion lactone mediated starting from 2,5-dihydrofurane;

4b – 5b) Allylic extraction to obtain furan which, after electrophilic oxygen insertion, leads to the formation of MA.

This proposed mechanism was obtained carrying out the reaction in unusual conditions: very low residence time or high *n*-butane/O_2 ratio is used, in this way the reaction atmosphere is more “reducing” and the desorption of olefins is possible.

Kinetic studies have shown that the first step, the alkane activation and its oxidative dehydrogenation to butenes, is the rate determining step. To obtain high MA selectivity this first step has to be faster than the one of oxygen insertion, in order to limit by-products that may be oxidized to other products than MA.

2. Aim of work

Nowadays the industrial production of Maleic Anhydride (MA) is achieved mainly by the selective oxidation of *n*-butane, a process catalyzed by V/P/O-based material, namely the vanadyl pyrophosphate (VPP), a compound with formula $(VO)_2P_2O_7$.

Although this process has been widely used since the '80s, the importance of MA as a building block in the chemical industry is still largely recognized and because of this, there is still an ongoing and continuous improvement of the technology and a deeper study of this reaction.

During my PhD I focused my work on the calcination step of the VPP-precursor in order to identify the effect of preparation parameters on catalytic performances. The starting material was an industrially-made precursor composed of vanadyl hydrogenphosphate hemihydrate (VHP) with formula $VOHPO_4 \cdot 0.5\ H_2O$. The activities were carried out at the Department of Industrial Chemistry "Toso Montanari" (University of Bologna) in collaboration with Polynt SpA, a company specialized in the production of organic anhydrides and their derivatives.

The aim of this research was to find out how the activation conditions (heat treatment) influence both the structure and properties of the final catalyst. In particular, the correlation between heat treatment environment and both the obtained phases and the observed catalytic activity have been investigated in depth. To do so, the obtained materials have been tested in the selective oxidation of *n*-butane in order to correlate the catalytic behaviour with the obtained structure. Since the ultimate purpose was to understand the effect of both operative conditions performed during the calcination and the intrinsic properties that characterized the precursor, a different industrially-made VHP was treated in the same conditions. This precursor differs from the previous one in terms of phosphorous/vanadium atomic ratio, carbon content remained from the synthesis in organic medium and amount of V^{5+}. Having regard to the differences between the precursors, the ultimate purpose was to try to develop a calcination method reproducible, in order to be able to provide useful information for the improvement of the industrial preparation of V/P/O catalysts.

3. Experimental

3.1. Catalysts preparation

The VPP catalysts were prepared employing different conditions during the thermal treatment (calcination) of two industrially-made precursors provided by Polynt SpA, composed of vanadyl hydrogenphosphate hemihydrate ($VOHPO_4 \cdot 0.5H_2O$, VHP).

The calcination experiments were carried out in a lab-scale continuous-flow fixed bed glass reactor, in which different atmosphere can be tested; the laboratory plant is schematized in Figure 16.

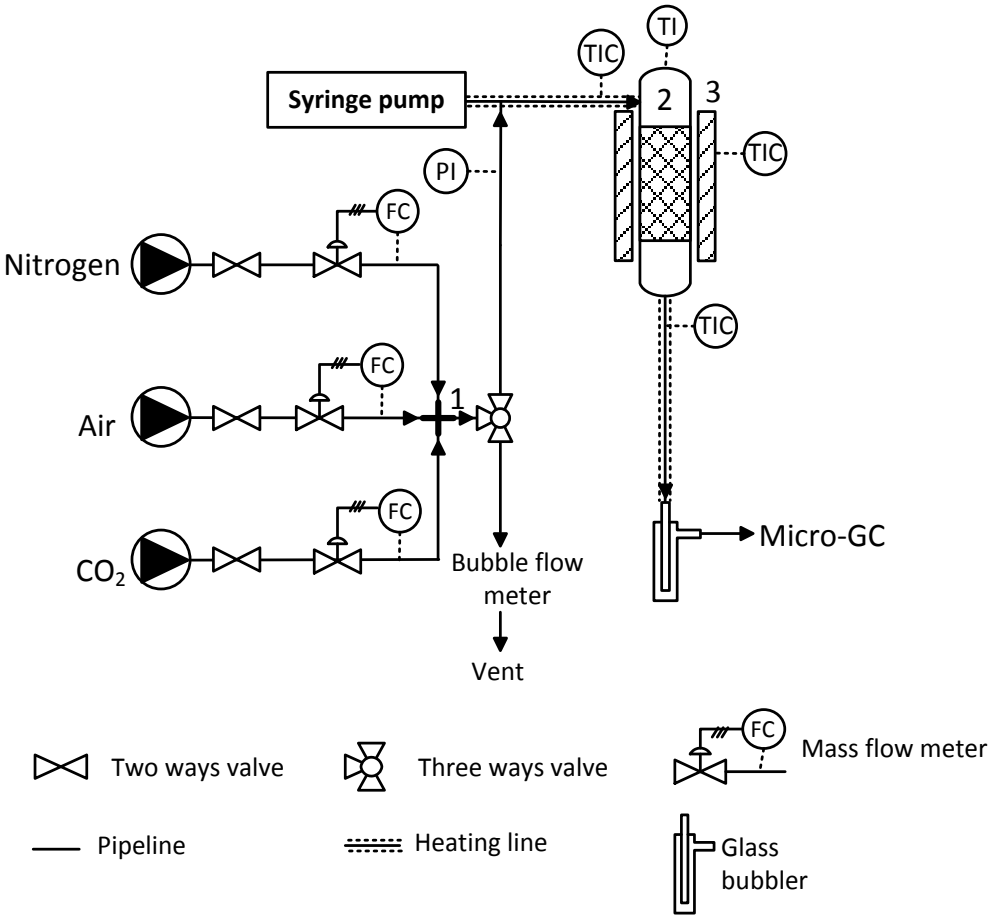

Figure 16. Scheme of the bench scale plant used for the thermal treatment.

The gases (air, nitrogen and carbon dioxide) were fed in separated stream or simultaneously, as a function of calcination test, by three mass flow meters; they were mixed (1) and sent to a three-ways valve, that was used to switch the feed inside the reactor or in a bubble flow meter, to check the real entrance flux. The water was fed by a syringe pump, properly calibrated for the desired quantity of liquid flow, and it was vaporized: gases and water were mixed in the same inlet line heated at 160°C and then fed to the reactor. The fixed bed reactor (2), operating at atmospheric pressure, is inserted

inside an oven (3) and the precursor powder is placed in its isothermal zone. The real temperature inside the bed it's regulated by a thermocouple (TI). At the reactor exit a heater string maintained at 160°C avoid the water condensation; the outlet stream was analysed by an online micro gas chromatograph Agilent 3000A. HP Plot-Q column, OV1 and Molecular sieve 5Å column are simultaneously used to separate water and carbon dioxide formed and oxygen consumed during the entire process; each column is equipped with a thermal conductivity detector (TCD) for the quantitative analysis.
If the water content at the outlet of the reactor was supposed to be higher than 10%, it was collected in a glass bubbler: in this way a damaging of the stationary phase of the columns was prevented.

3.2. Reactivity tests

3.2.1. Laboratory-scale plant

Catalytic tests were carried out in a continuous-flow, fixed bed, glass reactor designed to allow the variation of different parameters such as the feed composition, contact time and temperature inside the reactor. The laboratory plant is schematized in Figure 17 and it can be divided in three main parts:

1) Feed

Three different gases could be simultaneously fed, such as *n*-butane, air and helium, by three mass-flow meters. Butane and air, the reagents used for the synthesis of maleic anhydride, are sent to two three ways valve, that were used to switch the gases to a mixing point (1) or in two bubble flow meters in order to check the real entrance flux. After the mixing point a four-ways valve was present: using this valve the mixture of *n*-butane and air could be fed in the reactor or directly analyzed by GC (online sampling in the FID) to quantify the real entrance flow. During the sampling it was possible to feed He in the reactor using the four-ways valve.

2) Reaction

The fixed bed reactor (2) was constituted by glass tube, operating at atmospheric pressure. The thermocouple (TI) is positioned in the inner part of reactor, inside a thin glass tube at the level of catalytic bed, with which the real temperature inside the bed was measured. The reactor is inserted inside a Lenton oven (LFT 12/25/250) (3). The exit of the reactor emerging outside the oven is wrapped with a heater string kept at 250°C in order to avoid crystallization and condensation of the products.

3) Downstream

Upon exit from the reactor, the flow gas is splitted: opening the on/off valve (4) a part of flow is directly sent to the gas chromatograph and by a sampling valve it was possible to make directly the online analysis of the organic products and of the unconverted hydrocarbon on the FID column; the other part of flow pass through a crystallizer in which the organic products are collected in, and the incondensable gases are sent for online GC-TCD analysis.

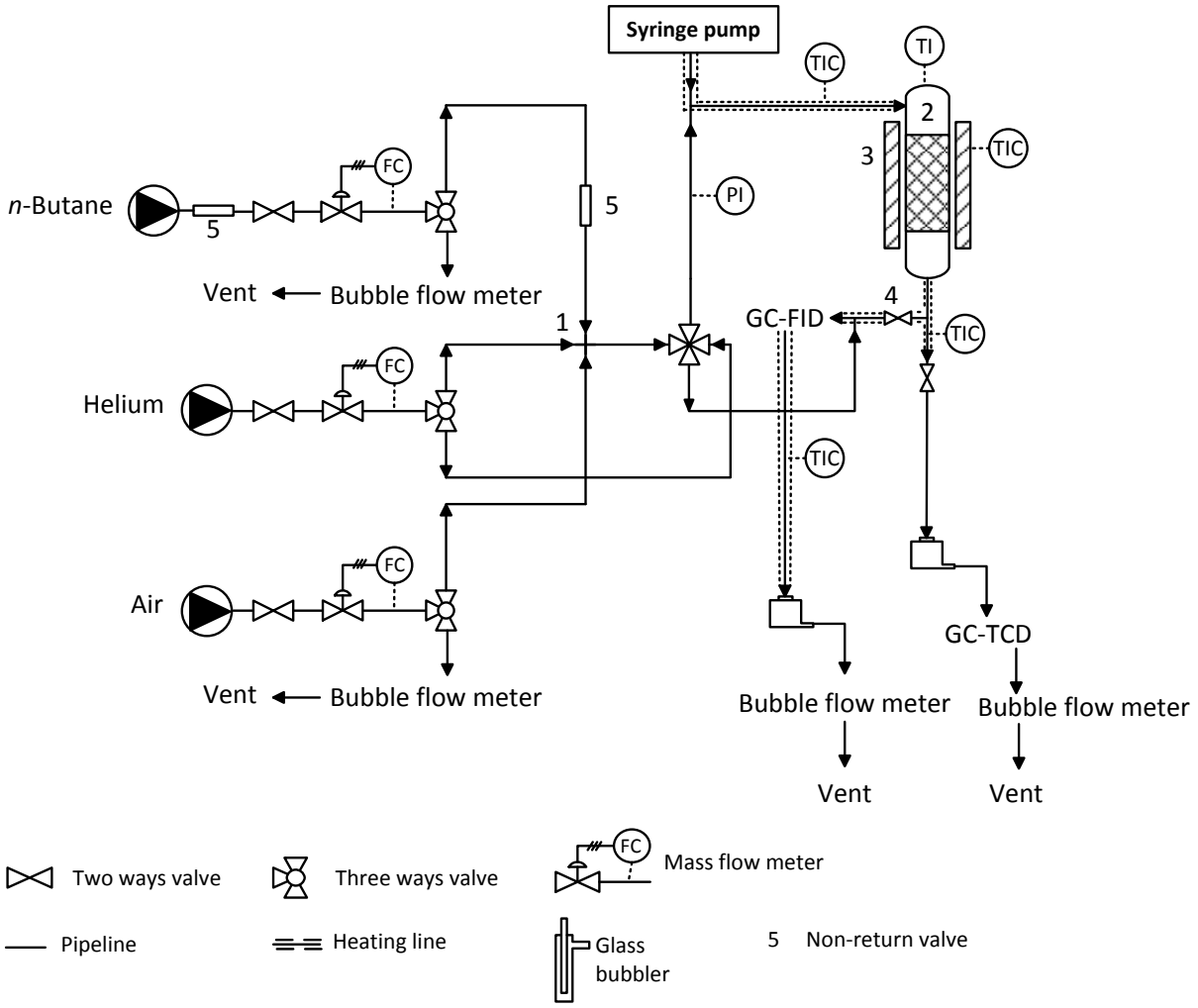

Figure 17. Scheme of lab-scale plant for the selective oxidation of *n*-butane to MA.

3.2.2. Analytical system

The reactants and products were analyzed by Agilent 6890 gas chromatograph equipped with:

- Semicapillar CPSil-5CB column (30 m length; i.d. 0.53 mm; stationary phase of dimethylpolysiloxane with a thickness of 3.00 μm. By this column are separated the maleic

anhydride, by-products (acetic acid, acrylic acid, and other light compounds, e.g., butenes), and *n*-butane (in and out). The correspondent detector is a FID.

- Packed Carbosieve SII column, of 2 m length, with a stationary phase formed by active carbons (mesh between 80 and 100). In this column CO, CO_2, O_2 and N_2 are separated and detected by a TCD.

Both the columns use helium as carrier gas; the temperature program of the oven was: 8 minutes at 40°C, heating up to 220°C at 30°C/min and final isothermal step at 220°C for 10 minutes.

3.3. Data elaboration

By gas chromatograph analysis, through calibration curve, it's possible to obtain a response factor (*F*) for each compound (*i*) and then the quantity (in mol) of it:

$$mol_i = \frac{Area_i}{F_i}$$

After that, the percentage values of conversion, yield and selectivity were determined, according to the following equations:

$$Conversion = \frac{mol_{reactant}^{IN} - mol_{reactant}^{OUT}}{mol_{reactant}^{IN}} \times 100$$

$$Yield_i = \frac{mol\ of\ product_i / stoichiometric\ coeff.}{mol_{reactant}^{IN} / stoichiometric\ coeff.} \times 100$$

$$Selectivity_i = \frac{Yield_i}{Conversion} \times 100$$

$$Carbon\ balance = \frac{\sum Yield}{Conversion} \approx 100$$

3.4. Catalyst characterization

3.4.1. Structural properties

X-ray diffraction of powder (XRD)

X-ray diffraction is a technique used to identify information about crystalline properties such as the nature of the crystalline phases, crystal size and possible distortions of the lattice; the information are given by the position, sharpness, intensity and width of the diffraction lines.

The measurements were carried out using Philips PW 1050/81 apparatus, with Cu Kα (λ=1.5406 Å) as radiation source, in the range of 10°<2θ<50° with a scanning rate of 0.05°/s and time-per-step=1s. Reflects attribution was done by the Bragg law: $2d \cdot sen\theta = n\lambda$ (where d is the spacing between two planes, 2θ is the diffraction angle, λ is the wavelength of incident X-ray beam, n is the diffraction order) and by using a software from PANalytical Company and the ICSD Database FIZ Karlsruhe library.

Specific surface area

The specific surface area was determined by physisorption of liquid nitrogen at 77K (the boiling temperature of N_2) using a MICROMERITICS ASAP 2420 instrument. The sample was heated at 150°C under vacuum, in order to desorb water and other molecules adsorbed on catalyst surface. After this pre-treatment, sample was maintained at 77K in a liquid nitrogen bath, while the instrument sent gaseous N_2, which was adsorbed on the surface. The instrument measures the volume of the adsorbed gas and, using the BET equation, it provides the value of sample surface area (this model was applied directly by the instrument).

Thermogravimetric analysis (TGA)

TG analysis was used to quantify the loss of weight of samples as a function of the time and temperature, providing important information about the adsorption of molecules over the solids.
The experiments were carried out in a DST Q600 TA Instrument, in order to quantify the weight loss during the transformation of the precursor in the final active phase vanadyl pyrophosphate. Generally 20 mg of samples was loaded in an alumina pan, air and/or nitrogen were fluxed (100mL/min) through the sample as a function of the test and the temperature is raised up at 2°C/min up to 500°C.

3.4.2. Surface properties

Raman spectroscopy

Raman spectroscopy was used with the aim to determine the phases on the catalysts surface after calcination and after reaction. The studies were performed using a Renishaw Raman System RM1000, equipped with Leica DLML confocal microscope, with 5x, 20x and 50x objectives, video camera, CCD detector and laser source Argon ion (514 nm) with power 25 mW. Generally, for all samples different spectra were recorded by changing the surface position. The parameters of spectrum acquisition are: 5 accumulation, 10 seconds, 25% of laser power to prevent sample's damage and 50x objective.

The Raman peaks used for compound identification are tabulated in Table 2.

Table 2. Raman bands of different Vanadium/Phosphorous phases.

V/P/O	cm^{-1}			
	1200-1100	**1100-1000**	**1000-900**	**900-400**
$(VO)_2P_2O_7$	1185, 1135		930, 920	
$(VO)HPO_4*0.5H_2O$	1155, 1100		985	342
$VOPO_4*2H_2O$		1039	988, 952	542
α_I-$VOPO_4$		1032	928	579, 541
α_{II}-$VOPO_4$		1091	993, 979, 945	433, 399
δ-$VOPO_4$	1200	1090, 1075, 1020	936	590
β-$VOPO_4$		1075	997, 986	892, 435
ω-$VOPO_4$	1188	1084, 1016	932	650, 589

Energy dispersive spectroscopy (EDX)

Energy dispersive X-ray spectroscopy (EDX) analysis is a surface characterization technique used for the elementary analysis or chemical characterization of the samples. The experiments were performed using Oxford Instrument INCA X-ACT and the spectra were registered for a 60 s collection time.

3.4.3. Composition

X-ray fluorescence (XRF)

XRF analysis consists in bombarding the sample with an X-ray source (i.e. electromagnetic radiations with wavelength equal to 0.01-11.3 nm or energy equal to 0.11-100 keV). This bombardment implies an excitation of electrons in the inner shell of the atoms and the subsequent emission of characteristic radiation. In WD system at 90 degrees (i.e. for fluorescence emission), a monochromator is located that allows the radiation to be dispersed and permits the discrimination for wavelength or energy (qualitative analysis), and afterwards a counter that allow the quantitative analysis. For the latter purpose several standards of the elements of interest are prepared in the working range; a calibration of the instrument should be done with the reading of the standards and, after that, the sample can be analyzed. This technique permits the determination of inorganic elements and the amount of each

element present in the materials. The analyses were carried out in a Bruker AXS S4 Explorer; the samples were grinded and mixed with a ligand before being pelletized pressing with 10 tons.

Carbon determination

LECO SC-144 DR instrument was used to determine the carbon content in the precursors by combustion and non-dispersive infrared detection. The sample was weighted into a combustion boat and placed in a pure oxygen flow regulated at 1350°C; the combination of high temperature and oxygen flow causes the total combustion of the sample, i.e. the oxidation of C to form CO_2. The gas flow pass through an anhydrone tube to remove moisture and then in a carbon IR cell that measures the concentration of carbon dioxide gas. The instrument, using an equation presents in the software that takes into account the sample weight and calibration, converts these values to a percentage/ppm value.

Vanadium oxidation state (Vox)

The Vanadium oxidation state was obtained by redox titration determining firstly the total vanadium content (renamed Vtot) and, later, the amount of V^{5+}:

$$Vox = 4 + \frac{\%\, V^{5+}}{\%\, V_{tot}}$$

The catalyst was dissolved in concentrated sulfuric acid; $KMnO_4$ 0.1 N was added until a persistent violet solution is obtained; the second step was a titration with Mohr salt solution (Fe^{2+}); in this way the total vanadium content was obtained.

For V^{5+}, the sample was dissolved in H_2SO_4 and then determined by titration with ammonium iron (II) sulfate (Mohr salt) 0.1N solution.

4. Results and discussion

4.1. Precursor characterization

Thermal treatment consists in inducing structural changes in the precursor by its exposure to a temperature ramp in controlled atmospheres.

To have a more complete overview and understand which phenomenon leads to obtain differences in the final catalyst, starting from the same precursor, it is necessary to analyse in detail all the phenomena that are involved during the process of calcination in order to assess if, and how, these can directly influence the calcination itself.

The reaction involved are:

1. Dehydration of vanadyl hydrogenphosphate hemihydrate to VPP:
   $2\ VOHPO_4 \cdot 0.5\ H_2O \rightarrow (VO)_2P_2O_7 + 2\ H_2O$
   This is a topotactic transformation in which the cis→trans electronic rearrangement of the dimer vanadyl groups is involved to form the active phase $(VO)_2P_2O_7$.
2. Oxidation of residual organic species present on the precursor from the synthesis in organic medium, with the concomitant loss of water molecules:
   $C + x\ O_2 \rightarrow CO + CO_2 + H_2O$
   Thus resulting in modification of the crystalline structure because the organics may lead to some local defect in the structure by steric hinderance or as a consequence of oxygen vacancies (the alcohol used for the synthesis could react with the structural oxygen to form carbon oxides).
3. Oxidation of VPP (V^{4+}) to form different polymorphic species with V^{5+}, namely the vanadyl orthophosphate:
   $(VO)_2P_2O_7 + 0.5\ O_2 \rightarrow 2\ VOPO_4$

The thermal treatment is a crucial step in the catalyst preparation, in fact the final structures (and consequently the catalytic performance) are strongly influenced by the composition of the gas mixture fed, temperature and time of treatment.

The focus of the present work was on the calcination step of the VPP-precursor catalyst in order to identify the effect of preparation parameters on catalytic performances. Special attention was on the influence of air and water co-fed during the thermal treatment on the structure and superficial phases of the final VPP catalyst, trying to increase the reproducibility of the entire process.

For this purpose, a series of VPP catalysts were prepared by using two different precursors renamed M16 and M17. They were composed of vanadyl hydrogenphosphate hemihydrate with formula $VOHPO_4 \cdot 0.5H_2O$ (VHP), provided by Polynt SpA and synthetized following the organic route[17]. The main differences of the two VHP are listed in Table 3.

Table 3. Precursors characteristics.

Precursor	P/V		C_{in} (ppm)	% V^{5+} prec.
	EDX	*XRF*		
M17	1.15	1.15	9490	0.006
M16	1.21	1.20	6344	0.040

The two hemihydrate precursors were analysed by means of EDX spectroscopy and X-Ray fluorescence analysis (XRF) to determine the Phosphorous/Vanadium atomic ratio: both the methods reveal that M17 has a lower P/V compared to M16. The differences in this parameter may affect the catalytic properties: it is generally accepted that an excess of P with respect to the stoichiometric requirement is necessary to have a good selectivity for MA[43,69].

The second main difference in the two precursors is the amount of carbonaceous species remained from the synthesis: this parameter is determined by LECO SC-144 DR instrument.

During the thermal treatment, the organic residues are burned and the topotactic transformation to obtain the VPP take place; the higher C content in M17 can make this process more difficult, taking too long, excessively destroying the structural layers and leaving less time for the structure to reorganize in an efficient way.

Finally, by redox titration with Mohr salt solution it has been determined the lower V^{5+} amount in M17 with respect to M16. It could be assumed that treating the two precursors in the same condition, the M16-derived catalysts will present higher vanadium oxidation state, i.e. less oxidant conditions may be required to have the optimal V^{5+}/V^{4+} ratio.

Figure 18 shows the room-temperature X-ray powder diffractogram pattern of the two precursors: the only compound identified was crystalline $VOHPO_4 \cdot 0.5H_2O$, as expected, in both samples (empty circle).

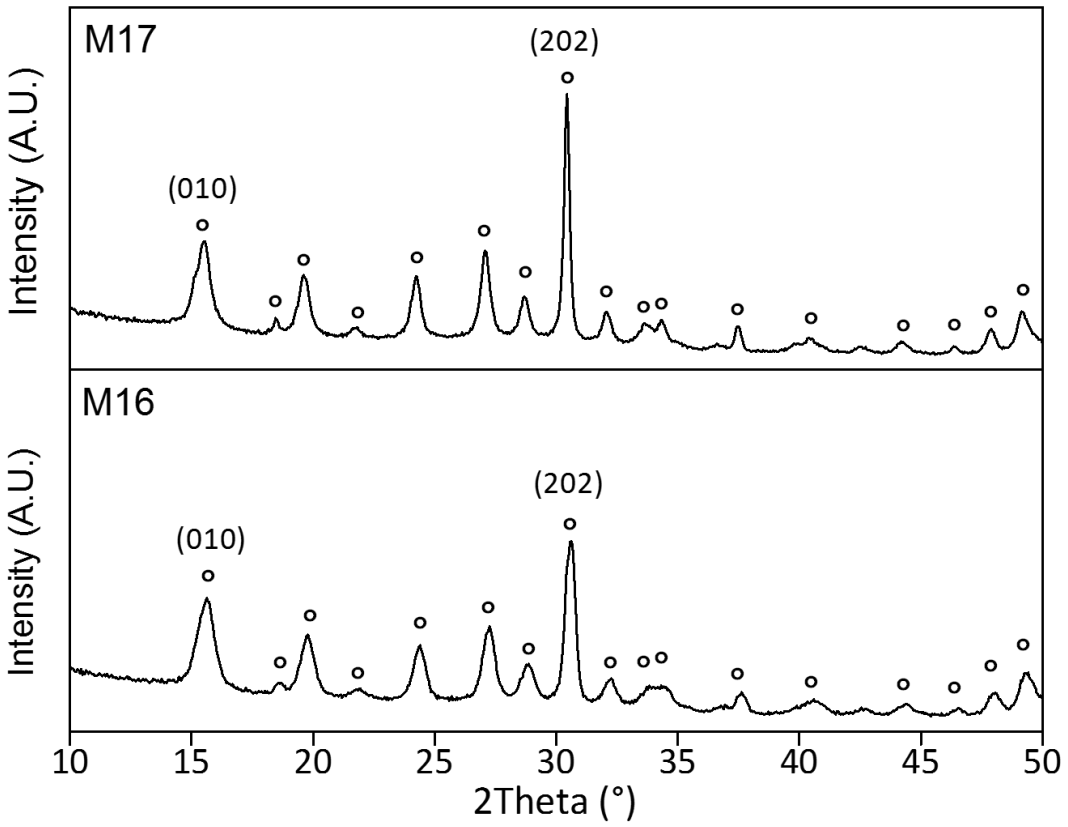

Figure 18. XRD patterns of precursors. Top: M17, bottom: M16. Symbols: ° = $VOHPO_4 \cdot 0.5H_2O$.

In regard to the reflections of hemihydrate vanadyl hydrogen phosphate, there is differences in crystallite morphology:

- The FWHM(202)/FWHM(010) ratio (FWHM means full width at half maximum and the ratio is often defined as the "aspect ratio", AR) gives information about the P/V ratio: in agreement with Cornaglia and co-workers[70] the lower the AR the lower is the P/V, attributed to a different crystallinity, induced by a different degree of structural disorder. M17 presents the lower aspect ratio with respect to M16 (0.39 and 0.54 respectively) demonstrating that the two precursors have different P/V ratio.
- The intensities of the two main peaks at 2θ=15.5° and 30.4° (related to (010) and to (202) planes, respectively) were different: extrapolating the data reported in literature[70] we can expect different reactivity results of the two precursors. M16, which presents the lower I_{202}/I_{010} ratio, will have greater selectivity in MA.
- Finally, the broadening and/or decrease in height of the reflection at 2θ=15.5° with respect to the one at 30.4° in M17 indicates an increasing in the disorder of the precursor and may be due to alcohol molecules trapped between the layers of the precursor which could produce

this disorder during drying; in fact it presents the higher Cin content (9490 ppm compared to 6344 ppm of M16)[20,71].

The first precursor tested was M17; M16 was used in the last part of the thesis trying to correlate the catalytic performances with the intrinsic characteristic of the VHP.

4.2. Choice of atmosphere conditions

Before starting with catalysts synthesis, it has been investigated the role of calcination environment (oxidant or inert) and the mechanism for the transformation of vanadyl hydrogenphosphate hemihydrate precursor to vanadyl pyrophosphate, the active phase for the selective oxidation of *n*-butane to maleic anhydride.

These preliminary tests were carried out focusing on the same vanadyl hydrogen phosphate hemihydrate, namely M17. It has been performed three thermal treatments, using the same heating ramp (schematized in Figure 19), changing the gas fed: a) the first step from room temperature up to 425°C flowing air and the second step from 425°C to 500°C in nitrogen atmosphere; b) during both step 1 and 2 was fed nitrogen; c) all the thermal treatment (step 1 and 2) was made flowing air.

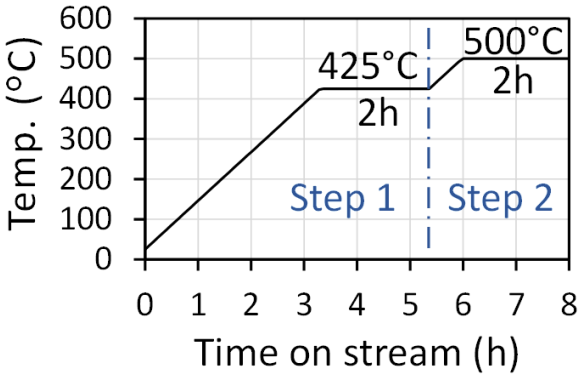

Figure 19. Heating ramp used for calcination tests. Heating rate 2°C/min. Case a) Step 1 in air and step 2 in nitrogen; b) Step 1 and 2 both performed in nitrogen flow; c) Step 1 and 2 in air.

The calcination tests were carried out both in a thermogravimetric apparatus, monitoring the weight loss during the treatment, and in a continuous flow lab-scale reactor, tracking the formation of H_2O and CO_2 and the consumption of oxygen.

Figure 20-a shows both the water (top) and carbon dioxide (middle), determined by an on-line micro-GC, formed during the thermal treatment in which air was fed only until 425°C (Figure 19-case a). On the other hand, the derivatives of weight loss (dTG) obtained by performing the same treatment with a TGA apparatus is reported bottom in Figure 20-a.

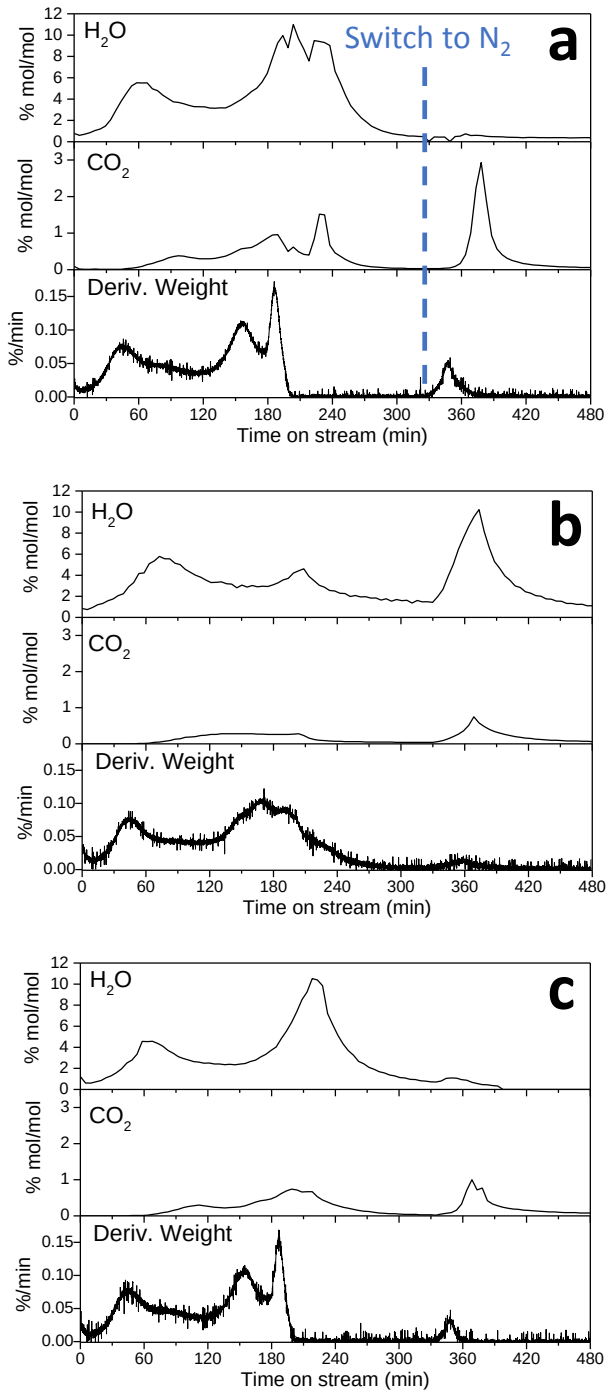

Figure 20. Water (top) and CO_2 (middle) formed during the thermal treatment and derivatives of the weight (bottom) as a function of time for air/nitrogen (a), only nitrogen (b) and only air (c) used as a carrier gas.

It is possible to observe a perfect correspondence between the loss in weight and the formation of combustion products: initial release of physiosorbed water and light organic compound (such as alcohols used for the precursor synthesis) after one hour (which correspond to the temperature of 120°C); between 350 and 425°C (respectively 2.5-4h) the combustion of organic species derived from the synthesis occurs, which correspond to the major formation of combustion products and loss in weight; finally it has been observed the formation of CO_2 after 6 hours, without concomitant release of water, when the carrier gas used was nitrogen. This latter phenomenon could be attributed to combustion reactions promoted by lattice oxygen of the catalyst with retention of water molecules inside the structure. The second test was performed using nitrogen as carrier gas during the entire process; the comparison between the micro-GC and the dTG analysis are reported in Figure 20-b: increasing time and temperature it has been observed an initial formation of water which correspond also to a loss in weight, similar to the previous case, meaning that this signal is actually due only to physisorption of molecules thanks to the increasing of the temperature, because it is the same regardless the gas fed is air (case a) or nitrogen (case b); after approximately 2 hours the combustion of organic species starts, but it is not complete in fact a lower quantity of water and CO_2 and a minor loss in weight has been detected, compared to the previous

case. Increasing the temperature up to 500°C one more formation of combustion products has been observed, probably it is permitted thanks to the high temperature (kinetically favoured reaction). Considering the inert atmosphere, the burning of organic molecules causes the reduction of the catalyst.

Finally, when the calcination is carried out only in air atmosphere from room temperature up to 500°C (Figure 20-c) a similar trend in terms of H_2O and CO_2 formed and loss in weight could be observed: initial release of water and light organic molecule physiosorbed on the precursor surface, combustion of organic species after 3 hours and then formation of CO_2 without co-production of water when the temperature reaches 500°C is observed.

Treating the precursor in different atmosphere and tracking the transformations with thermogravimetric analysis, leads to demonstrate the relationship between the precursor, the carbonaceous species and the air feed: the VHP acts as source of oxygen atoms for the combustion of organic compounds leading to the formation of H_2O and CO_2 and a reduction in vanadium oxidation state occurs. Later the oxygen feed is reduced and replenished in form of O^{2-} inside the structure, re-oxidizing the catalyst and minimizing the loss in weight. This cycle of reduction and oxidation reactions is commonly known as Mars-Van Krevelen mechanism.

The demonstration of this hypothesis is given by the comparison of the total weight loss in the three cases: when only nitrogen is used as carrier gas (Figure 21-b), the total loss in weight is the highest (14.5%): the combustion starts but in the absence of air the cycle cannot take place, this means that the lattice oxygen was not replaced and the total weight loss was the highest. Moreover, the mean vanadium oxidation state (Vox) determined by titration (Table 4) was lower than 4, meaning that the vanadium acts as an oxidizing agent in relation to organic molecules, consequently undergoing a reduction. Feeding only air for the entire thermal treatment (Figure 21-c), allows a greater replenishment of oxygen which correspond to the minor weight-loss (11.2%). When the temperature reaches 500°C, an increase in weight was observed: an over-oxidation due to the air fed still happens and the Vox was the higher, with a value equal to 4.66, compared to the other.

In accordance to the hypothesis previously made, when both air and nitrogen are used (Figure 21-a) an intermediate value of loss in weight (12.3%) was observed, and the sample is characterized by a lower Vox with respect to the one obtained only in air (case c), because the second step was performed in nitrogen instead of air.

Table 4. Vanadium oxidation states after thermal treatment in (a) air and N_2, (b) only in N_2 and (c) only in air.

	Atmosphere	Vox
Case a	RT→425°C Air 425→500°C N_2	4.52
Case b	RT→500°C N_2	3.85
Case c	RT→500°C Air	4.66

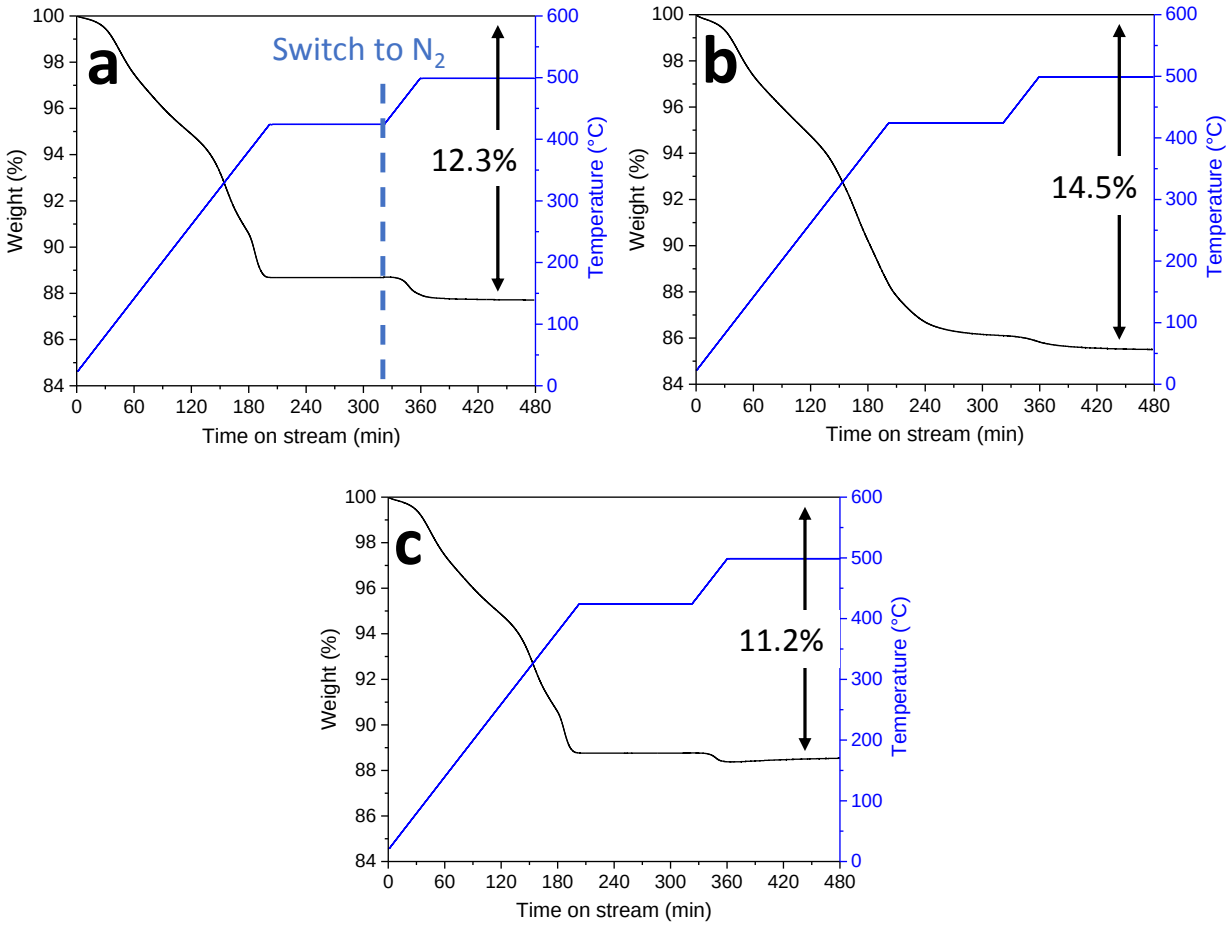

Figure 21. TGA as a function of time for air/nitrogen (a), only nitrogen (b) and only air (c) used as a carrier gas. Black line represents the percentage loss of weight and blue lines represent the temperature ramp.

The samples obtained after the calcinations were characterized by means of X-ray powder diffraction and Raman spectroscopy and the results are reported in Figure 22 left and right respectively.

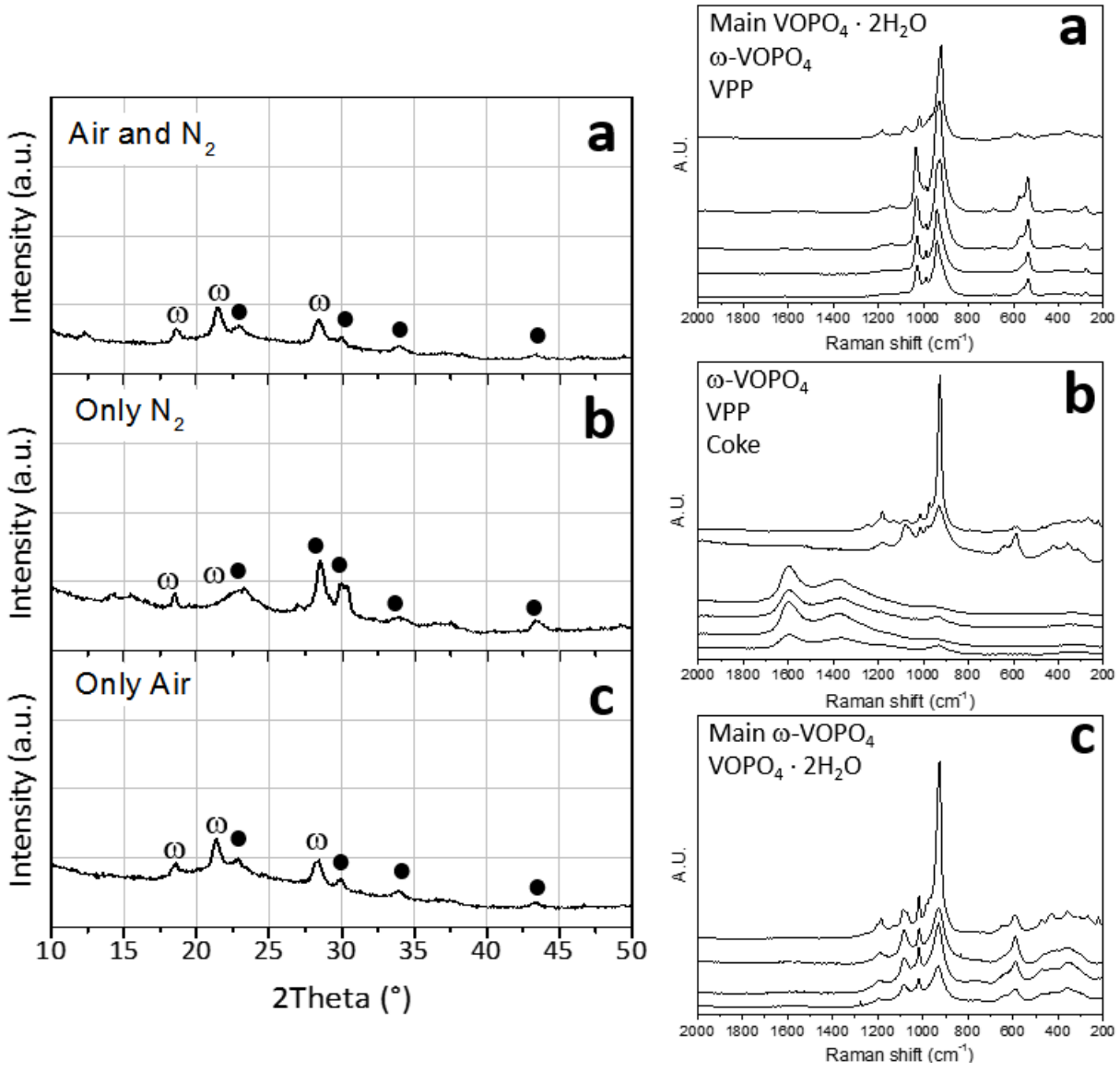

Figure 22. XRD analysis (left) and Raman spectra (right) for samples obtained with air/nitrogen (a), only nitrogen (b) and only air (c) as a carrier gas for the calcination. Symbols: ω = ω-$VOPO_4$; ● = VPP.

The sample obtained after the thermal treatment performed in air in the first step and ended in nitrogen flow (Figure 22 - case a) is composed mainly of ω-$VOPO_4$ (represented by the symbol ω) in the bulk structure (X-ray diffractogram to the left), with traces of the active phase for the selective oxidation of *n*-butane, namely VPP (full circle). The Raman spectra collected in several points presents pattern attributable to $VOPO_4 \cdot 2H_2O$ (1039, 988, 952, 542 cm^{-1}) and ω-$VOPO_4$ (1188, 1084, 1016, 932, 650, 589 cm^{-1}) as major phase; it is also presents the most important bands of VPP (1185, 920 cm^{-1}). The presence of the dihydrate phase could be explained looking at the combustion products formed in nitrogen flow when the temperature reaches 500°C (Figure 20 - a): it was detected the formation of

CO_2, without co-production of water that probably remain trapped in the structure leading to the formation of hydrated phases.

When the precursor is subjected to thermal treatment in nitrogen flow (case b) the Mars-Van Krevelen mechanism begins to take place but without the air it could not be completed: the XRD diffractogram reveals the presence of VPP, but a lot of carbonaceous species unburnt are still presents on the catalyst surface (broad band at 1650 and 1450 cm^{-1} in the Raman spectra in Figure 22-b, right). Without feeding air the precursor hemihydrate starts to transform because the vanadium acts as oxidizing agent, but this is not enough to promote the total combustion of organic species remained from the synthesis, allowing the topotactic transformation and production of vanadyl pyrophosphate.

In the case c, in which only air was fed for the entire calcination process, it is possible to observe that:

- X-ray powder diffraction analysis is the same as the case a: the crystallinity is low but it has been detected the ω-$VOPO_4$ and traces of VPP; this means that the transformation from VHP to the final VPP is achieved in the temperature range between room temperature and 425°C, the common step in the two treatments.
- Raman spectra reveal the presence of ω-$VOPO_4$ (1188, 1084, 1016, 932, 650, 589 cm^{-1}) as a main phase and traces of $VOPO_4 \cdot 2H_2O$ (1039, 988, 952, 542 cm^{-1}); no bands attributable to VPP has been observed on the catalytic surface, confirming that feeding air for the entire treatments leads to an over-oxidize catalyst. The minor amount of dihydrate phase compared to the case a (in which both air and nitrogen were fed) could be due to the minor combustion products observed during the isothermal step at 500°C, reported in Figure 20-bottom: at this temperature lower %mol of CO_2 was detected, which correspond to lower water formation and lower loss in weight.

Even though both in VHP and VPP vanadium is present in the same 4+ oxidation state, an oxidizing atmosphere is necessary for the transformation and the obtainment of the active phase: without air fed during the calcination the Mars-Van Krevelen cycle does not occur; for these reasons, it has been decided to perform all the future calcination using an oxidizing atmosphere up to 425°C and then switch to nitrogen atmosphere from 425°C to 500°C, avoiding an overall oxidation state too high, because it is known that an oxidized catalyst shows worse performances in the synthesis of MA from *n*-butane[30].

4.3. Vanadyl pyrophosphate catalysts prepared by thermal treatment in presence of water

4.3.1. Synthesis and characterization of calcined catalysts

Since it is known that the presence of water during the calcination promotes the formation of the active phase VPP[28], different experiments were carried out increasing its partial pressure, co-feeding air, varying the air/water ratio, in other world the content of oxygen in the gas mixture fed during the calcination.

The catalysts obtained has been renamed L0, L10, L40 and L70, in which 0, 10, 40 and 70 are the %mol of water and the remaining part (100, 90, 60 and 30% respectively) is air:

- L0: only air is used as a carrier gas for this calcination from room temperature to 425°C. The starting point was a thermal treatment in which the structural transformation occurs in total absence of water, so in highly oxidizing condition (100%mol of air, 21% of oxygen), in order to define the role of water in the formation of VPP.
- L10: the calcination is carried out using a gas mixture composed of 10%mol of water and the remaining 90%mol air (which correspond to 18.9%mol O_2) up to the end of the isotherm at 425°C. The aim was to identify how the low amount of water influence the transformation of VHP precursor.
- L40: a mixture composed of 40%mol of water and 60%mol of air (12.6%mol O_2) was fed from 180°C to 425°C.
- L70: the higher %mol of water was used for this experiment, in particular 70% of it and the remaining 30%mol was air (6.3% mol O_2); in other word the lower oxidant power mixture was fed until the end of isothermal step at 425°C. This is the condition used in the industrial calcination plant.

The calcination conditions used to investigate the role of water in VPP-based catalyst preparation are summarized in Figure 23.

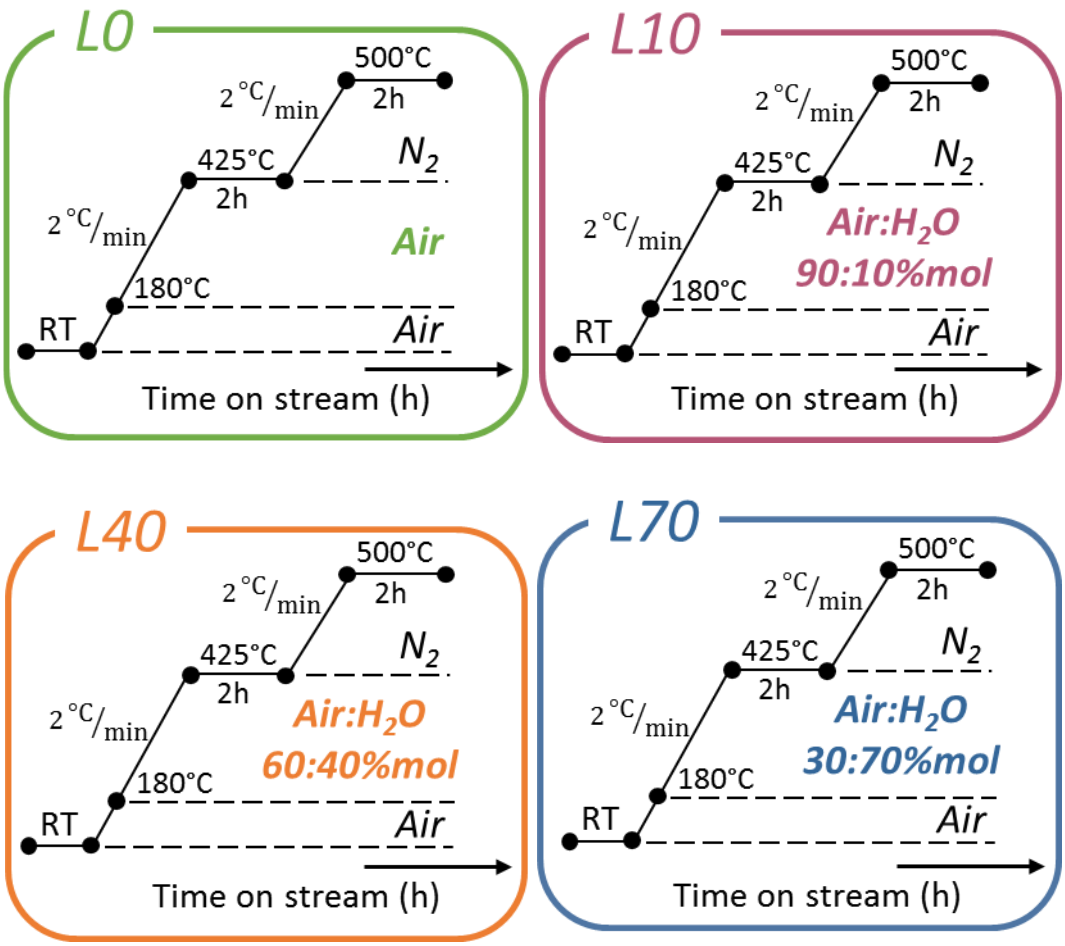

Figure 23. Heating ramp and atmosphere performed during the thermal treatments of VHP to study the effect of water in the synthesis of VPP.

During the thermal treatments performed in a tubular glass reactor the formation of H_2O and CO_2 and the consumption of oxygen were monitored by an online microGC.

In Figure 24 are reported the results obtained for the catalyst L0, calcined without water:

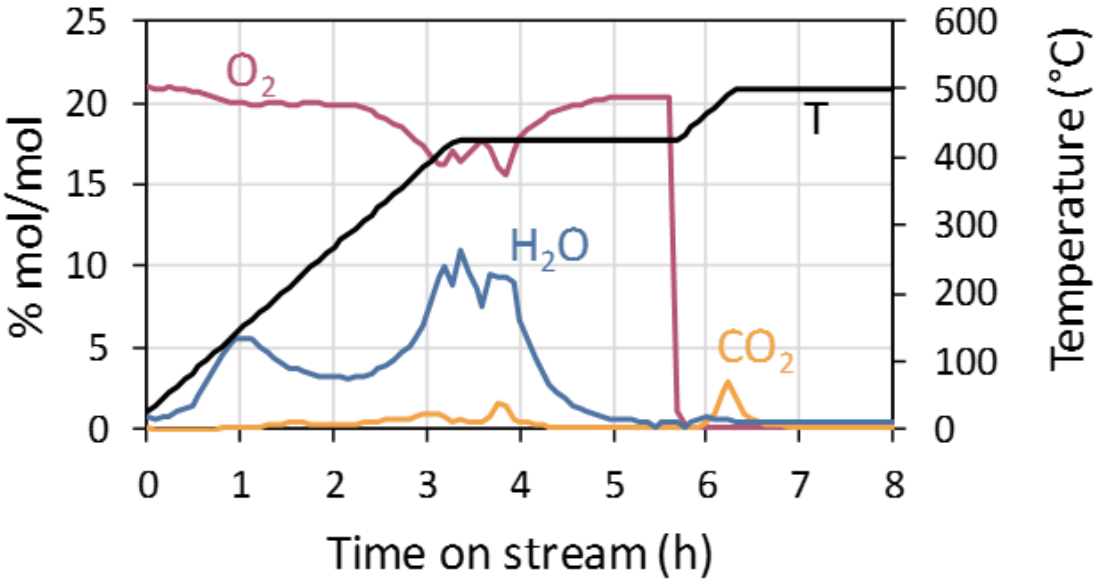

Figure 24. Consumption of oxygen (pink) and formation of water (blue) and CO_2 (orange) during the calcination without water (L0).

Increasing time and temperature, it could be noticed that there is consumption of oxygen used for the oxidation of the precursor to give the final catalyst; at the same time there is the formation of CO_2 and water, due to the oxidation of organic components in the precursor, deriving from the synthesis. In particular:

- After 1 hour it has been observed the formation of water physiosorbed on the precursor surface layer.
- Between 300 and 425°C (which correspond a time on stream between 2.5h and 5h) the oxidation/combustion of organic compounds remained from the synthesis in organic medium occurs: an oxygen consumption and water/CO_2 desorption are observed, and the transformation of VHP to give the final catalyst takes place.
- Finally it was observed a formation of carbon dioxide when the temperature reaches the isothermal step at 500°C; the latter happens in inert atmosphere, in which only nitrogen was used as carrier gas. This phenomenon must not seem surprising and can be attributed to a further combustion, due to the high temperature, by reticular oxygen in the catalyst, which would take place with retention of water molecules inside the structure (because no water formation was detected by gas chromatographic analysis). Otherwise it could be hypothesized that at this temperature a desorption of CO_2 previously formed and trapped inside the structure could take place thanks to the high temperature.

After the calcination treatment the sample obtained was characterized by means of Raman spectroscopy: it is particularly suitable technique for the structural characterization of

vanadium/phosphorous mixed oxide, because it allows, by surface investigation in several points, to differentiate the various phases composing each sample, because several V(IV) and V(V) phosphate phases exist in the VPO system and the presence/amount of them influence the catalytic performance. Figure 25 shows the Raman ex-situ spectra recorded in different spots of sample L0, calcined in absence of water: it is mainly composed of oxidized vanadium phases (V^{5+}), in particular were identified α_I-$VOPO_4$ (1032, 928, 579, 541 cm^{-1}), ω-$VOPO_4$ (1188, 1084, 1016, 932, 650, 589 cm^{-1}), the dihydrate phase $VOPO_4 \cdot 2H_2O$ (1039, 988, 952, 542 cm^{-1}) and traces of VPP (1185, 1135, 920 cm^{-1}). The main superficial phases are the dihydrate and α_I which are convertible according to the environment and the reaction temperature[42].

Despite the anhydrous atmosphere used in the treatment, the final catalyst L0 has a considerable amount of dihydrate phase, but considering the water and CO_2 formed during the calcination and monitored by microGC, it was observed that around 500°C (in nitrogen flow) CO_2 was detected with no co-production of water (as reported in Figure 24). Can be conceived that water formed during the last combustion of organic residues it is retained by the structure, forming the dihydrate oxidized vanadium phase ($VOPO_4 \cdot 2H_2O$).

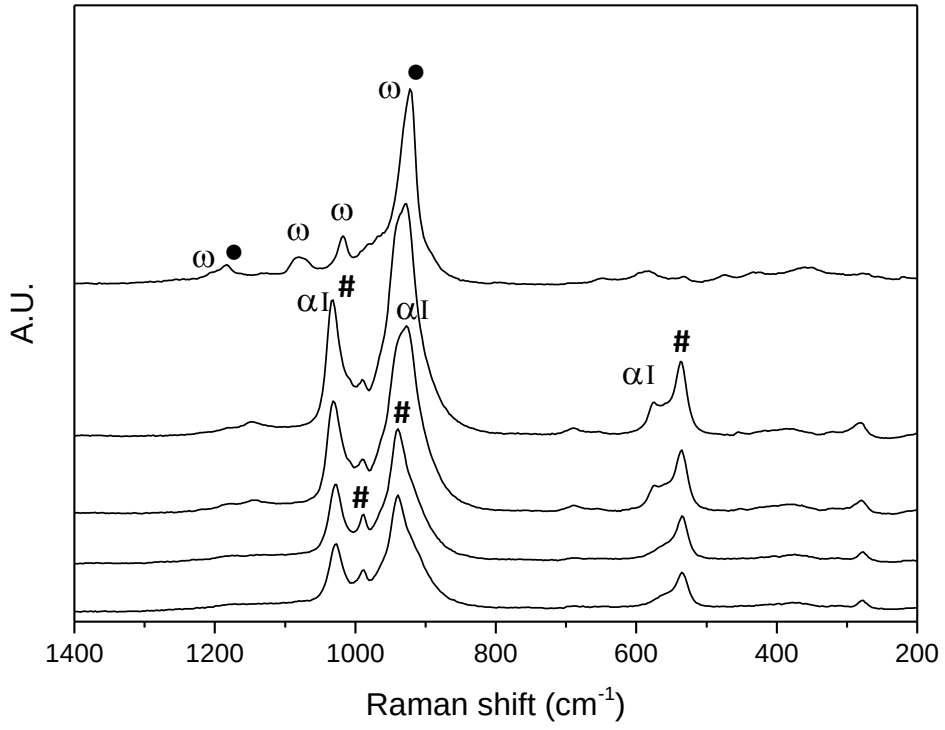

Figure 25. Raman spectra of L0 catalyst (obtained without water, 21% of oxygen).

Symbols: ω = ω-$VOPO_4$; α_I = α_I-$VOPO_4$; # = $VOPO_4 \cdot 2H_2O$; ● = VPP.

Increasing the partial pressure of water co-fed with air, i.e. L10, L40 and L70 (respectively calcinating the precursor with air:water ratio equal to 90:10%mol, 60:40%mol and 30:70%mol) led to analogues trends, reported in Figure 26, Figure 27 and Figure 28.

For these catalysts, the water in the outlet stream has to be condensed and removed before entering the microGC, because it would damage the columns.

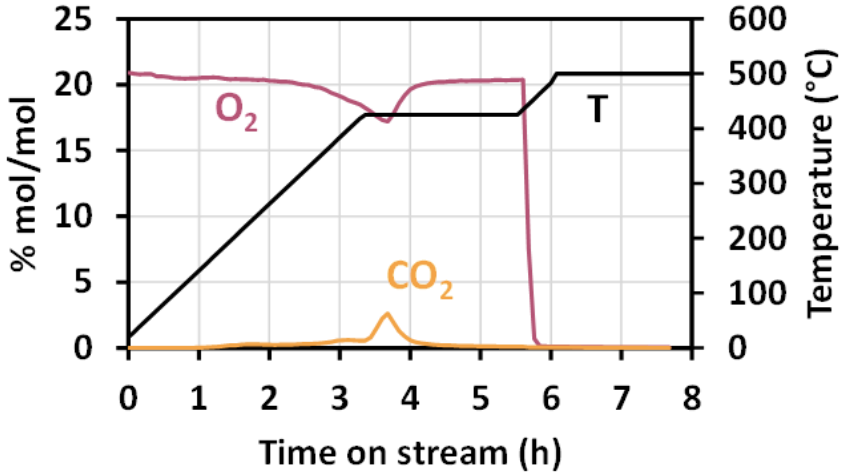

Figure 26. Consumption of oxygen (pink) and formation of CO_2 (orange) during the calcination performed with 10%mol of water and the remaining part 90% air (L10).

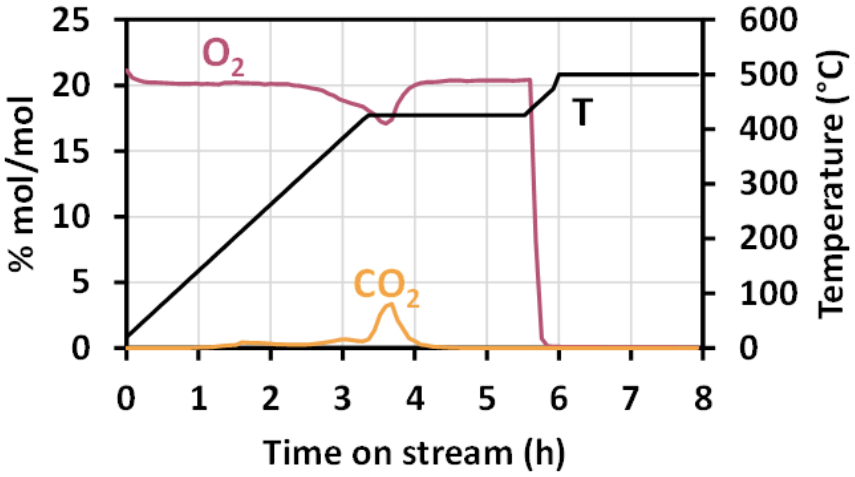

Figure 27. Consumption of oxygen (pink) and formation of CO_2 (orange) during the calcination performed with 40%mol of water and the remaining part 60% air (L40).

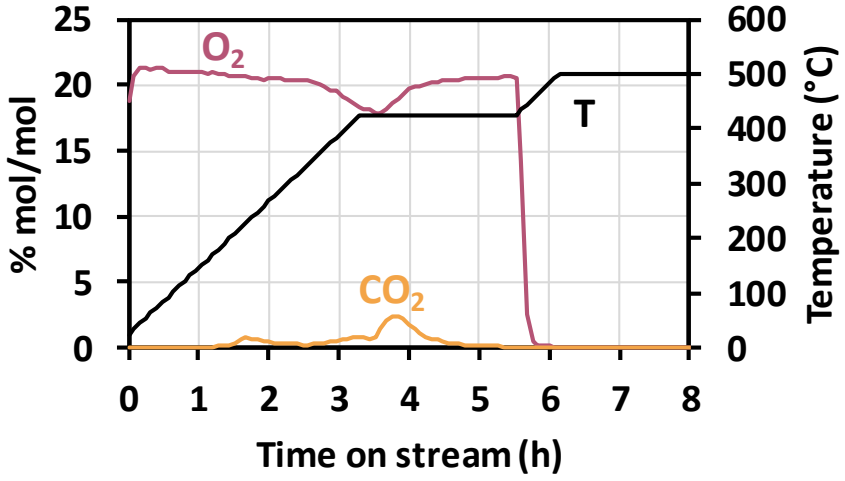

Figure 28. Consumption of oxygen (pink) and formation of CO_2 (orange) during the calcination performed with 70%mol of water and the remaining part 30% air (L70).

The trends for the three cases are quite similar: oxygen concentration starts to decrease after the first hour of heating, at the same time a slight increase in CO_2 was observed. The significant consumption of oxygen, in the case of L10, L40 and L70 occurs when the temperature reaches 425°C as for L0. On the other hand, the main difference when water is co-fed with air is in the formation of carbon dioxide in nitrogen flow at 500°C, which is observed only in the calcination performed in anhydrous condition (for L0 catalyst). The most plausible hypothesis is that the water fed, thanks to the high temperatures, favours the kinetics of combustion by facilitating superficial reforming reactions of organic residues present. In conclusion water helps and speed up the resulting desorption of CO_2 at lower temperature and time on stream (before changing the atmosphere to nitrogen); during this combustion the structural modification takes place and VPP phase is formed.

In Figure 29 are reported the Raman spectra of sample L10 (obtained calcinating with a gas mixture Air:H_2O 90:10%mol). Dihydrate $VOPO_4$ (1039, 988 and 542 cm^{-1}) and ω-$VOPO_4$ (1188, 1084, 1016, 932, 650 and 589 cm^{-1}) are the main phases identified; also VPP in traces has been detected, principally in the first spectrum, associated to the bands at 1185 and 920 cm^{-1}.

Comparing the spectra of these first two catalysts L0 and L10, it is possible to note that L0 presents α_I-$VOPO_4$ phase that it is known to be unselective for the oxidation of *n*-butane to MA; on the other hand, L10 is composed of ω-$VOPO_4$, a V^{5+} phase that, in the reaction temperature range, it could rearrange leading to δ-$VOPO_4$, the selective phase for the reaction[38,72].

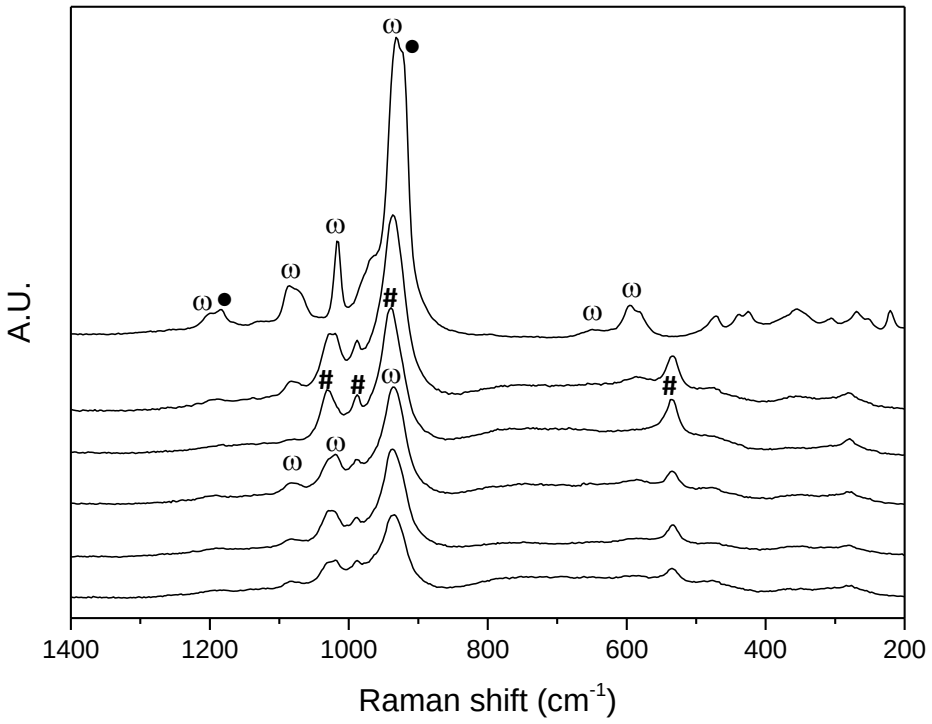

Figure 29. Raman spectra of L10 catalyst (10%mol of water, 90%mol of air).

Symbols: ω = ω-$VOPO_4$; # = $VOPO_4 \cdot 2H_2O$; ● = VPP.

Increasing the partial pressure of water (i.e. decreasing the %mol of oxygen) in the feeding mixture the VPP phase is gradually increased: the Raman spectra collected on a different spots of the L40 catalyst show the presence of both ω-$VOPO_4$ and VPP as main phases: the simultaneous presence of these two phases is proved by the broad bands at 1190 and at 930-920 cm^{-1} which are probably due to the overlapping of the individual bands of the two compounds (Figure 30). The band at 542 cm^{-1} is attributed to $VOPO_4 \cdot 2H_2O$.

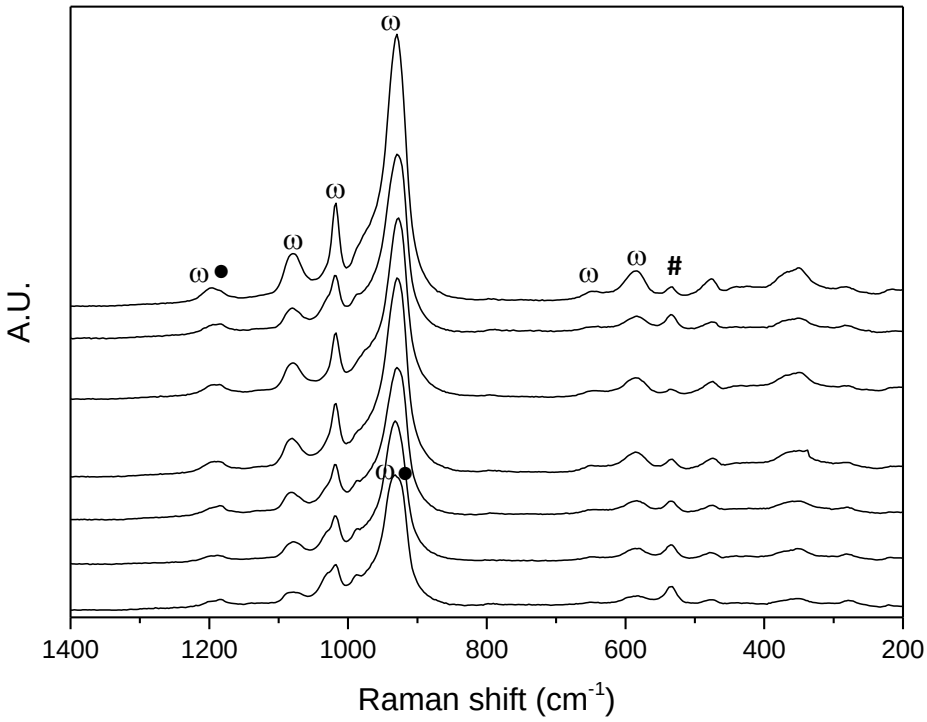

Figure 30. Raman spectra of L40 catalyst (40%mol of water, 60%mol of air).
Symbols: ω = ω-$VOPO_4$; # = $VOPO_4 \cdot 2H_2O$; ● = VPP.

Finally, for the catalyst L70, calcined with only 6.3%mol of oxygen in mixture with water, the spectra collected in different spots revealed the presence of VPP (1185 and 920 cm^{-1}) together with ω-$VOPO_4$ (1188, 1084, 1016, 932, 650 and 589 cm^{-1}) and the dihydrate $VOPO_4$ (1039, 988 and 542 cm^{-1}) (Figure 31). The first spectrum on the top shows only one difference: a double bands at 1090 and 1075 cm^{-1}, instead of a single and broad band at 1084 cm^{-1} characteristics of ω-$VOPO_4$: this fact reveals the presence of δ-$VOPO_4$.

Increasing the amount of water from 40 to 70%mol led to the formation of more V^{4+} phases on the catalyst surface, in fact in the latter VPP is present in each point analysed and all its bands are clearly distinguishable (in particular the most important one at 920 cm^{-1}). The presence of hydrated phase and ω-$VOPO_4$ is particularly important because, in the reaction conditions they could be transformed into the selective δ-$VOPO_4$[38,42].

The combination of these two phenomena, together with high presence of VPP, would therefore lead to obtain a very active and selective catalyst in the synthesis of maleic anhydride.

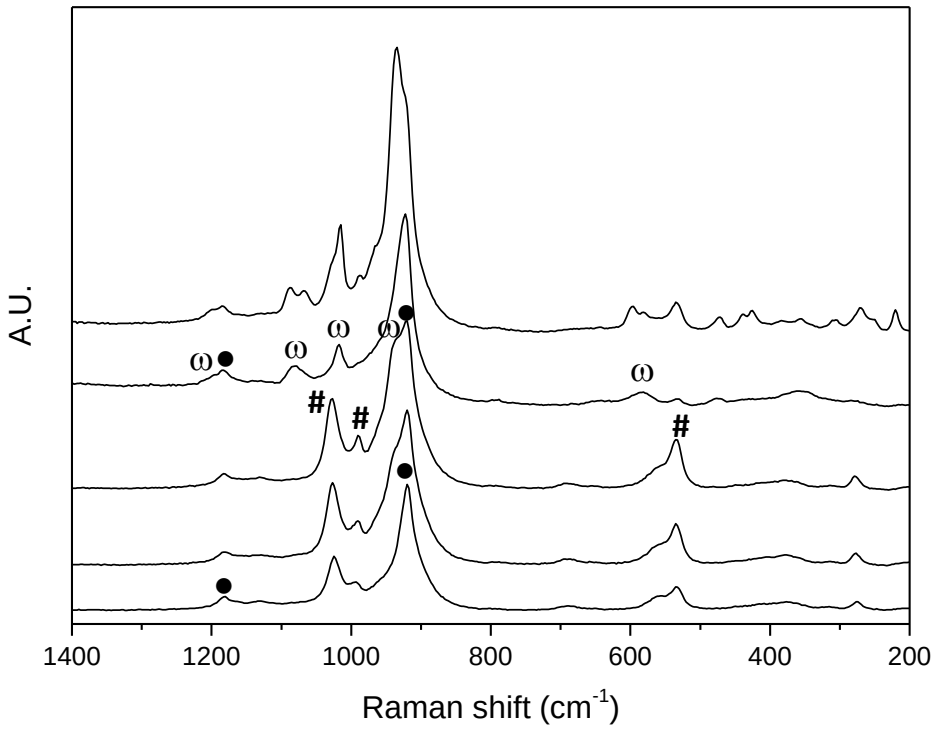

Figure 31. Raman spectra of L70 catalyst (70%mol of water, 30%mol of air).
Symbols: ω = ω-$VOPO_4$; # = $VOPO_4 \cdot 2H_2O$; ● = VPP.

The X-ray diffraction powder analysis (XRD) was carried out for all the catalysts: there were evident differences between them (Figure 32): L0 (green line - no water was used for calcination) presents a very low crystallinity; just adding 10% of water (L10 - pink line) during the calcination the crystallinity increases.

Both these two samples contain V^{5+} oxide as a main phase (18.6° and 21.4° the most important pattern), with low reflection attributable to VPP phase (23°). It is plausible that in these conditions, the combustion of organic compound remained from the synthesis causes a reduction in vanadium oxidation state, but due to the highly oxidant atmosphere (21%mol of oxygen and 18.9%mol respectively for L0 and L10), the final catalysts result over-oxidized (Mars-Van Krevelen mechanism). It is generally accepted that an higher oxidation state (in other word V^{5+} phases in the *bulk*) is detrimental for the catalytic performances, both in terms of activity and selectivity to the desired products (maleic anhydride)[17,30]. Although XRD analysis do not allow the identification of the different $VOPO_4$ phases, comparing it with the Raman spectra (Figure 25 and Figure 29), revealed additional information about the samples: the bulk structure is composed for both L0 and L10 of ω-$VOPO_4$ with traces of VPP.

Increasing the partial pressure of water (i.e. 40% and the remaining 60% air, orange line) an increase in VPP phase crystallinity and the concomitant decreasing of $VOPO_4$ (in the structural form of ω-$VOPO_4$, identified by Raman spectra in Figure 30) are observed considering the most important reflection at 2θ=23° and 21.4° respectively.

In the last condition represented by the blue line, obtained after thermal treatment with 70% of water and 30% of air the main crystalline phase is constituted of VPP (V^{4+}), the active one for the reaction, with only a small amount of V^{5+}, confirming the results of Raman spectra, meaning that the same composition is presents both in the bulk and in the active layer.

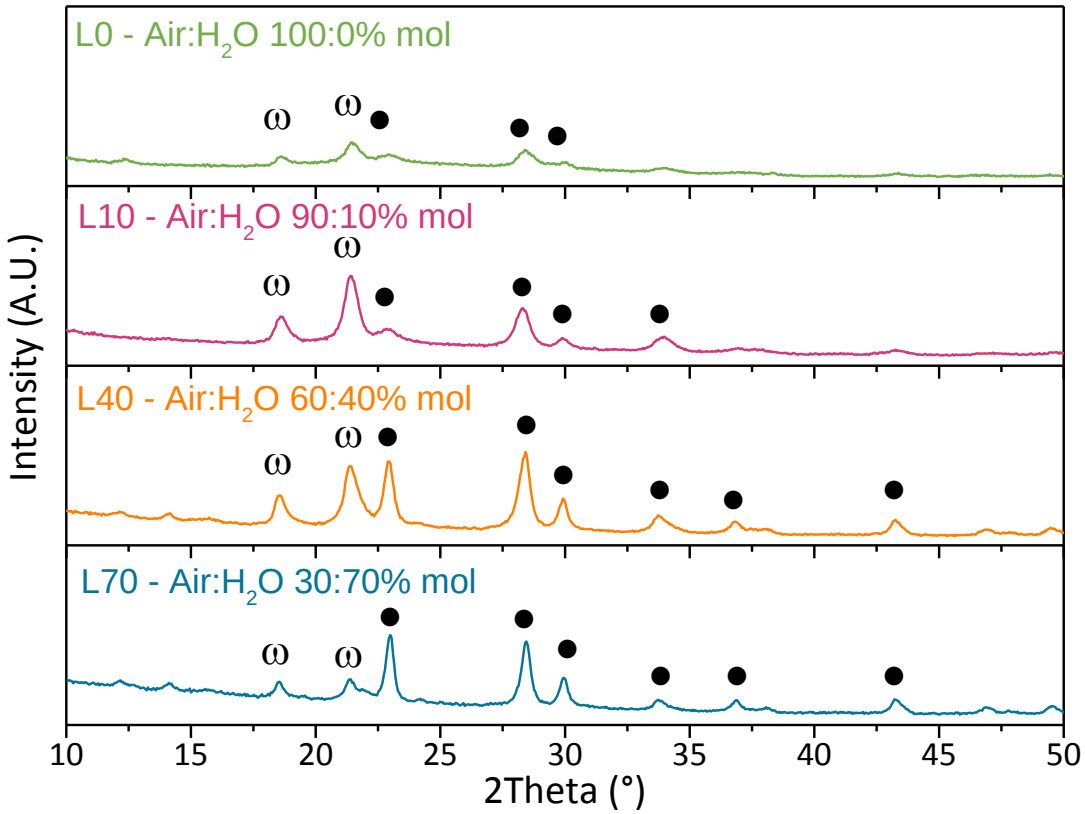

Figure 32. XRD diffractograms of catalyst after calcination without water (green), with 10%mol H_2O (pink), 40%mol H_2O (orange), 70%mol H_2O (blue). Symbols: ω = ω-$VOPO_4$; ● = VPP

These experiments revealed the double effect of water:

- Even in small amounts, it was necessary to promote the crystallinity of the final catalyst (observed by comparing the XRD of the first two samples, the green and the pink ones), a desired and necessary characteristic for the achievement of V/P/O catalytic system with good catalytic performance;

- It could be assumed that water leads to a better structural reorganization: monitoring the combustion products formed during the calcination performed in the tubular reactor (Figure 24 and Figure 26) in the case of L0 and L10, it was observed that adding water in the feeding mixture facilitate the combustions, because of the CO_2 formation was complete at lower times and temperatures; in this way the catalyst structure has more time to stabilize and reorganize after the loss of combustion products, resulting in a more crystalline phases.
- Increasing the partial pressure of water (or, on the other hand, decreasing the %mol of oxygen in the feeding mixture) promotes the formation of the desired crystalline phase vanadyl pyrophosphate (pink, orange and blue catalysts) despite to the oxidized ones ($VOPO_4$).

After the calcination, the catalysts were also characterized to evaluate the mean vanadium oxidation state and the specific surface area: the first one was evaluated by means of a titration with $KMnO_4$ and Mohr salt, the second parameter was obtained with the BET analysis.

The results are reported in Table 5:

Table 5. Surface area and Vanadium oxidation state for calcined samples.

Catalyst	SSA (m^2/g)	Vox
L0	9	4.52
L10	12	4.53
L40	11	4.41
L70	7	4.21

Regarding the surface area, no relationship between its value, the crystallinity and the amount of water was observed, they all present a very low value. The oxidation states of vanadium, instead, were consistent with the previous conclusions observed analysing the XRD and Raman spectra: increasing the water, causes a decreasing of the oxidizing power of the mixture used for the thermal treatments, causing a decreasing in the vanadium oxidation state; same results were observed looking at the clear inversion in the crystallinity of the two most intense peak at 21.4° and 23°, respectively attributed to V^{5+} phosphate phase and VPP (Figure 32).

4.3.2. Reactivity of V/P/O systems obtained after thermal treatment in presence of water

First, it has been carried out a blank experiment in order to study the reactivity of *n*-butane in gas phase as function of temperature, without any catalyst. The tests were performed both with the empty

reactor and with the empty space in the reactor filled in with an inert material (steatite). The range of temperature chosen was that typically used for *n*-butane oxidation to maleic anhydride, that is between 360 and 440°C. The feed composition was the same used for the catalytic tests: 1.7%mol *n*-butane, 17%mol oxygen and the remain inert.

When steatite was used as a filler material (green bar in Figure 33) the *n*-butane conversion was lower than 10% in the entire temperature range investigated; the only products detected were CO ad CO_2 due to the total combustion reaction. On the other hand, if the test was carried out in a completely empty reactor (blue circle in Figure 33) a significant conversion was observed: since at 360°C it was nearly 50%. The products distribution was not reported because it was formed COx and a few unknown products.

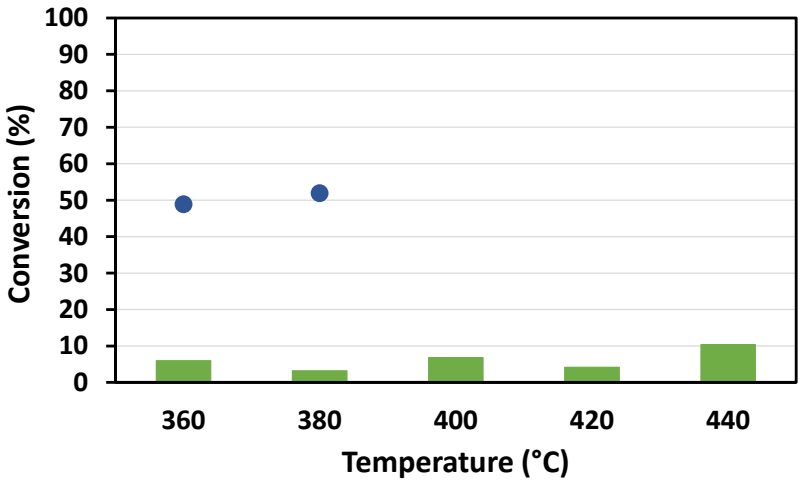

Figure 33. *n*-butane conversion as a function of temperature with empty reactor (blue circle) and with steatite filling the reactor (green bar).
Feed composition: 1.7%mol *n*-butane, 17%mol O_2, remain inert; W/F = 1.33 g·s·mL^{-1}.

Based on these results steatite was used as inert filler material for the further catalytic tests, in this way side reactions occurring in homogeneous phase has been limited.

The reactivity tests were carried out with calcined samples with the aim to evaluate the catalytic activity as a function of temperature for the selective oxidation of *n*-butane to maleic anhydride (MA). An equilibration step was previously performed by letting the catalyst at 400°C in the reactive mixture for a period of about 50h, until constant catalytic performance is achieved. After that, catalytic tests were carried out at the temperatures of 400, 420 and 440°C.

Because of its explosion hazards (lower flammability limit=1.8% and upper flammability limit=8.4%), *n*-butane has to be fed in limited inlet concentrations: 1,7%mol butane and 17%mol O_2 has been chosen as feed composition (the remain was inert). A mass of catalyst to volumetric gas

flow ratio (W/F) equal to 1.33 $g \cdot s \cdot mL^{-1}$ was used and the catalyst was in forms of pellets sized in 30-40 mesh.

In Figure 34-Figure 37 are reported the catalytic performance in terms of *n*-butane conversion (blue rhombus), selectivity in the desired product maleic anhydride (red square) and the sum of selectivity of CO and CO_2 (orange circle), for the catalyst L0, L10, L40 and L70, in function of temperature. The main by-products detected and quantify were acetic and acrylic acid, not reported because of its low amount (yield lower than 5%).

When the precursor was treated in anhydrous athmosphere (100%mol air, 21% O_2), the obtained catalyst L0 presents very poor performances (Figure 34): at 400°C the conversion was 12% with 20% of selectivity in MA. The selectivity in the combustion products were very high (nearly 65%) in the entire temperature range tested.

Increasing in tempereature causes an increase in conversion, reaching the value of 22% at 440°C: not only the kinetics of the reaction is favoured, enhancing the conversion of *n*-butane under the same contact time, but also the capacity of the catalyst to produce and desorb the desired product improves, in fact the selectivity in MA increases with temperature, up to 30% at 440°C.

The problem is that side reaction such as total combustion becomes the favorites: extrapolating the yield in COx, its value increses with temperature from 8% to 15%, making it the main product (MA yield increses with temperature but it still has very low values, equal to 2% at 400°C and 7% at 440°C).

The very low catalytic activity of this catalyst could be explained with the characterization: both in the *bulk* and on the catalytic surface the VPP was found only in traces, leading to the formation of an inactive catalyst. The very low selectivity, instead, could be caused by the α_I-$VOPO_4$ presents as a main phase in the fresh catalyst, toghether with the $VOPO_4$ dihydrate: in the reaction condition could dehydrate forming even more α_I, the latter being detrimental for the catalytic performance[42].

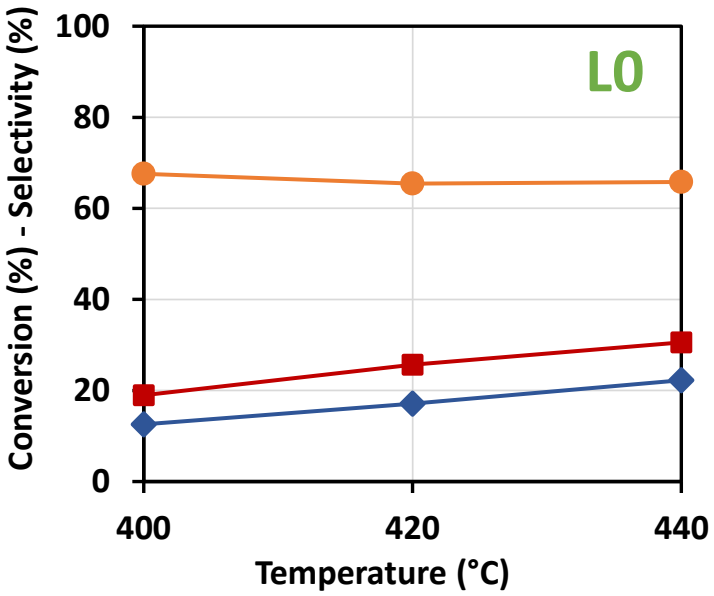

Figure 34. *n*-butane conversion (♦), MA (■) and COx (●) selectivities for L0 (100:0%mol Air:H_2O) in function of temperature.

Feed composition: 1.7%mol *n*-butane, 17%mol O_2, remain inert; W/F = 1.33 g·s·mL^{-1}.

In Figure 35 has been reported the catalytic behavior of L10. The trends and the value obtained are similar to L0: the activity increases with the temperature reaching the maximum value of 24% at 440°C.

Regarding the selectivity in MA, L10 shows higher performances: at 400°C was 35% and improves with temperature, achieving 41% at 440°C (10 points higher than for L0). Thus affects the selectivity in COx: the latter presents the constant value of 52%, regardless of temperature changes and it is lower than in L0.

This means that the increasing in conversion observed as a function of the temperature for the catalyst L10 is mainly due to the selective formation of MA.

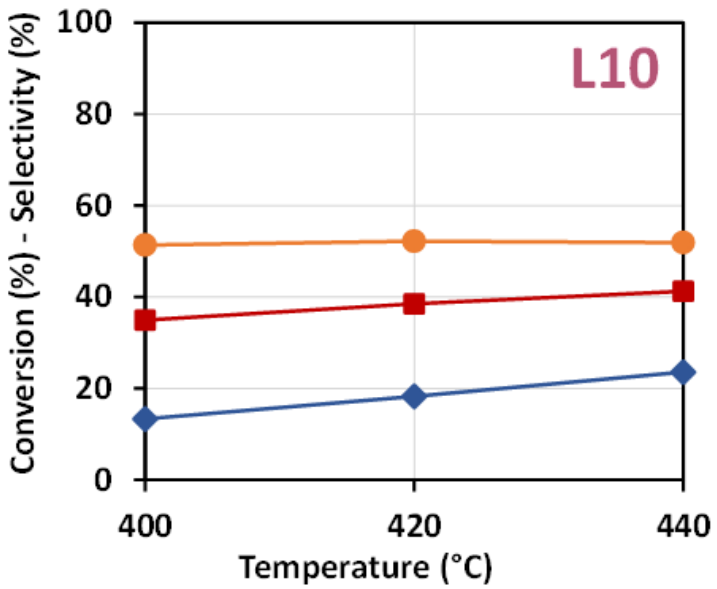

Figure 35. *n*-butane conversion (♦), MA (■) and COx (●) selectivities for L10 (90:10%mol Air:H_2O) in function of temperature.

Feed composition: 1.7%mol *n*-butane, 17%mol O_2, remain inert; W/F = 1.33 g·s·mL^{-1}.

Comparing the catalytic behaviour of L0 and L10, the latter does not present α_I-$VOPO_4$ in the characterization before reaction, but it was only composed of $VOPO_4 \cdot 2H_2O$ (main phase), VPP in traces and ω-$VOPO_4$ in slightly large quantities than L0; the latter causes the increse in selectivity in MA, because it is reported in literature that this ω- phase is in-situ transformed into the δ-$VOPO_4$ in the reaction conditions (400°C and 1.7% *n*-butane in air), which is considered the selective form of orthophosphate phases[38]. The low content of VPP, instead, confirm the very low conversion in the entire temperature range tested.

Increasing the partial pressure of water from 10 to 40%mol, causes an inversion in the selectivity trends: L40 presents higher selectivity in MA compared to COx (Figure 36). This is due to the ω-$VOPO_4$ that was found in each point analyzed by Raman spectroscopy; this phase is known to be transformed into the selective δ during the reaction, when *n*-butane and air were fed at temperature equal to 400°C[38,42].

The conversion increases with temperature from 14 to 28% (at 400 and 440°C respectively); at the same time the increasing in the kinetic of the reaction causes an increase in yield both for MA (from 8 to 16%) and for COx (from 5 to 13%).

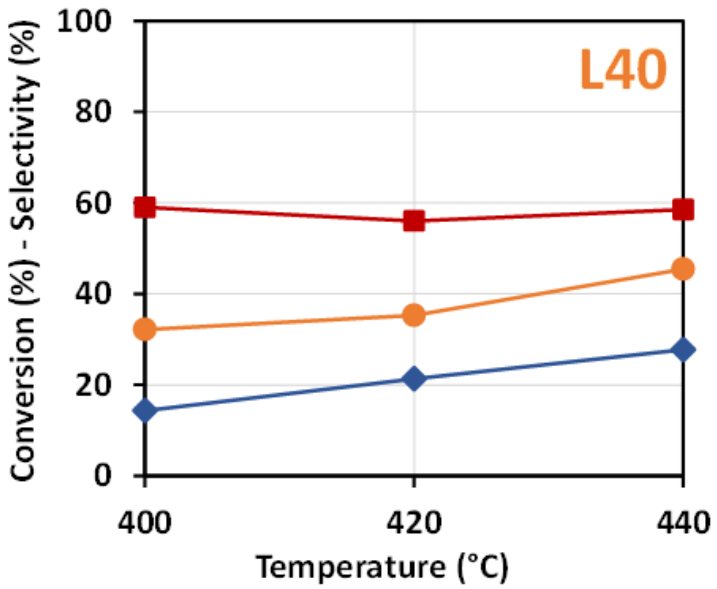

Figure 36. *n*-butane conversion (♦), MA (■) and COx (●) selectivities for L40 (60:40%mol Air:H_2O) in function of temperature.

Feed composition: 1.7%mol *n*-butane, 17%mol O_2, remain inert; W/F = 1.33 g·s·mL^{-1}.

Finally, to study the effect of changing the amount of water co-fed with air during the calcination, the catalytic activity of L70 was studied and the results are reported in Figure 37.

The catalytic performance as a funtion of reaction temperature for the sample L70 is much better than L0, L10 and L40, both in terms of activity and selectivity.

The increase in conversion in this case is much more marked than the previous catalysts, doubling its value in the temperature range detected, and reaching the 46% at 440°C: increasing the water amount, favours the formation of crystalline VPP, which is the active phase for the selective oxidation of *n*-butane to MA.

The selectivity in MA presents nearly a constant value (55%) in the entire temperature range investigated, probably because no phase transformation occurs during the experiment. Moreover, its value is the same with respect to the one obtained previously with L40: they presents the same phases (ω-$VOPO_4$ and VPP) in the fresh catalyst, but the higher $VOPO_4$ content in L40 causes its lower conversion.

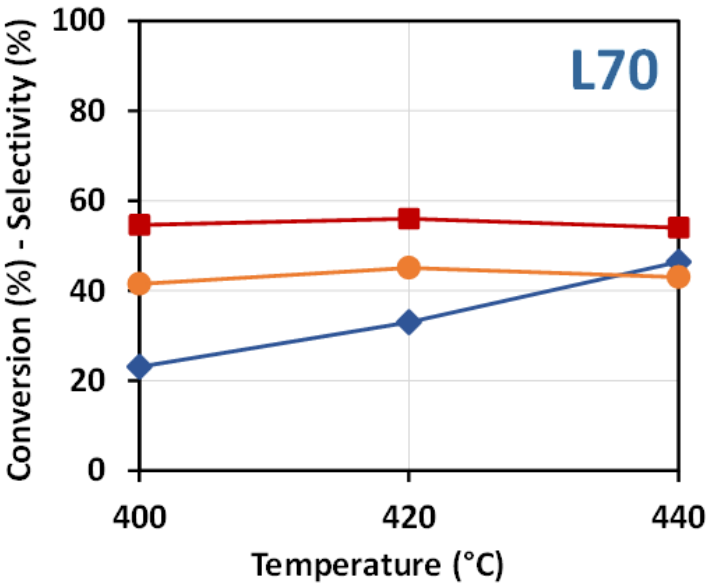

Figure 37. *n*-butane conversion (♦), MA (■) and COx (●) selectivities for L70 (30:70%mol Air:H_2O) in function of temperature.

Feed composition: 1.7%mol *n*-butane, 17%mol O_2, remain inert; W/F = 1.33 g·s·mL^{-1}.

4.3.3. Relationship between catalytic test and characterization

Figure 38 reports a summary of catalytic behaviour, plotting the conversion and the selectivity at 400°C for all the catalysts. Once again, it is possible to figure out the incremental effect on catalytic performances achieved by the increasing quantities of water (or, at the same time, the decreasing of the remaining oxygen molar ratio):

- L0, L10 and L40 presents nearly the same conversion of *n*-butane (slightly higher than 10% at 400°C) but it is interesting to note the trends of selectivity in MA and COx: increasing the amount of water from 0%mol to 40%mol, a corresponding increase in MA selectivity and the decreasing into COx was observed. These results are consistent with the vanadium oxidation state measured: these three catalysts presents nearly the same, and very high, value, equal to 4.5 (Table 5), and the over-oxidation of catalyst surface considerably affect the catalytic performances, enhancing the rate of the successive reaction to carbon oxides of the maleic anhydride formed, decreasing the yield in the desired product.[71]
- L70 presents higher activity with respect to the previous catalysts: the selectivity in MA was the same as for L40, but the higher conversion leads to obtain higher yield both in MA (13% for L70 compared to 8% for L40) and in COx (10% for L70 compared to 5% for L40).

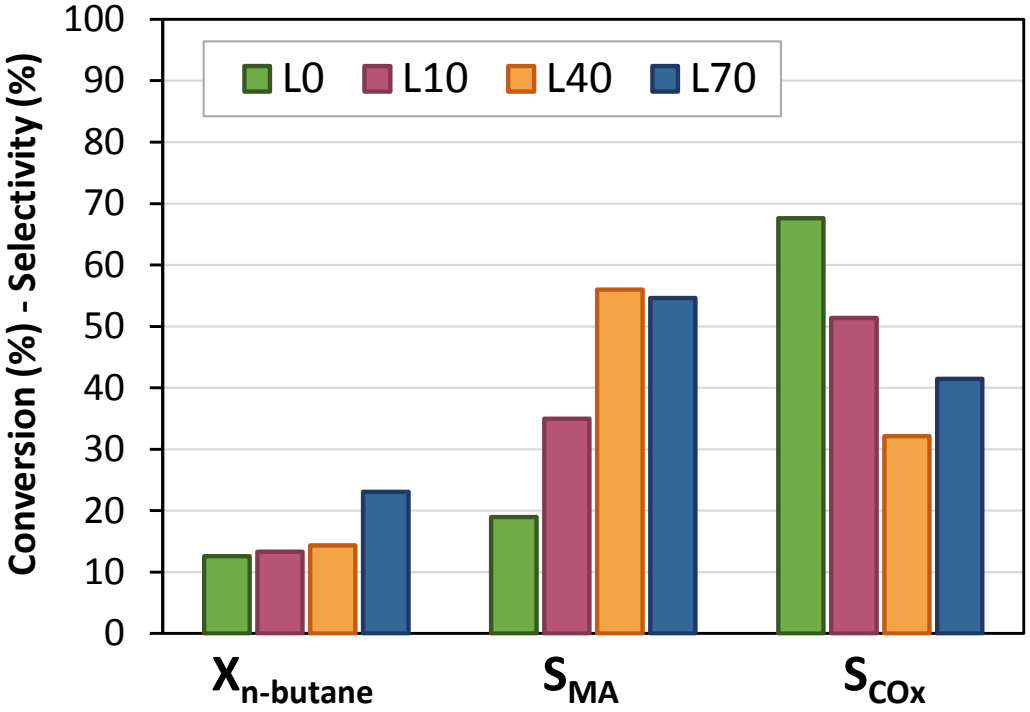

Figure 38. Catalytic performance of equilibrated L0 (green), L10 (pink), L40 (orange) and L70 (blue) at 400°C. Other by-products not reported: acetic acid, acrylic acid.
Feed composition: 1.7%mol *n*-butane, 17%mol O_2, remain inert; W/F = 1.33 g·s·mL^{-1}; T=400°C.

It is worth noting that the different behaviour was not simply due to the specific surface area (Table 5) because very similar values were obtained for L0, L10, L40 and L70 catalysts.

The characterization of used catalyst may be helpful to interpret the catalytic results, since the latter are consequence function of the surface and *bulk* composition effectively developed under reaction conditions.

The XRD patterns are reported in Figure 39 and presents the reflections of ω-$VOPO_4$ (ω) and VPP (●) as in the fresh catalysts; but a new line attributable to α_I-$VOPO_4$ (2θ=28.9°) is also presents.

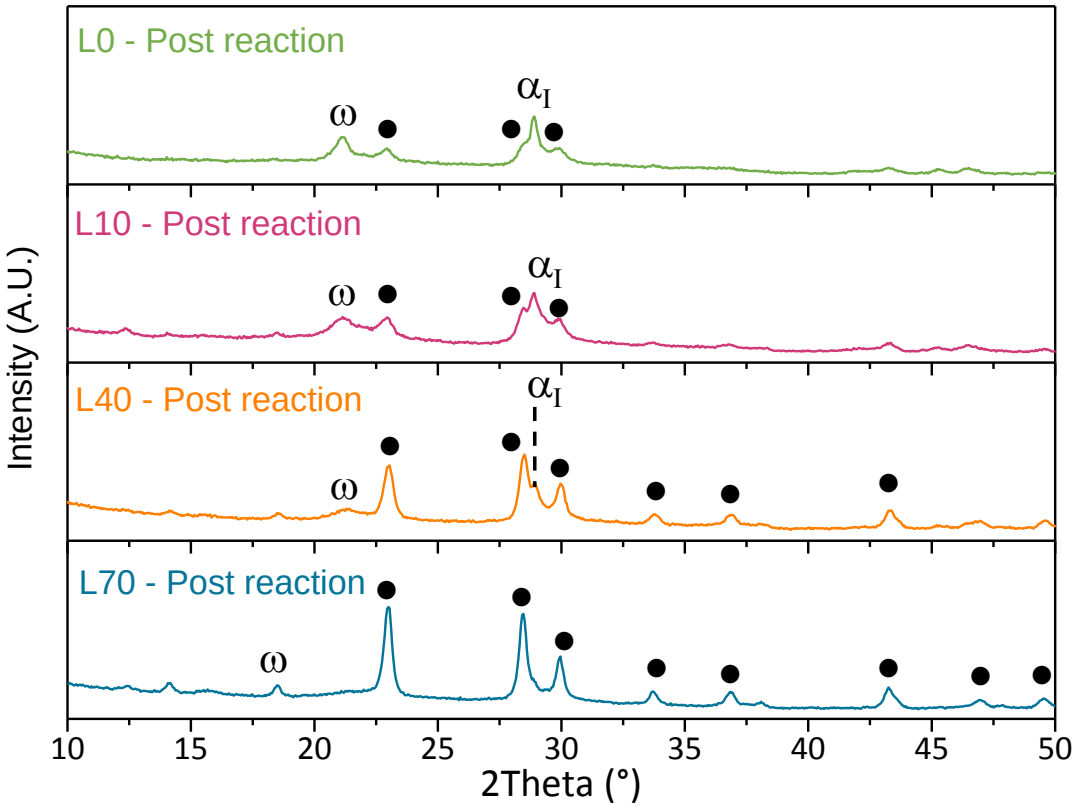

Figure 39. XRD analysis of used catalysts. L0 (green line) 100:0%mol Air:H_2O; L10 (pink) 90:10%mol Air:H_2O; L40 (orange) 60:40%mol Air:H_2O; L70 (blue) 30:70%mol Air:H_2O.
Symbols: ω = ω -$VOPO_4$; α_I = α_I-$VOPO_4$; ● = VPP.

A direct relationship between the partial pressure of water fed during the calcination of the precursor, the catalytic performances and the phases detected in the used catalysts has been found: increasing the amount of water (or decreasing the oxidant power of the gas mixture) enhanced the reactivity performances in terms of selectivity into MA and, at the same time, decreases the formation of α_I phase detected in the catalysts after reaction. L70, which was the best catalyst compared to the other, do not show any α_I pattern in the diffractogram; moreover, the latter presents VPP as a main phase both in the fresh and in the spent catalyst and this is related to the higher conversion detected during the experiment in the entire temperature range investigated.

Concluding, in the last condition used for the thermal treatments it is possible to obtain a "stable" catalyst, that does not undergo structural changes due to the temperature and/or feed composition.

The Raman characterization (Figure 40) are consistent with XRD diffractograms.

In the case of L0 and L10 samples only α_I-$VOPO_4$ was detected on the surface; increasing the amount of water and considering L40 VPP and δ-$VOPO_4$ composing the surface layer of the catalyst, together with α_I-$VOPO_4$ as in the previous two cases. L70 presents the same phases detected also in L40 (i.e.

δ-$VOPO_4$, α_I-$VOPO_4$ and VPP) but it is different the distribution of each compound: VPP was found in each spectrum recorded and there are more points where it was found δ with respect to α_I V(V) phosphate. The main peculiarity of VPP showing the best performance is the one able to generate in-situ "patches" of δ-$VOPO_4$ dispersed on VPP surface. Finally, no dihydrate phase was found in any catalysts (which was presents in the fresh samples): it is possible to assume that the latter phase undergoes a dehydration leading to the formation of the α_I-$VOPO_4$.

In accordance with the literature: (i) the formation of an active layer made up of α_I-$VOPO_4$ that develops on the catalysts surface during reaction gives the worst performance[42]; (ii) increasing water leads to a concomitant decreasing of this un-selective phase and increases the VPP at the same time, leading to the greater performances both in terms of activity and selectivity; (iii) finally, when relatively large amounts of $VOPO_4$, including the δ- phase, are present over the catalyst surface the catalytic behaviour is unsatisfactory.

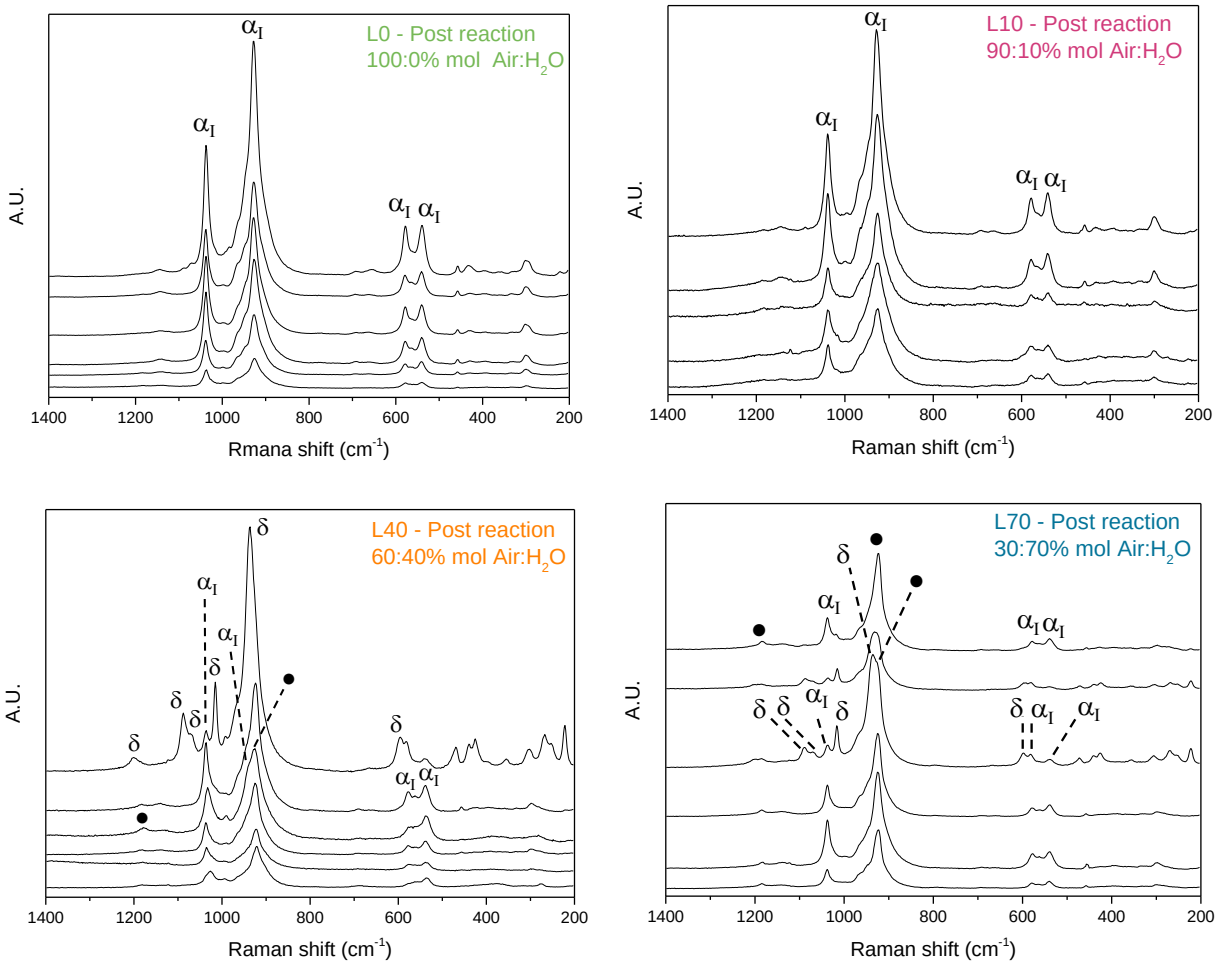

Figure 40. Raman spectra of used L0 (top left), L10 (top right), L40 (bottom left) and L70 (bottom right). Symbols: δ = δ -$VOPO_4$; α_I = α_I-$VOPO_4$; ● = VPP.

From the tests conducted so far the importance of the atmosphere used for the thermal treatment of vanadyl hydrogen phosphate (VHP) was demonstrate: increasing the oxidizing power of the mixture used for the calcinations, favours the formation of different V^{5+} species both in the fresh and used samples and also influence the VPP content, leading to very different catalytic results.

4.4. Thermal treatment: the role of oxygen

Since in the previous tests two parameters have been simultaneously varied, and looking at the results obtained in terms of phases formed after the calcination procedures, further experiments were carried out to observe and isolate the effect on structural changes only gives by the variation of oxygen molar ratio fed.

It has been decided to firstly evaluate the precursor transformation when it was subjected to different calcination conditions in which the oxidizing power of the mixture was changed diluting the air with nitrogen in different amount, with the aim to demonstrate if it was the different percentage of oxygen (instead of water) in the feeding gas that played a role in the formation of the active phase VPP, considering that both the VHP and the VPP are composed of V^{4+}.

The calcination atmosphere performed are reported in Table 6, note that the first step in air from room temperature (RT) to 180°C and the last from 425°C to 500°C in N_2 are common for all the thermal treatments; changes in oxygen content were employed only from 180°C to the end of the isothermal step at 425°C.

The samples have been renamed as a function of the atmosphere used for the calcination, in which 0, 40, 70 and 100 indicates the amount of diluting agent and N indicate that nitrogen was used as a diluting agent for air:

- L0: only air was used, without any diluting agent. Note that it is the same catalyst used in the previous paragraph when the influence of the water-added thermal treatment was investigated.
- L40-N: 40% of nitrogen was used to dilute the air, in this way the molar ratio of oxygen was decreased from 21%mol to 12.6%mol.
- L70-N: to obtain this catalyst it was used a mixture of air and nitrogen in the molar ratio equal to 30:70%mol (which correspond to 6.3%mol O_2).
- L100-N: only nitrogen was fed during all the thermal treatment.

Table 6. Calcination atmosphere used from 180°C to 425°C: the role of oxygen.

Sample name	Mix (%mol)		%mol O_2
	Air	N_2	
L0	100	0	21
L40-N	60	40	12.6
L70-N	30	70	6.3
L100-N	0	100	0

The experiments were carried out in a lab-scale tubular glass reactor equipped with an on-line micro GC used to control and quantify both the formation of water and CO_2 and the oxygen consumption. For the L0 sample the results are reported in Figure 41:

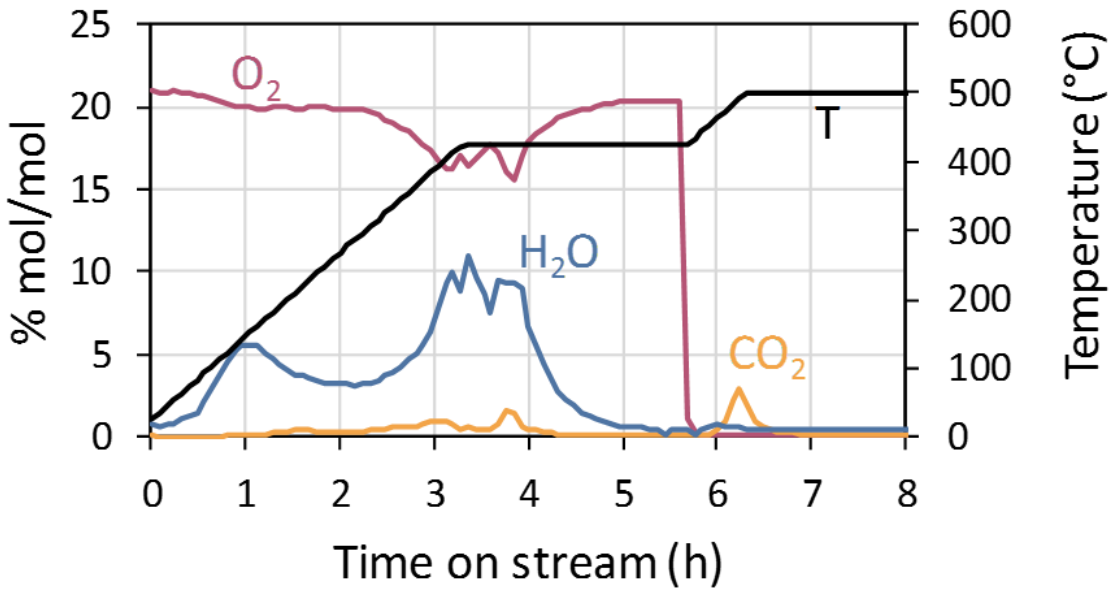

Figure 41. Consumption of oxygen (pink) and formation of water (blue) and CO_2 (orange) during the calcination of L0 sample.

Increasing time and temperature, there is consumption of oxygen used for the oxidation of the precursor to give the final catalyst; at the same time there is the formation of CO_2 and water, due to the oxidation of organic components in the precursor, trapped within the layers after the synthesis. At the temperature of 100-150°C the formation of water was observed, accordingly to the low temperature it has been assumed that this was water physisorbed on the surface.

The most important desorption of combustion products (water and CO_2) was observed after 3.5h of time on stream; at the same time was detected the consumption of oxygen: at this temperature the transformation of VHP to give the final catalyst takes place thanks to the lattice oxygen; the vacancies formed were replaced by the gaseous oxygen (Mars-Van Krevelen mechanism). As mentioned above the further formation of CO_2 when the carrier gas was changed to N_2 and the temperature reaches 500°C could be attributed to a further combustion, due to the high temperature, or it has been hypothesized that at this temperature a desorption of CO_2 previously formed and trapped inside the structure could takes place thanks to the high temperature.

In the literature several studies regarding the characterization of vanadium/phosphorous/oxide catalysts with Raman spectroscopy are reported; this technique provides greater sensitivity to the phase composition in metal oxide, such as V/P/O system, permitting to distinguish the various phases that can be assumed by the catalyst.

The ex-situ Raman analyses on different spots of L0 sample (Figure 42) reveal that it is mainly composed of oxidized vanadium phases (V^{5+}), in particular were identified α_I-$VOPO_4$ (1032, 928, 579, 541 cm^{-1}), ω-$VOPO_4$ (1188, 1084, 1016, 932, 650, 589 cm^{-1}), the dihydrate phase $VOPO_4 \cdot 2H_2O$ (1039, 988, 952, 542 cm^{-1}); also traces of VPP (1185, 1135, 920 cm^{-1}) were detected. The main superficial phases are the dihydrate (probably formed when the last combustion in nitrogen atmosphere takes place without co-production of water) and α_I which are convertible according to the environment and the reaction temperature[42].

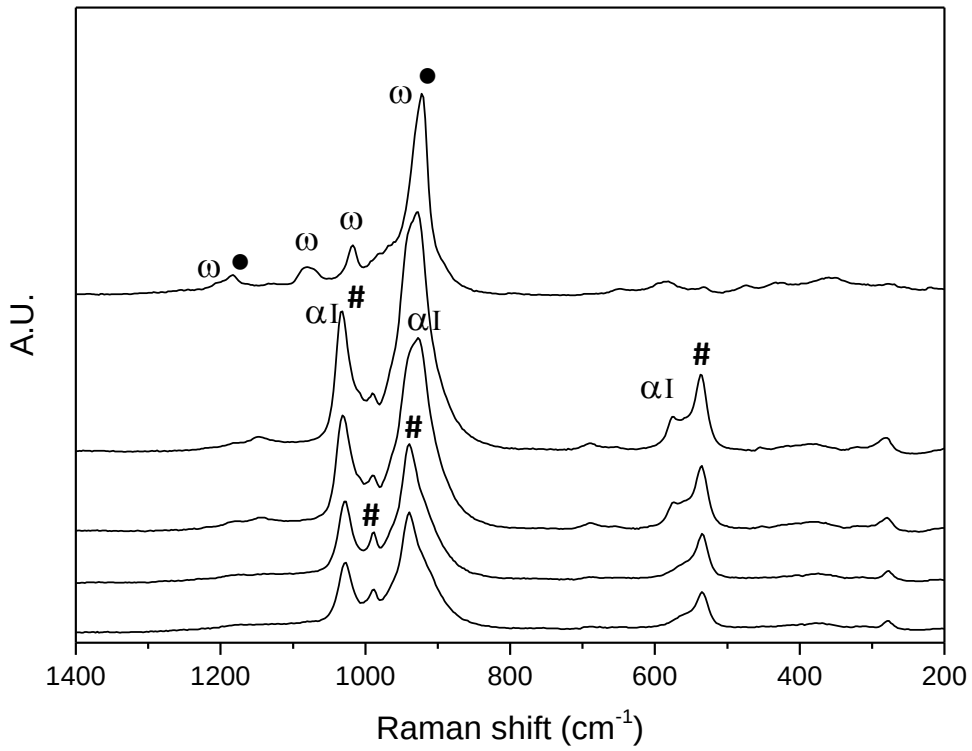

Figure 42. Raman spectra of L0 catalyst (obtained with 21% of oxygen).

Symbols: ω = ω-$VOPO_4$; α_I = α_I-$VOPO_4$; # = $VOPO_4 \cdot 2H_2O$; ● = VPP.

In the case of L40-N, the precursor was treated with a mixture of air and nitrogen in a molar ratio equal to 60:40%mol respectively. Decreasing the oxidizing power of the mixture a similar trend was observed when the outlet stream from the reactor was analysed with a micro gas chromatograph. Figure 43 shows the evolution of oxygen, water and CO_2 molar ratio as a function of time on stream and temperature. It was detected an initial desorption of water physisorbed; at the temperature of 180°C the feeding gas was changed from air to air:N_2 60:40%mol, in fact the molar ratio of oxygen decreases from 21% to 12.6%mol. After 2 hours an oxygen consumption was observed and at the same time water and carbon dioxide were both formed: in this range of temperature the precursor starts to transform, and the organic molecules are burned. Also in this experiment, a further development of CO_2 was observed, without co-production of water, when the carrier gas was switch to nitrogen (T=500°C).

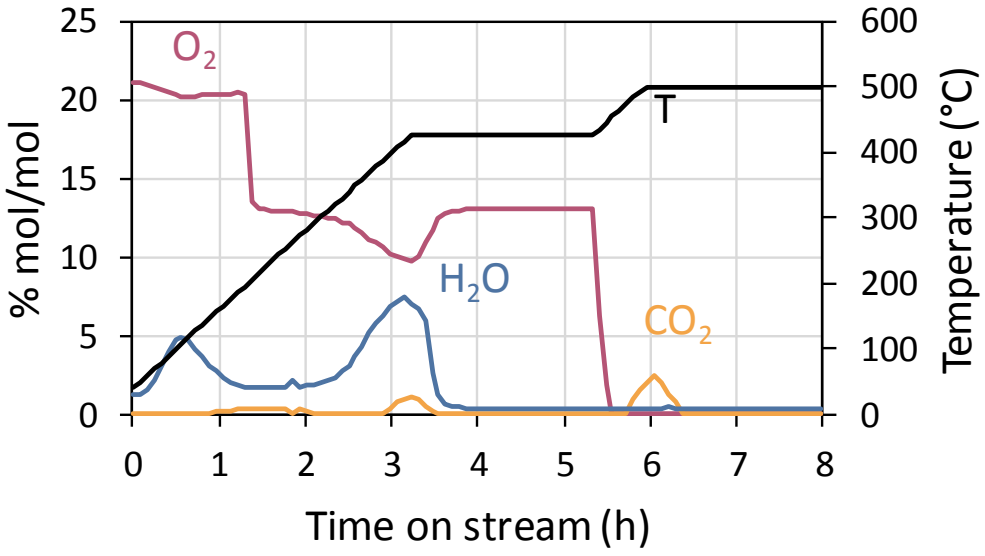

Figure 43. Consumption of oxygen (pink) and formation of water (blue) and CO_2 (orange) during the calcination with 60%mol air and the remain 40% of nitrogen (L40-N).

In the case of L40-N the Raman spectra (reported in Figure 44) reveal a quite inhomogeneous phase distribution on the surface: the first spectra shows the typical bands of α_I-$VOPO_4$ (α_I) together with VPP (full circle), the second spectra is related to another structural form of $VOPO_4$, namely the ω. In the last three spectra, although the very poor resolution, the main characteristic bands of VPP and $VOPO_4 \cdot 2H_2O$ (#) were distinguished, to confirm that probably the latter phase was formed as a consequence of water deriving from the combustion and trapped inside the structure.

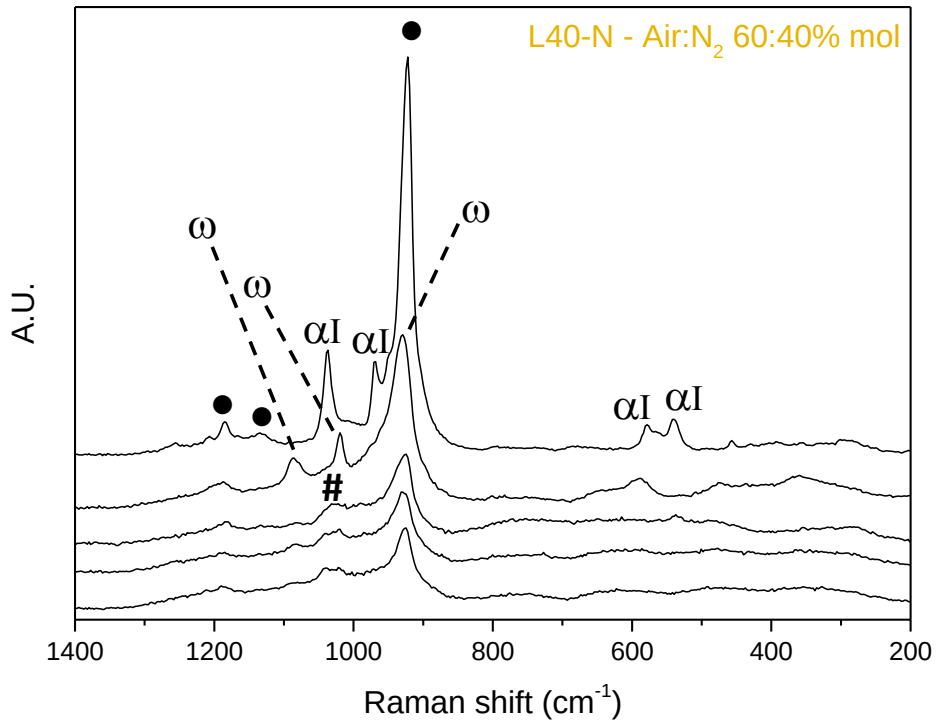

Figure 44. Raman spectra of L40-N catalyst (obtained with 12.6% of O_2 and 40% N_2).
Symbols: α_I = α_I-$VOPO_4$; ω = ω - $VOPO_4$; # = $VOPO_4 \cdot 2H_2O$; ● = VPP.

Figure 45 shows the evolution of O_2, H_2O and CO_2 during the thermal treatment of L70-N, in which only 30%mol of air was used (the remain 70% was nitrogen).

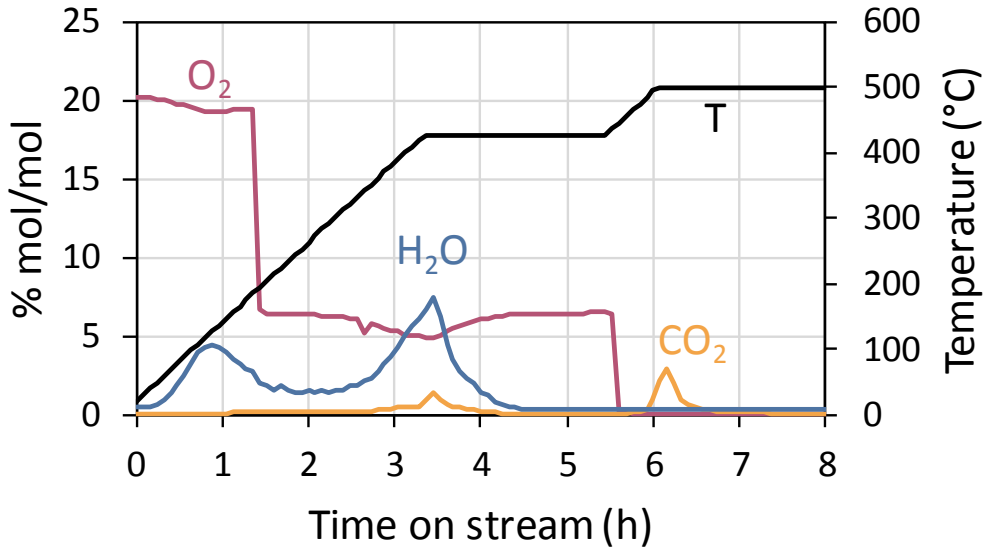

Figure 45. Consumption of oxygen (pink) and formation of water (blue) and CO_2 (orange) during the calcination with 30%mol air and 70% of nitrogen (L70-N).

Increasing time and temperature there is the release of water physisorbed; at the temperature of 180°C the air has been diluted with 70%mol of nitrogen, for this reason the oxygen molar ratio decreases until it reaches 6.3%mol. As in the previous two cases the combustion reaction and the transformation of the precursor to give the final catalyst takes place mainly at 425°C; at 500°C in nitrogen flow only CO_2 is observed, again without co-production of water.

In fact, the Raman spectra collected in several point of L70-N catalyst after calcination (Figure 46) reveal the presence of hydrated phase namely $VOPO_4 \cdot 2H_2O$ (#), a specific orthophosphate phase in which the vanadium is presents as V^{5+}. On the surface are also presents VPP (full circle) and δ-$VOPO_4$ as main phases: the first is the real active phase for the reaction, the latter is already known to enhance the selectivity to maleic anhydride.

Comparing the micro-GC molar ratio recorded for L70-N with the ones obtained for L70 (Figure 28) it immediately appears that the main difference is in the CO_2 formed: when water was used to dilute the air (L70) no CO_2 was desorbed at 500°C, demonstrating that the water facilitate the combustion of the organic species trapped between the layer of the precursor, and leading to a more orderly structure.

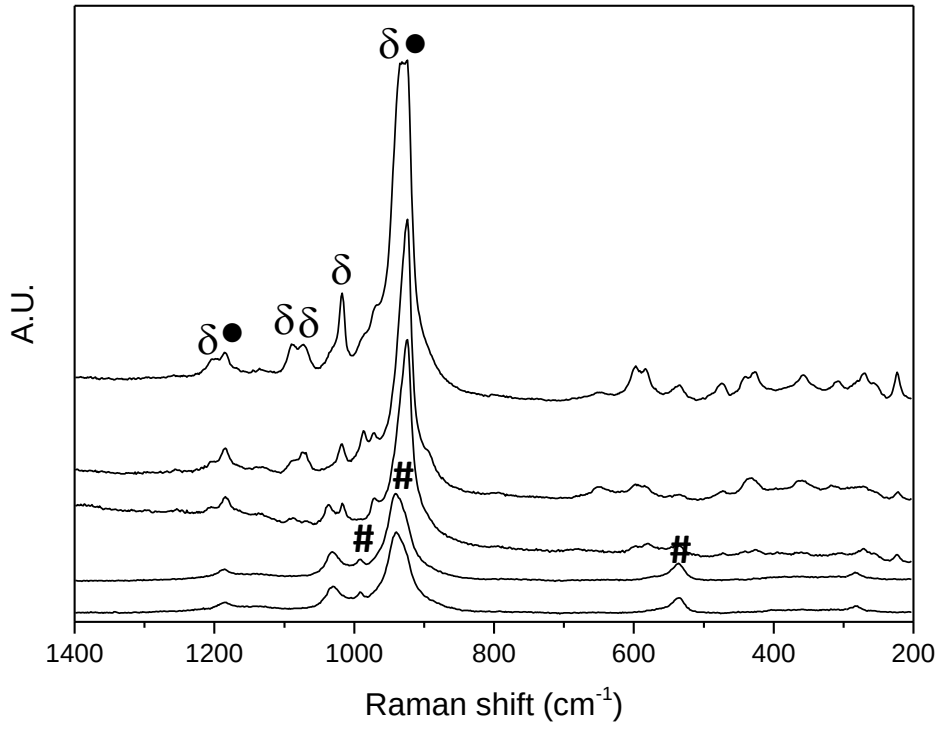

Figure 46. Raman spectra of L70-N catalyst (obtained with 6.3% of O_2 and 70% N_2).
Symbols: δ = δ-$VOPO_4$; # = $VOPO_4 \cdot 2H_2O$; ● = VPP.

Comparing the three experiments it is possible to conclude that decreasing the oxygen molar ratio fed during the thermal treatments promote the formation of vanadyl pyrophosphate (VPP) instead of vanadyl orthophosphate ($VOPO_4$), but this could be easily explained if you consider that both the precursor VHP and the VPP are made up of vanadium in 4+ oxidation state. For this reason, a further experiment was carried out in totally inert atmosphere, with the aim to understand if without air the transformation to produce the VPP takes place, totally avoiding the formation of oxidized $VOPO_4$ species, which would results in poor performance. The catalyst obtained has been renamed L100-N.
The micro-GC results and the Raman spectra are reported in Figure 47 and Figure 48 respectively.
The first part of the calcination leads to the release of water as in the previous case; when the oxygen was totally replaced and only nitrogen was fed (which correspond to 180°C) the temperature continues to increase but only a very small amount of combustion reactions take place: as shown in Figure 47-bottom the molar ratio of carbon dioxide was lower than 1% and also the co-production of water was lower than the previous cases.
It could be assumed that vanadium acts as oxidizing agent, leading to the formation of combustion products, but without oxygen replacement the process cannot be completed. The Raman spectra, in fact, show a not perfect homogeneity of the catalyst, due to the presence of carbonaceous species that cover the catalytic surface which constitute the main phases detected (represented by the bands at 1590 and 1376 cm^{-1})[73,74]. The bands at 1188, 1084, 1016, 932, 650, 589 cm^{-1} are related to the ω-$VOPO_4$ phase; traces of α_I-$VOPO_4$ (1032, 928, 579, 541 cm^{-1})[75] and VPP (1185, 1135, 920 cm^{-1}) were also identified.

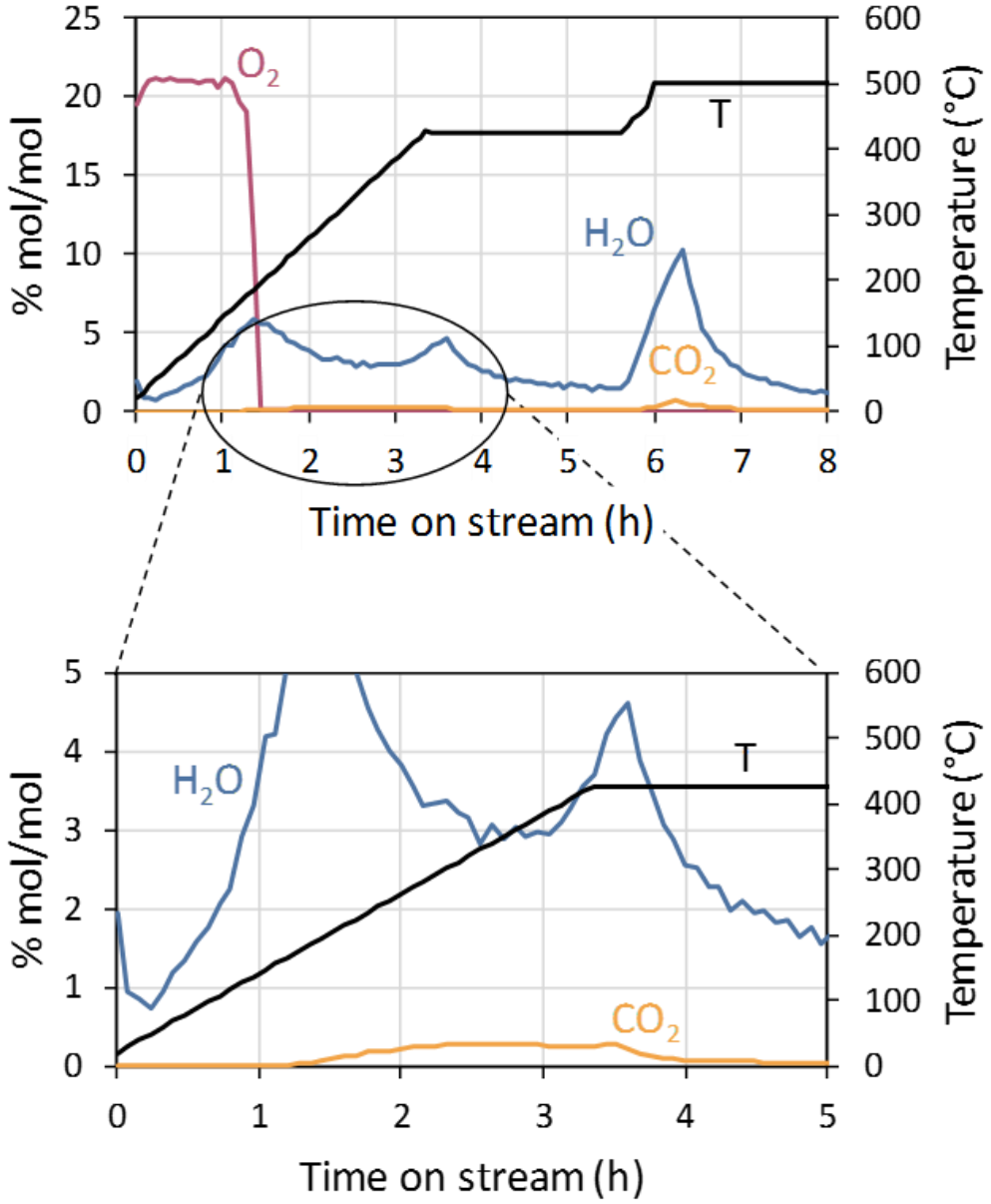

Figure 47. Consumption of oxygen (pink) and formation of water (blue) and CO_2 (orange) during the calcination with 100%mol of nitrogen (L100-N).

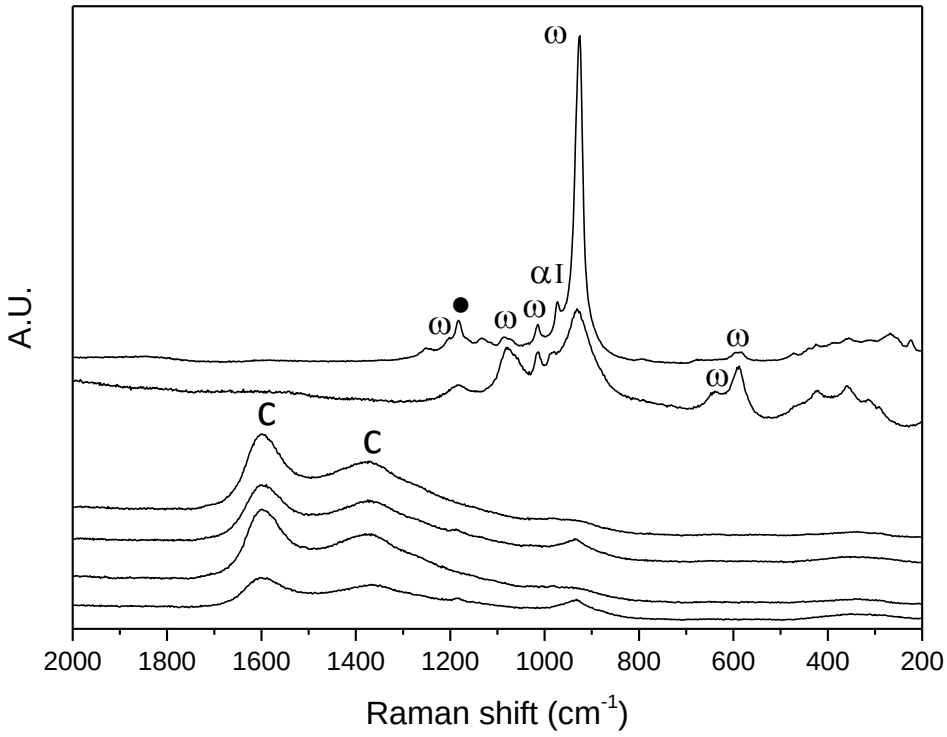

Figure 48. Raman spectra of L100-N catalyst (obtained with 100% N_2).

Symbols: ω = ω-$VOPO_4$; α_I = α_I-$VOPO_4$; ● = VPP ; c = Coke.

The X-ray powder diffraction analyses (Figure 49) revealed additional information about samples characterization. All the four samples are characterized by the presence of two crystalline phases and the characteristic reflections have been highlighted: the first one was the active phase VPP (full circle) and the other was $VOPO_4$ phase, namely the ω-$VOPO_4$ (ω), in which the vanadium is present in 5+ oxidation state.

The catalyst L0 (green line) calcined in highly oxidant condition (no nitrogen was fed to dilute the air stream) shows the pattern attributable to oxidized vanadium species, in agreement with the Raman spectra previously reported (Figure 42); this means that both the superficial phases and the bulk presents the same composition.

Decreasing from 100% to 60% the molar ratio of air fed (sample L40-N, yellow line) leads to the formation of VPP together with $VOPO_4$, even though it is not the main phase.

The diffractogram of L70-N (red line, obtained with only 30%mol of air) shows the presence of VPP as a main phase, with only traces of vanadyl orthophosphate phase.

Finally, the catalyst obtained feeding only nitrogen (L100-N, black line) presents a very low crystallinity (due to the carbonaceous species on the surface) but the pattern can be attributed to VPP phase.

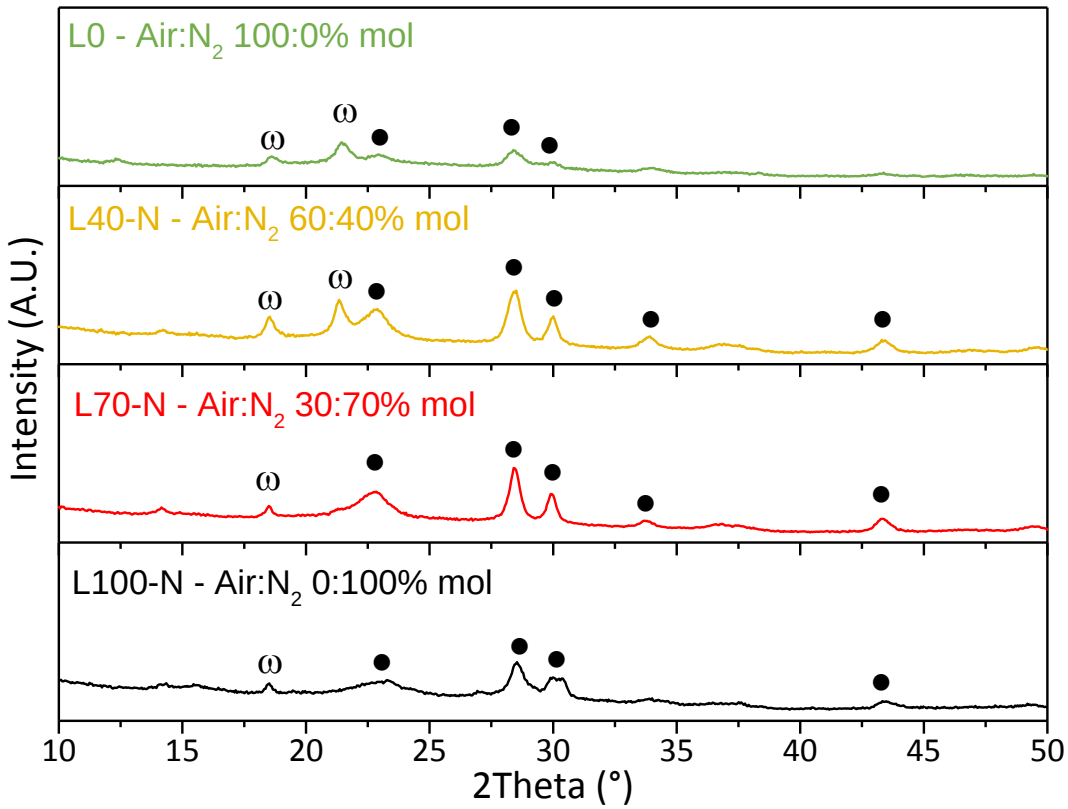

Figure 49. X-ray powder diffraction analysis of calcined L0 (100% air), L40-N (60:40%mol Air:N_2), L70-N (30:70%mol Air:N_2) and L100-N (100%mol N_2).

Symbols: ω = ω-$VOPO_4$; ● = VPP.

As previously mentioned with the Raman spectra, the calcination atmosphere greatly influences the final catalyst, and this is very clear comparing the diffractograms: decreasing the molar ratio of oxygen fed, it was observed the inversion in the trend which occurs between the relative intensities of VPP (2θ=23°) and $VOPO_4$ (2θ=21.4°). Same trends were also observed when the molar ratio of oxygen was decreased by the increasing of water content: L10, L40 and L70 shown a progressive reversal of the two main peaks considered just above (Figure 32).

To better understand the effect of diluting air with water or nitrogen, XRD analyses of L40, L40-N, L70 and L70-N after the calcination treatment are compared in Figure 50.

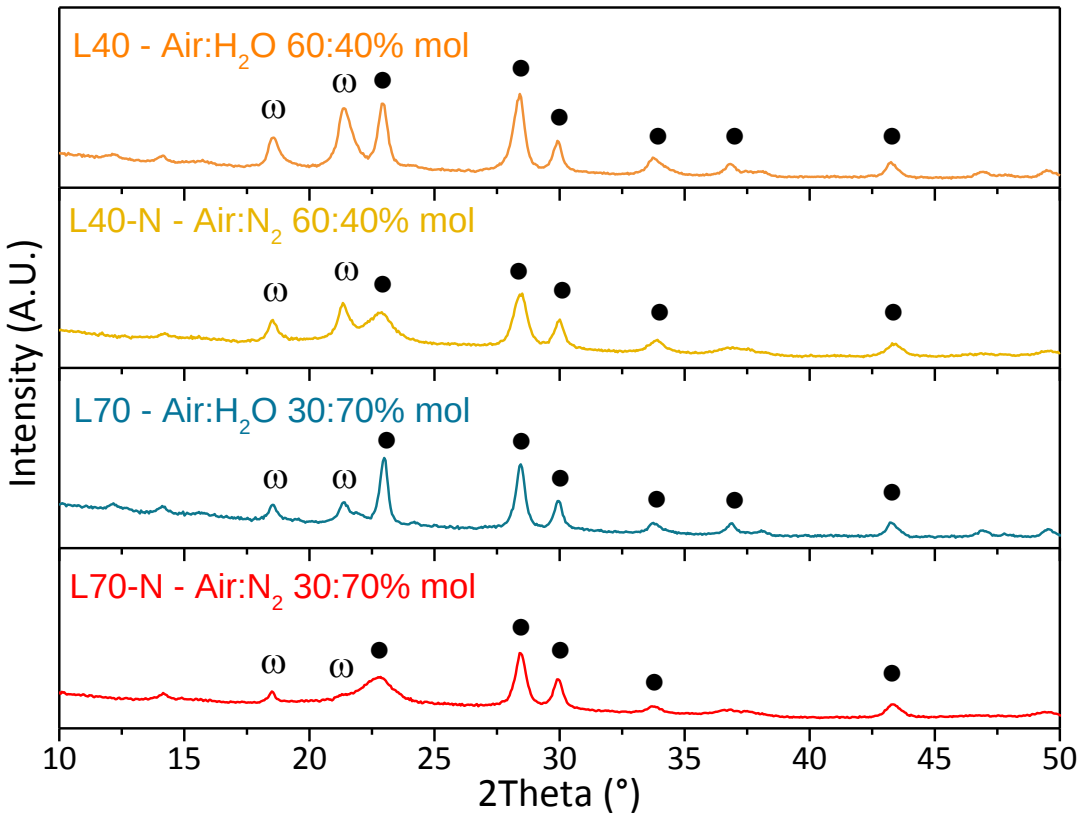

Figure 50. XRD analysis: comparison of diluting 60%mol and 30%mol of air with water or nitrogen. Symbols: ω = ω-$VOPO_4$; ● = VPP.

Comparing L40 and L40-N, which were obtained using 60%mol of air in both cases, but in the first the remaining 40% was water and in the second N_2, the diffractograms reveal no differences in the phase distributions and the relative intensity of the reflections.

The last two diffractograms, obtained from the catalysts calcined with only 30%mol of air (and diluted with 70%mol of water or nitrogen) decreasing in the intensity of the peak at 2θ=21.4° related to ω-$VOPO_4$ and, on the other hand, increasing in the VPP (2θ=23°) were observed if compared to L40 and 40-N; the important thing to note is that this phenomenon occurs in both cases, regardless of the diluting agent.

In the case of treatments performed adding water, greater intensity (crystallinity) of all signals were observed both for L40 and L70, with respect to the ones obtained in the same oxidizing conditions but using nitrogen instead of water.

It is now clear that the role of oxygen is in the formation of the phases that constitute the bulk of each catalyst, i.e. in the final vanadium oxidation state (Table 7): the higher the molar ratio of oxygen, the higher the formation of V(V) phosphate phases, regardless of the type of diluting agent used; however, even if in relatively low amount, it is necessary to allows the transformation of VHP into

VPP and to promote the combustion reaction in order to eliminate the organic residue. The importance of adding water is, instead, related only to the crystallinity.

Table 7. Vanadium oxidation state of L40, L40-N, L70 and L70-N after calcination.

Catalyst	Vox
L40	4.41
L40-N	4.47
L70	4.21
L70-N	4.25

4.5. Thermal treatment: the role of water

It has been already demonstrated that the oxygen affects the phases formed during the calcination, thus modification both in the vanadium oxidation state and catalytic performance occurs: the precursor transforms into VPP but the highly molar ratio of oxygen causes an over-oxidation of the material leading to the formation of $VOPO_4$ phases, not only on the surface of the catalyst but also in the bulk.

For completeness, a series of catalysts were synthetized by using the same molar ratio of air and diluting it with different amount of water in order to confirm its role in the thermal treatment, and separate its role to the effect given by the oxidizing power of the mixture (i.e. the molar ratio of oxygen). It has been previously hypothesized that water causes an increase in the crystallinity, because it favours the combustion of organic residue thus leading to a more efficient recrystallization of the material.

It was decided to study the effect of water when 30%mol of air was fed during the calcination treatments, because L70 was the catalyst with the best catalytic performance, in the reactivity tests conducted so far in this thesis, regarding the selective oxidation of *n*-butane to MA.

The aim is to find out the calcination method that is as reproducible as possible and it is able to combine the need for water to promote crystallinity and the right fraction of oxygen in order to obtain a catalyst with the optimal oxidation state for vanadium.

To demonstrate this, have been synthetized the samples renamed as L70-N (30:70%mol Air:N_2), L10:60 (30:10:60%mol Air:H_2O:N_2), L40:30 (30:40:30%mol Air:H_2O:N_2) and L70 (30:70%mol Air:H_2O), obtained with increased molar ratio of water (0%, 10%, 40% and 70%mol respectively), but the same 30%mol of air.

The heating ramp used are summed up in Figure 51.

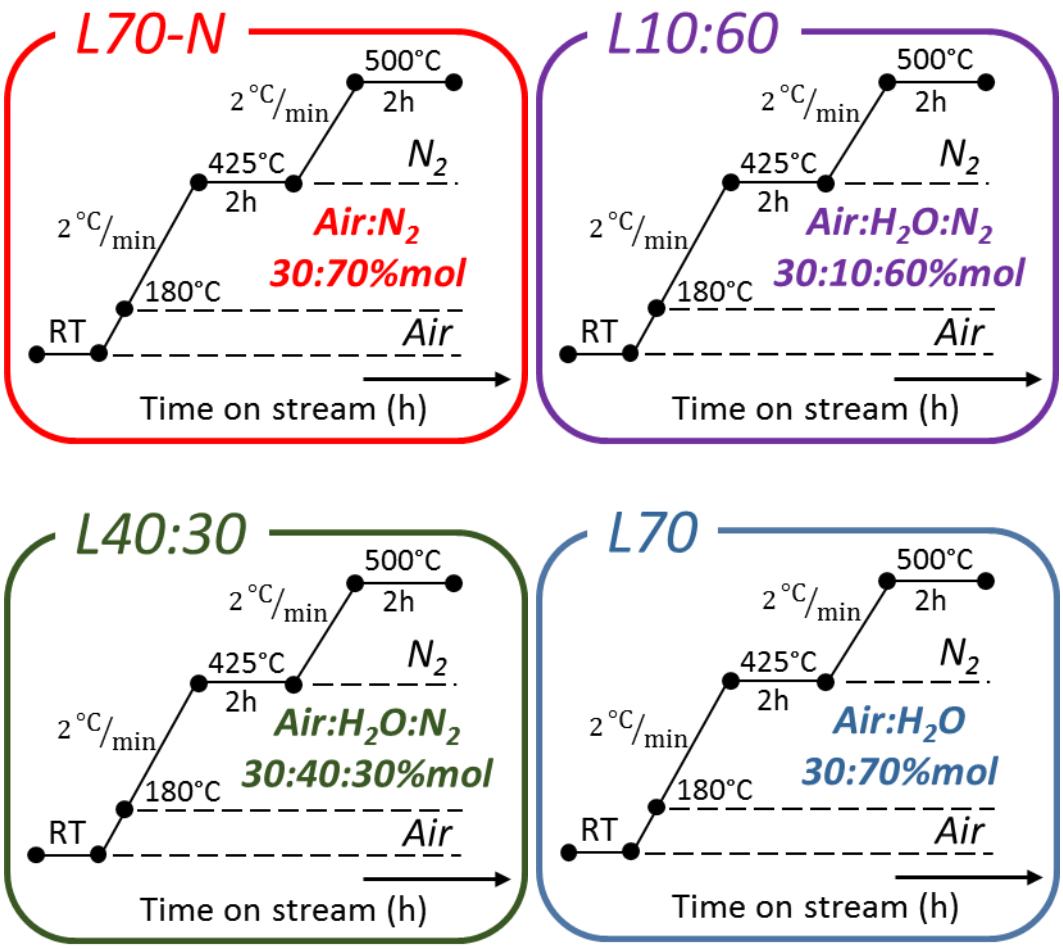

Figure 51. Heating ramp and atmosphere performed to study the effect of water in the transformation of VHP.

The oxygen consumption and the water and CO_2 formed due to the combustion of carbonaceous species and the transformation of hemihydrate precursor to give the final catalyst were monitored in the outlet stream with an on-line micro GC, for the entire thermal treatments (reported in Figure 52). It is important to note that, if water was fed in a mixture with air and/or nitrogen as a function of the experiment performed, in the outlet it has to be condensed and separated, in order to avoid column damages in the micro GC.

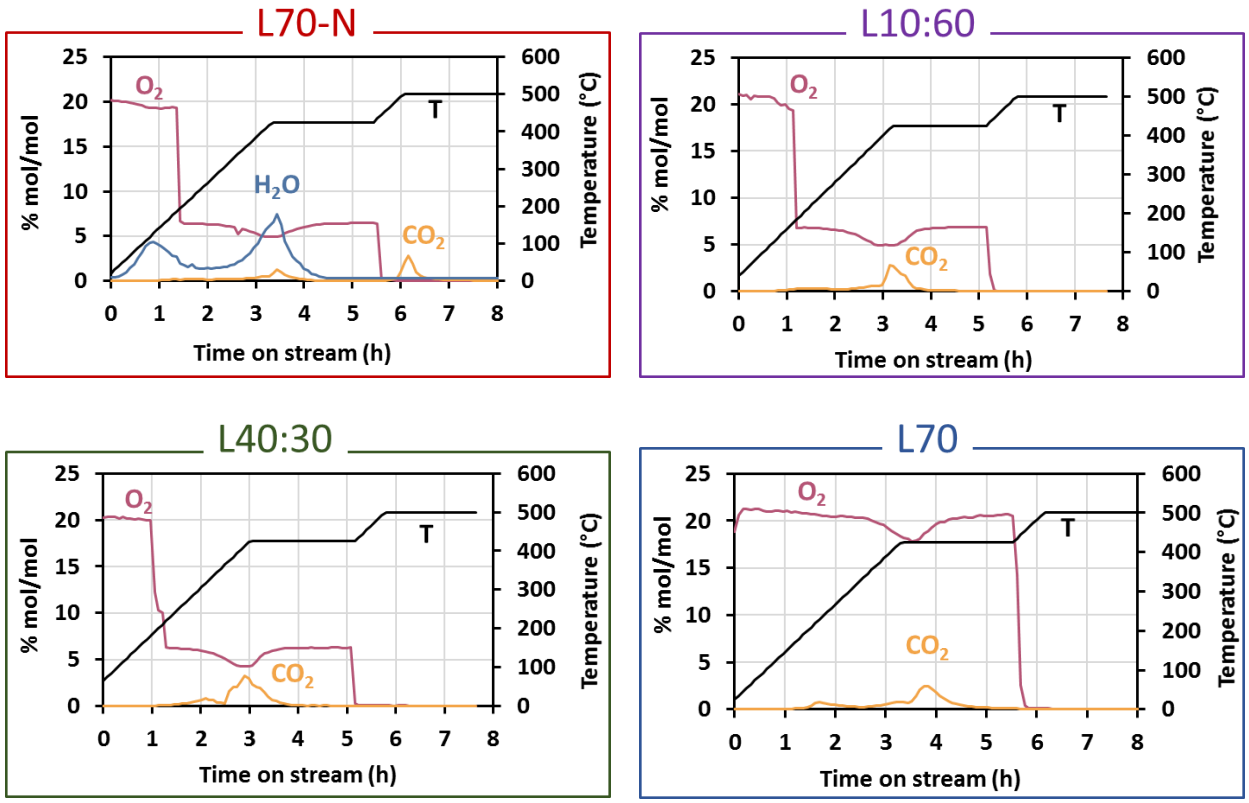

Figure 52. Consumption of oxygen (pink) and formation of water (blue) and CO_2 (orange) during the calcination of L70-N (top, left), L10:60 (top, right), L40:30 (bottom, left) and L70 (bottom, right).

In anhydrous conditions (L70-N, red), a gradually liberation of CO_2 has been observed during the entire calcination process: the combustion of organic residues takes place more hardly, and the process can only be completed by reaching high temperature (500°C). Same trend was previously observed when the VHP was treated only with air, leading to the obtainment of the catalyst L0 (Figure 24).

Adding water, even if in small percentage (10%mol, L10:60, purple), in a mixture with nitrogen, a more marked development between the three and four hours was detected (which correspond to 350-425°C), after that the combustion process is complete.

Similar trend has been observed also when higher amount of water was fed (L40:30 and L70): the role of water is to promote the desorption of combustion products and/or it favours reforming reaction of organic compounds trapped between the layer of catalyst due to the synthesis of the precursor in organic solvent, regardless the oxidizing power of the mixture used for the thermal treatments.

Figure 53 compares the XRD spectra of these four samples; surprisingly they are not very different in the phases that constitute them: the pattern is attributable VPP as a main phase (full circle), with traces of ω-$VOPO_4$. Thereby demonstrating that the phases formed are influenced only by the partial

pressure of oxygen (6.3%mol in these cases) used for the thermal treatment, whether it is diluted with nitrogen, water or a mixture of the two. A further demonstration is given by similar value for all the catalysts in the vanadium oxidation state measured by titration (Table 8).

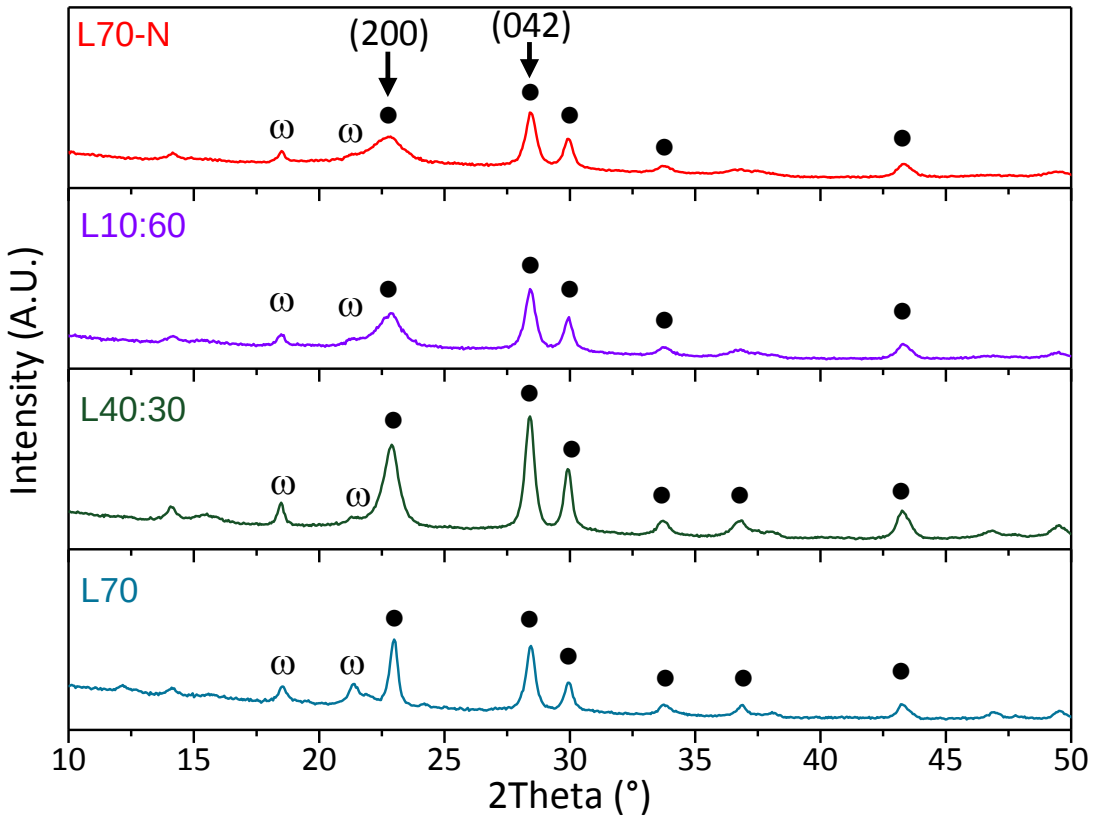

Figure 53. XRD pattern of L70-N (30:70%mol Air:N_2), L10:60 (30:10:60%mol Air:H_2O:N_2), L40:30 (30:40:30%mol Air:H_2O:N_2) and L70 (30:70%mol Air:H_2O). Symbols: ω = ω-$VOPO_4$; ● = VPP.

Table 8. Surface area and Vox value for calcined catalyst: L70-N, L10:60, L40:30 and L70.

Catalyst	Surface area (m^2/g)	Vox
L70-N	14	4.25
L10:60	11	4.19
L40:30	n.a.	n.a.
L70	7	4.21

Even if the phases detected were the same in all the four samples, changes in crystallinity were observed. In particular, increasing the amount of water fed during the calcination (passing from the top to the bottom in Figure 53):

1- A general increase in crystallinity for all the reflections is observed but, if the partial pressure of water is too high (in the case of L70), the crystallinity decreases again and changes in the intensity ratio (I_{042}/I_{200}) was observed, passing from ratio higher than 1 to value lower than 1 for L70. Every reflection is associated to a specific lattice plane and different intensity means a preferential growth of the material in a specific plane rather than other. In the field of catalytic materials, it is well known that this results in a different reactivity. From the literature, V/P/O catalysts with a well-ordered stacking of the (200) planes (lower intensity ratio) offer the best yield in MA[28].
2- The second important point is in the structural disorder that characterized the catalysts after calcination as a function of the atmosphere used: increasing water, a gradually decreasing in disorder along the (200) plane was observed, as shown by the width of (200) reflection if compared with that of (042): this parameter, usually called aspect ratio (defined as $FWHM_{042}/FWHM_{200}$), is a measure providing information on the preferential exposure of the (100) crystallographic plane of VPP (which possess the higher density of active sites)[43,45]. Disorder along (200) cleavage planes of VPP increased the number of active sites responsible for the *n*-butane activation even if, Cavani et al. demonstrate that the selective oxidation of *n*-butane to MA is a "structure sensitive reaction", this means that the broadening of the line (200) is responsible for the higher activity but did not influence the nature of the active centres, thus not changing the selectivity of the reaction[34,71,76].

Horowitz and co-workers[22] demonstrate that trapped alcohol molecules between the layers of the precursor affect the nature of the vanadyl pyrophosphate that results from calcination: they observed that calcinating the precursor in air the X-ray pattern presents all the reflections with equal sharpness; on the other hand, when argon was used as a carrier gas, instead of air, the resulting VPP exhibits a disproportionately broadened (200) reflection. They claimed that this difference is due to an impediment to phase transformation caused by alcohol trapped within the layers when inert conditions were used for the thermal treatment.

Same trends were observed with our catalysts as a function of partial pressure of water used for the thermal treatments, demonstrating that water promotes reforming to more easily oxidizable molecules or it encourages the desorption, leading to a more efficient recrystallization of the structure, causing an increase in VPP crystallinity: comparing the GC analysis for L70-N and L70 reported in Figure 52 it was observed that without water the combustion reaction takes place also at high temperature (500°C, in N_2 atmosphere).

The "easier combustion" caused by the addition of water during the thermal treatment leads to obtain a more crystalline catalyst, decreasing the disorder along (200) planes.

Raman spectroscopy, moreover, permits the characterization of all the species on the catalyst surface. In Figure 54 are reported the spectra collected by focussing the beam over other spots, for the four samples renamed L70-N (top-left, red), L10:60 (top-right, purple), L40:30 (bottom-left, dark green) and L70 (bottom-right, blue).

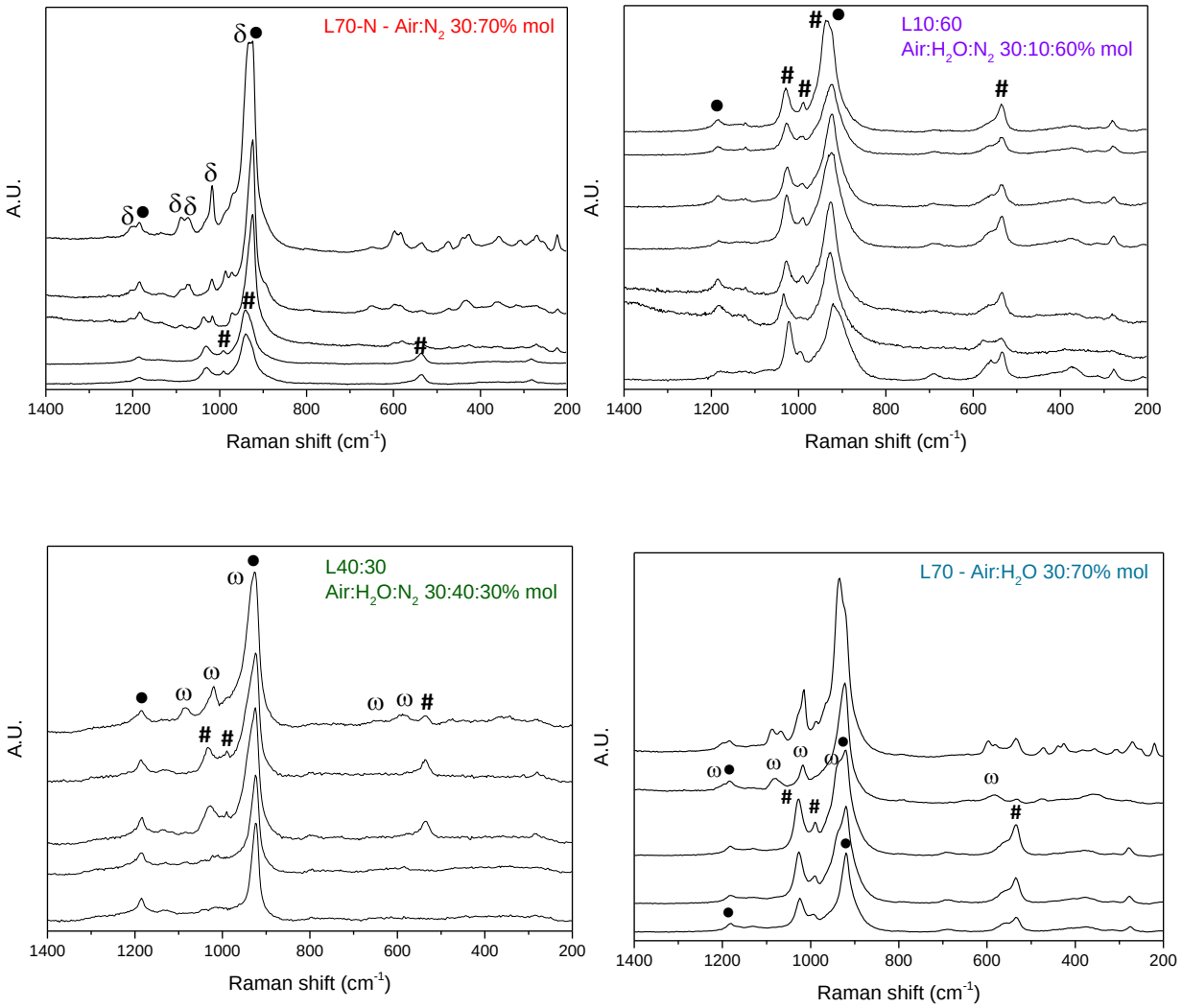

Figure 54. Raman spectra of L70-N (top, left), L10:60 (top, right), L40:30 (bottom, left) and L70 (bottom, right) catalysts.

Symbols: ω = ω-$VOPO_4$; δ = δ -$VOPO_4$; # = $VOPO_4 \cdot 2H_2O$; ● = VPP.

L70-N, calcined with a mixture of air and nitrogen in the molar ratio equal to 30:70%, presents on its surface mainly δ-$VOPO_4$ (1200, 1090, 1075, 1016, 936, 590 cm^{-1}) that could enhance the selectivity of the catalyst, and it was not detected from XRD analysis. The second main phase, detected in all

the five spots is VPP (1185 and 927 cm^{-1}), the active phase for the reaction. Also traces of $VOPO_4 \cdot 2H_2O$ (1039, 988 and 542 cm^{-1}) were detected.

The surface of the catalyst L10:60 is quite homogeneous: all the spectra recorded are very similar and composed of $VOPO_4 \cdot 2H_2O$ (1039, 988 and 542 cm^{-1}). This hydrated phase is known to be transformed into the selective δ-$VOPO_4$ in the reaction temperature range and together with the *bulk* constituted of vanadyl pyrophosphate (Figure 53) could let to a very performing catalyst[42].

Also the active layer of L40:30 is characterized by the same phases: ω-$VOPO_4$ detected in the first spot analysed and $VOPO_4 \cdot 2H_2O$ in the other two. Moreover, the bands associated to VPP has been detected in all the spectra.

The Raman spectra of L70 were previously descripted, the important thing to note is that it is constituted mainly of VPP, ω-$VOPO_4$ and dihydrate phase.

Focusing on the main signal at about 920-930 cm^{-1}, a shift in the peak maximum was observed: in the case of L70 it was positioned at 919 cm^{-1}, for L70-N and L10:60 (which are characterized by the broadening of the line at 2θ=23° in the XRD) it is centred at 927 cm^{-1}. In the case of L40:30 the reflection in the X-ray diffractogram at 2θ=23° presents an intermediate width: it is more sharp compared to L70-N and L10:60, but less wide if compared to the blue sample (L70), obtained with the higher molar ratio of water; the same trend was observed also in the peak maximum: in this case it was centred at 924 cm^{-1}. Differences were observed, in addition to the ones observed analysing the diffractograms, also comparing the Raman spectra, demonstrating that effectively two different VPP composed our catalysts and they are caused by different symmetry relationship between V and P, which are not identical in two structure. The possibility of the existence of two polytypes for vanadyl pyrophosphate was taken into consideration by a number of authors[22,31,33–35,77–80]: they reported that the morphology of calcined VPP was affected by preparation and calcination conditions and these variation were due to differences in orientation of adjacent dimeric vanadium polyhedral.

It is not already clear in which conditions the formation of one structure is encouraged rather than the other or which one is more stable, but it has been demonstrated that water has a great influence not only in the crystallinity but also in the morphology of the final catalyst, because, as mentioned above, the shift in the Raman spectra of VPP is associated to different structure, which probably exhibits different catalytic performance.

In conclusion, thermal treatments performed using the same %mol of air (30%mol) and with the remaining part nitrogen or water leads to the obtainment of catalysts with different morphology and for this reason a different reactivity for L70-N with respect to L70 was expected.

The reactivity tests were carried out in a gas-phase reactor, for the mild oxidation of *n*-butane; the catalysts were previously equilibrated by letting at 400°C in the reactive mixture for a period of about 50 hours. The reaction conditions were the following: 1.7%mol *n*-butane, 17%mol of O_2 and W/F=1.33 g·s·mL^{-1}.

For samples L70-N, L10:60 and L70 the *n*-butane conversions are plotted in Figure 55, while Figure 56 reports the MA and CO+CO_2 (COx) selectivities, respectively to the left and right, all plotted in function of the reaction temperature (400-440°C).

For completeness, other products detected in traces (in yield less than 5%) and not reported were acetic acid and acrylic acid.

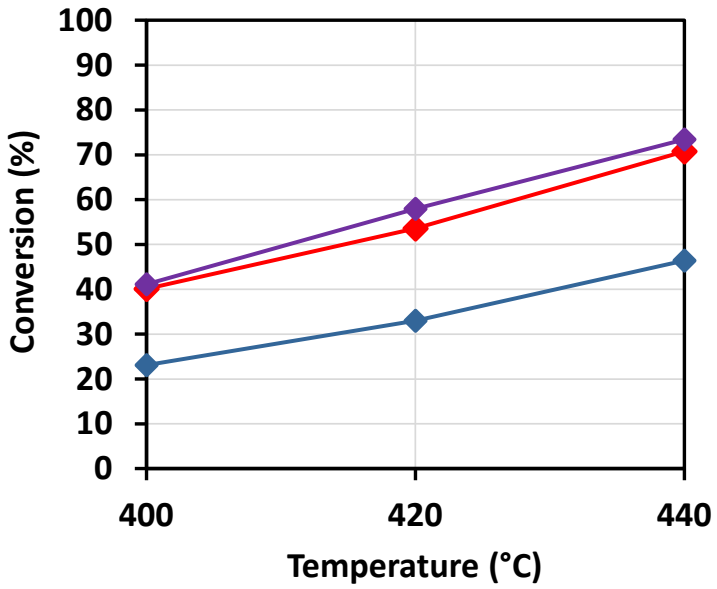

Figure 55. Conversion of *n*-butane for L70-N (♦), L10:60 (♦) and L70 (♦) samples. Feed composition: 1.7%mol *n*-butane, 17%mol O_2, remain inert; W/F = 1.33 g·s·mL^{-1}.

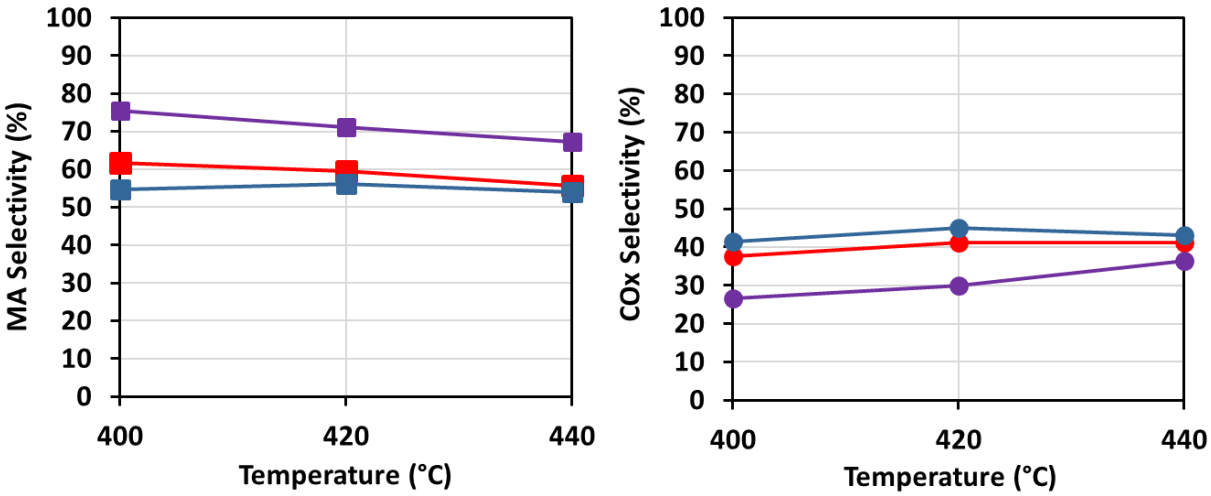

Figure 56. Maleic anhydride (left) and COx (right) selectivity for L70-N (■ and ●), L10:60 (■ and ●) and L70 (■ and ●) samples. Feed composition: 1.7%mol *n*-butane, 17%mol O_2, remain inert; W/F = 1.33 g·s·mL^{-1}.

For all catalysts the *n*-butane conversion increased with temperature, as expected, and the values are in agreement with the disorder along (200) plane: L70-N and L10:60 shows higher disorder, which correspond to a preferential exposure of the (100) crystallographic plane, in fact higher conversion in the entire temperature range investigated were reached. For the same reason L70 presents the lowest value (approximately 20 percentage points lower): this is probably due to the combination of the sharpness reflection at 23° and the lower specific surface area with respect to the other two (Table 8). Regarding the selectivity: L70 (blue) is the catalyst with the lower selectivity to MA, with a nearly constant value during the entire experiment (about 55%), contrary to what it would be expected considering the lower aspect ratio, with respect to the other two catalysts. The Raman characterization performed after the reaction (Figure 57) reveal the presence of V^{5+} in each point analysed, together with VPP. In particular, the presence of α_I-$VOPO_4$ is a further cause of low selectivity values.

When anhydrous conditions were used for the calcination (the case of L70-N) higher selectivity to maleic anhydride was reached and the Raman spectra do not show the formation of α_I-$VOPO_4$. Considering the experimental data reported in the work of Busca and co-workers[71], the texture of the catalyst influences its redox properties, in particular disorder along (200) plane reduces the rate of oxidation of V^{4+} to V^{5+}; same results are deduced from our post-reaction characterization: L70-N that was the one with the higher disorder, shows only Raman bands attributable to VPP (Figure 57), whereas L70, which showed the most sharp reflection in the fresh diffractograms, is the samples with the higher presence of oxidized vanadium phases ($VOPO_4$). The stabilization of vanadium^{4+} with

respect to its oxidized phase is an important factor for the catalytic performances, leading to an increasing in selectivity to MA instead of total combustion products.

Nevertheless L10:60 is the catalyst with not only the best conversion of *n*-butane but also the best selectivity if compared with the catalysts tested so far. Probably the key point in the calcination treatment of hemihydrate precursor to obtain the best performance is in the air and water mol% in the overall mixture fed.

If different structures of VPP really exist, which differ in the relative orientation of the vanadyl groups, as mentioned above about the so-called polytypes, disorder as revealed in the relative intensities (intensity ratio, I_{042}/I_{200}) or width (aspect ratio, $FWHM_{042}/FWHM_{200}$) of XRD reflections can be originated from co-crystallization of more than one structure; in our catalysts L10:60 may be made up of both the VPP polytypes, because presents an intermediate intensity and width between L70-N and L70. The high conversion is due to the disordered reflection in the peak at 2θ=23°, as for L70-N, and the lower FWHM leads to an increases in the MA yield value[28].

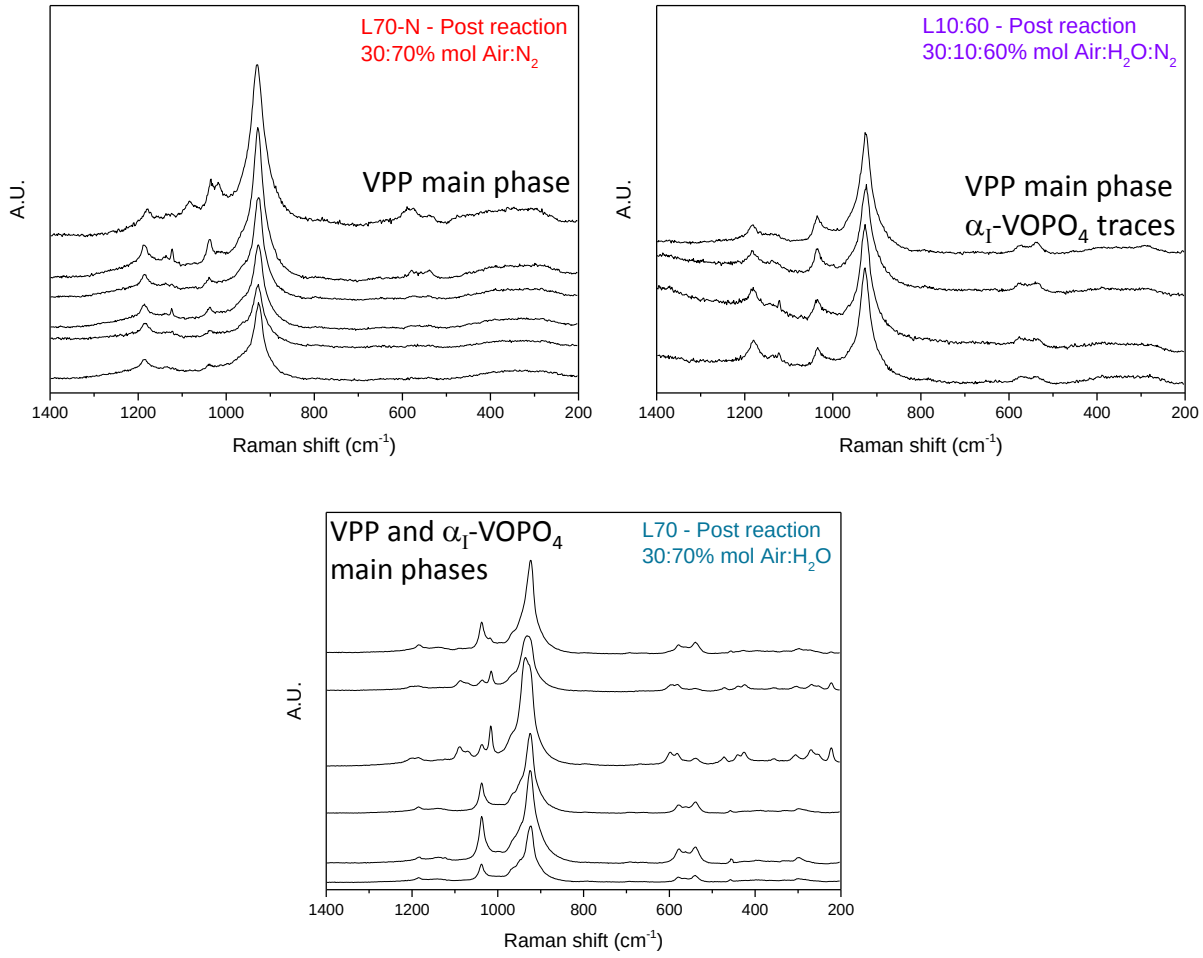

Figure 57. Raman spectra of used catalysts. Top left: L70-N, top right: L10:60 and bottom: L70.

No differences in the XRD patterns of used catalysts were observed: they have been compared in Figure 58 and presents only reflection attributable to VPP phase. This means that structural modification as a function of the calcination atmosphere and reaction condition occurs only in the superficial layer of the catalysts and the *bulk* did not changes its composition, leading to a stable catalytic performance regardless the time on stream and reaction temperature, preventing catalyst deactivation.

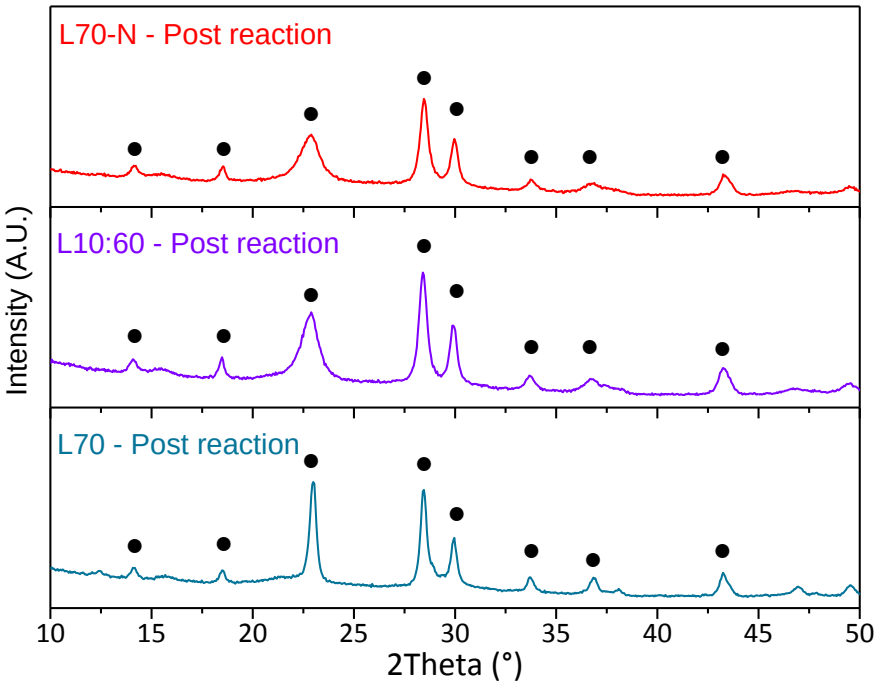

Figure 58. XRD patterns of L70-N, L10:60 and L70 used samples. Symbols: ● = VPP.

These tests demonstrate the need for water in the calcination environment, essential to promote desorption and decomposition of the organic species present on the surface of the catalyst, also thanks to reactions such as catalytic reforming. Secondly, it pointed out that not high amount of water is necessary to obtain an highly performing catalyst and that the percentage of oxygen can also be modulated with an inert diluent (nitrogen for example), significantly decreasing the costs associated with vaporization and steam supply in the case of industrial applications.

All data indicate that it is possible to obtain, depending on the method of calcination, a different morphology and phase distribution in the final catalyst and that two parameters (water and oxygen) affect at the same time the transformation of VHP to VPP.

The design of the L10:60 catalyst allow to get the best catalytic performance, because it was obtained with the best air and water molar ratio in the inlet stream, with the aim to exploit both the positive effects given by the water and those given by the lower oxidizing power of the calcination mixture.

4.6. Thermal treatment: the role of the diluting agent

From the experiments conducted so far, it is possible to conclude that both water and air are important in order to obtain an active and selective catalyst, but they possess a different role: the amount of oxygen influences the phases that are formed as a results of the thermal treatment, in other word, it is responsible for the vanadium oxidation state in the sample. Water, instead, influences the crystallinity that characterized the final catalyst, leading to the formation of different levels of structural disorder, which consequently, modify the reactivity. But it has been already demonstrated that water it is not necessary to achieve the formation of VPP phase and, above all, not large quantities are needed to obtain a highly performing catalyst.

Considering the peculiar effect of water, that is one of the two products formed during the thermal treatment, finally a calcination using a mixture of air and CO_2 was performed, to evaluate if also the second co-product formed during the thermal treatment has the same effect on the precursor transformation to VPP.

For this purpose, three different samples have been compared:

- L70: obtained calcinating VHP with 30% mol of air and 70%mol of water; these corresponds to the industrial condition.
- L70-N: a mixture composed of 30%mol of air (6.3%mol O_2) and the remaining 70% of nitrogen was used; the same oxidizing power compared to the sample L70, using nitrogen as diluting agent instead of water. The aim of this experiment was to evaluate if the formation of vanadyl pyrophosphate is accomplished with water or the remaining air.
- L70-C: the same oxidizing condition was used, which correspond to 30%mol of air, and the remaining part (70%mol) was CO_2.

During the calcination, carried out in a lab-scale tubular glass reactor, the oxygen consumption and the water and CO_2 formed were monitored by an online micro GC and the results are summarized in Figure 59.

Some remarks:

- The same heating ramp was used in the three cases: from room temperature to 180°C only air was fed, from 180°C to the end of the isothermal step at 425°C the experiments were carried out with the mixture of air with water (L70), nitrogen (L70-N) or CO_2 (L70-C), the last step

from 425°C up to 500°C was performed in nitrogen atmosphere. The heating rate was 2°C/min.

- In the case of L70 the trend of water was not reported because of its high molar ratio that damages the separation columns in the gas chromatograph.
- At the temperature of 180°C the decrease in oxygen molar ratio was due to the diluting agent added (in the case of L70 no decreasing was observed because of the water condensation before the GC entrance, but the real molar ratio inside the reactor was 6.3%mol as in the other cases); at this temperature in the case of L70-C also CO_2 was fed and its molar ratio increases reaching 70%mol.

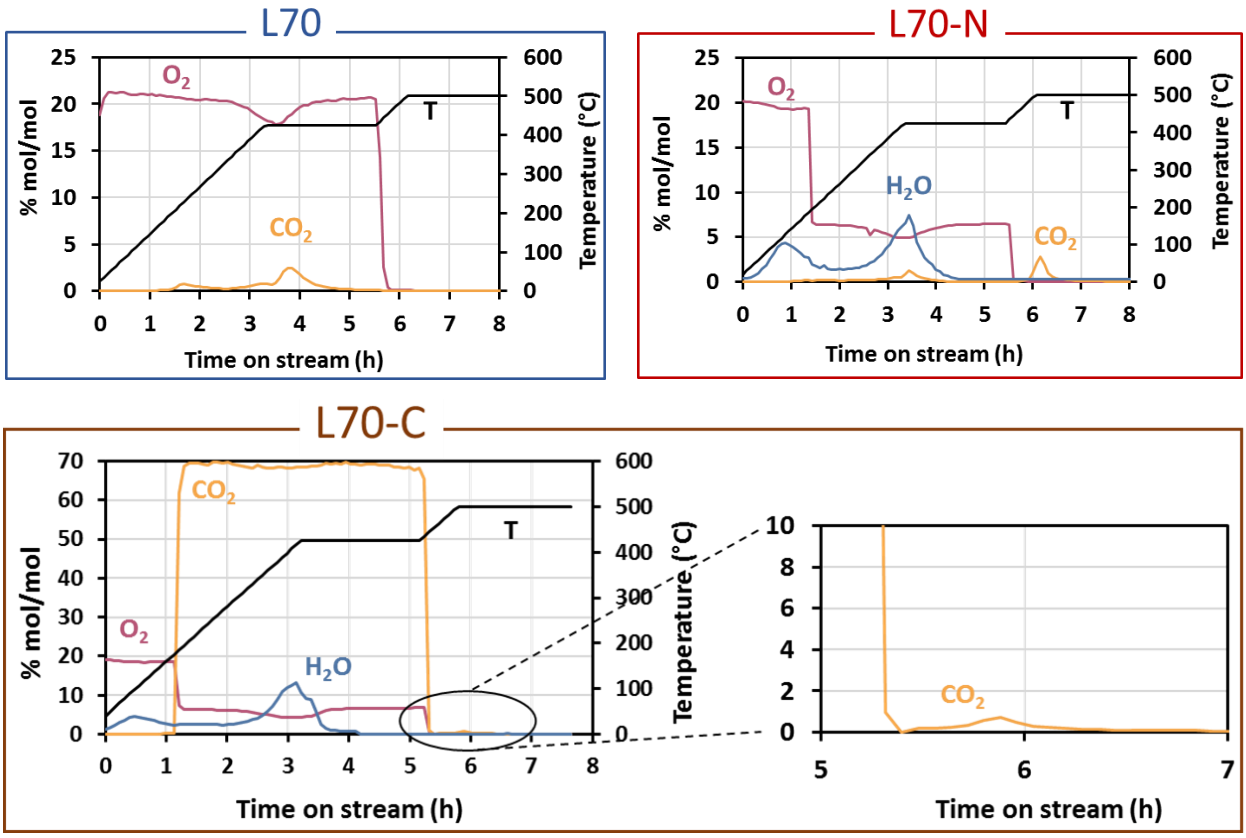

Figure 59. Consumption of oxygen (pink) and formation of water (blue) and CO_2 (orange) during the calcination of L70 (top, left), L70-N (top, right), L70-C (bottom).

Comparing the trends registered for the water formation, in the two cases where it was possible to measure it, they appears very similar: initial desorption of phisisorbed water (around 100-120°C); at the temperature of 300°C a great amount of water begins to desorb, reaching the maximum value at 425°C, at this temperature correspond also the formation of CO_2 and the consumption of oxygen:

both the transformation from VHP to VPP and at the same time the combustion of organic species remained from the synthesis occurs.

The main differences in the three cases is in the CO_2 formation: as already mentioned in the previous paragraph, when water was added in the inlet stream, the combustion is facilitated and it was completed at the end of the isothermal step at 425°C; in the case of L70-N, in which anhydrous condition was used, the most important formation of CO_2 happens at 500°C (without co-production of water). The new experiment conducted with a mixture of air and CO_2, reveal a further combustion at 500°C, even if a minor quantity of CO_2 was detected if compared to the one obtained during the calcination of L70-N, always with no co-production of water; this means that probably CO_2 does not exploit the same effect of water in the calcination procedure.

The characterization after reaction is reported in Figure 60: the XRD patterns were very similar because the reflections are attributable to VPP as a main phase (full circle), with very low intensive peaks characteristics of ω-$VOPO_4$ (ω).

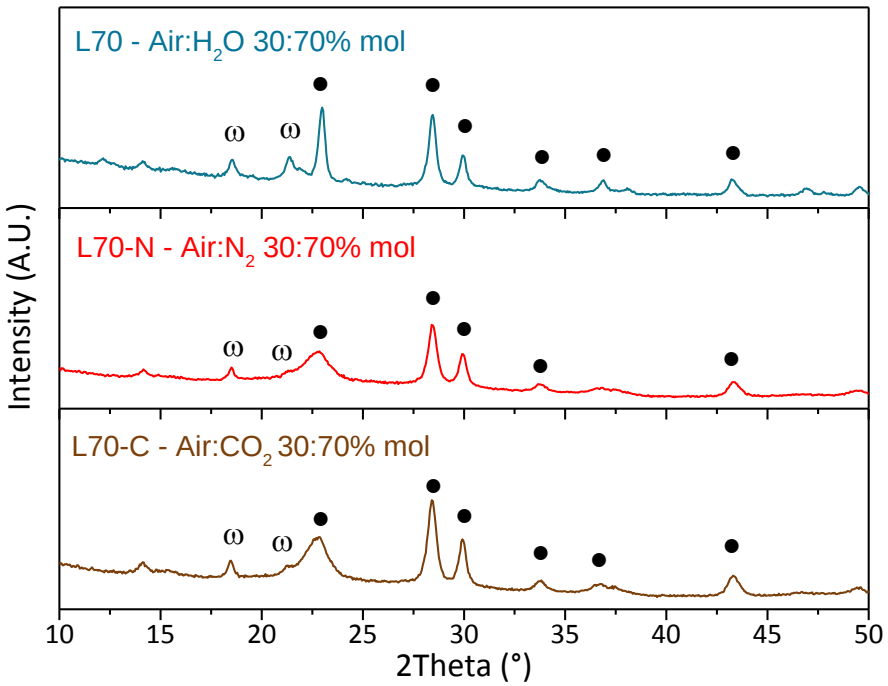

Figure 60. XRD analysis: comparison of L70, L70-N and L70-C to evaluate the role of the diluting agent. Symbols: ω = ω-$VOPO_4$; ● = VPP.

Thus demonstrate that under the same oxidizing power condition (30%mol air), changing the diluting agent from water to nitrogen or carbon dioxide (blue, red and brown lines respectively) no changes in the *bulk*-phase constituting the final catalyst are observed: it is mainly constituted of VPP. The difference in the three samples was, again, in the crystallinity. Looking at the most intense reflection

(23°): adding water (blue diffractogram) it appears sharp, whereas in the red sample (obtained with a mixture of air and nitrogen in 30:70%mol ratio) the signal appears broad, sign of major structural disorder. In the case of air diluted with 70%mol of CO_2 an intermediate situation is observed.

Comparing the crystallinity to the results monitored with the micro GC it was observed a correlation of the two: the increases in crystallinity correspond to the smaller amount of CO_2 formed in nitrogen atmosphere, i.e. in the case of combustion completed at lower temperature and time on stream, in order L70, L70-C and L70-N, the final structure presents a well-crystallized vanadyl pyrophosphate. Chemical analysis (Table 9) confirm that similar vanadium oxidation state have been obtained in the three cases, demonstrating that they are composed with similar V^{4+} and V^{5+} phase distribution. Notable are instead the value of surface area, probably correlated to the crystallinity observed with X-ray analysis: increases in disorder along (200) planes ($2\theta=23°$) is related to an higher specific surface area, which correspond to an higher activity per unit volume, in fact the lower the surface area, the more limited is the *n*-butane conversion. As evidence of this fact, L70 and L70-N, which are characterized by the greatest difference in terms of stacking disorder along (200) plane, possess very different conversion (the complete reactivity of these two catalysts were previously reported): 23% for L70 and 40% for L70-N, at the temperature of 400°C.

Table 9. Surface area and V oxidation state for L70, L70-N and L70-C calcined catalysts.

Catalyst	Surface area (m^2/g)	Vox
L70	7	4.21
L70-N	14	4.25
L70-C	15	4.20

Using CO_2 instead of water, considering that it is the second combustion product with water, does not allow to obtain the same results as observed when an water-added treatment was performed: it shows intermediate trends (both in the micro-GC results monitored during the calcination and in the X-ray diffractograms) between L70, which presents higher crystallinity and no CO_2 formed at 500°C, and L70-N, characterized by a disorder along (200) plane, at $2\theta=23°$, and an higher molar ratio of carbon dioxide released when the temperature reaches 500°C in the calcination plant (sign of a more difficult combustion).

Changing the diluting agent is a valid method, alternative to the standard preparation of vanadyl pyrophosphate catalyst, considering that the active phase is formed regardless the type of carrier gas used. Analysing the Raman spectra (Figure 61), however, those that characterize L70-C appears with

a very low intensity (lower signal/noise ratio) compared to the other two; this peculiar effect is usually due to organic molecules adsorbed on the surface. We are not able to observe and quantify the amount of CO_2 formed during the calcination, because the signal is influenced by the feeding mixture, but observing the spectra it is presumed that in these condition the organic molecules are not totally burned, at least as regards the more superficial layers.

An aspect to be further explored, however, is the effect that this method of preparation will have on catalytic performance, when the selective oxidation of *n*-butane is the reaction of interest.

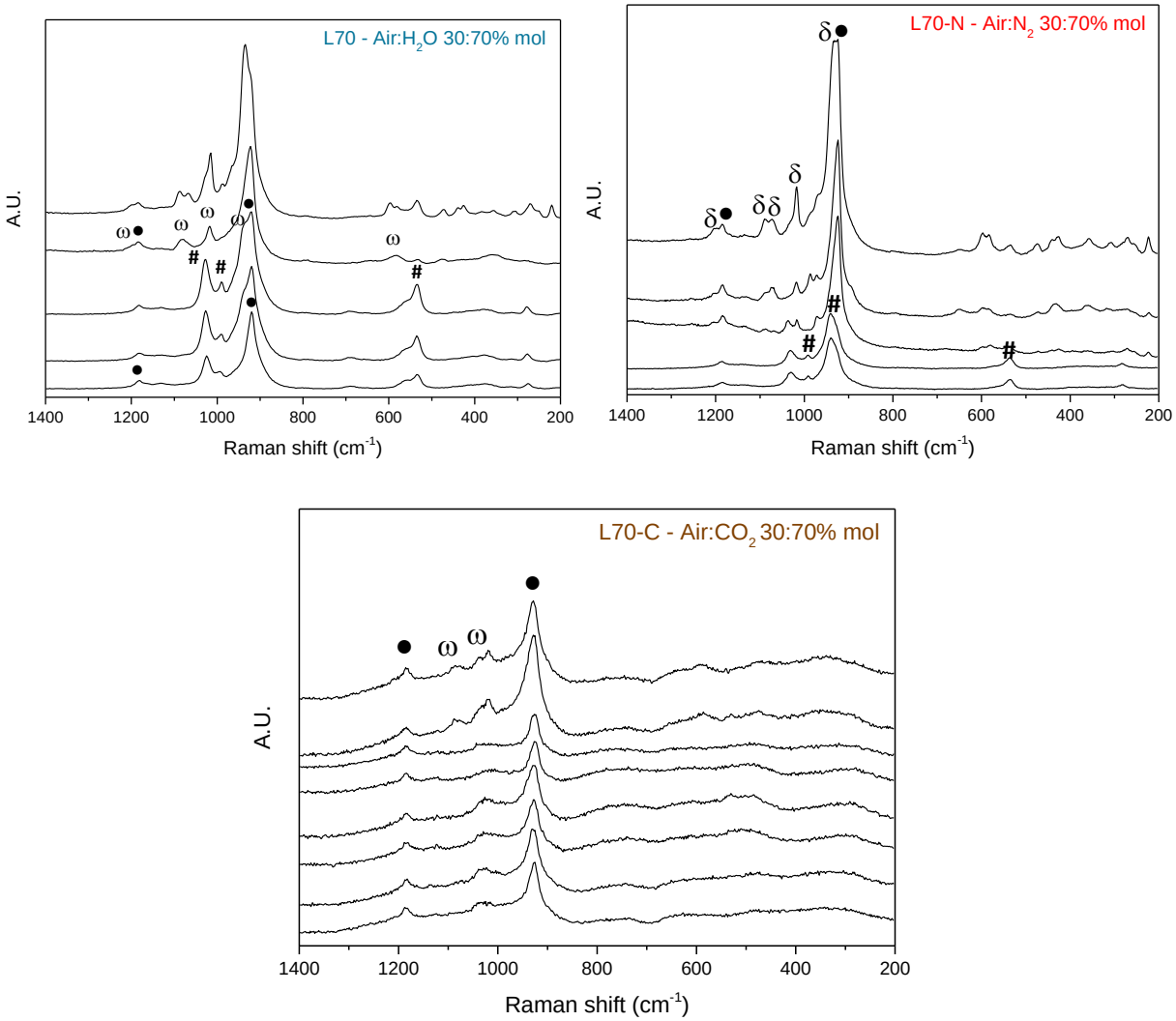

Figure 61. Raman spectra after calcination with 70%mol of water (L70, blue), 70%mol of N_2 (L70-N, red) and 70%mol of CO_2 (L70-C, brown). The remaining 30% was air.

In conclusion, the gaseous feeding mixture used for the thermal treatment acts on two different phenomena that occur simultaneously: the combustion of organic molecules derived from the synthesis and the dehydration of vanadyl hydrogenphosphate hemihydrate (VHP, precursor) to give

the final vanadyl pyrophosphate (VPP). Water is the only molecule that participates in both reactions and, because of it, shows its particular and unique effect: it is responsible for the increasing in crystallinity and it is necessary to promote reactions that favours the combustion of organic molecules, even if this is not directly correlated to greater catalytic performance, as shown from the results of L70 and L70-N; in fact we have previously demonstrated that the best catalytic performances are reached with only a small amount of water (L10:60 sample).

4.7. The role of the heating ramp

Once it has been understood the role of water and oxygen in the transformation of hemihydrate precursor to obtain vanadyl pyrophosphate, a study varying the heating ramp has been done.

During the industrial calcination of the precursor they has been observed differences when the thermal treatment was performed in the pilot plant (PP) or in the industrial one (PI). In particular the main difference is in an isothermal step at 350°C: during the calcination in the PI the heat supplied by the resistance of the oven in lower than the one needed for the dehydration of the precursor and, at the same time, for maintaining the heating rate according to the ramp used, for this reason a so-called "endothermic step" was formed. As mentioned in the initial part of the results, the two main reactions that occur during the calcination of VHP are the dehydration to form VPP and the combustion of organic residues due to the synthesis in organic medium, the first one is endothermic and the second exothermic. This means that the "endothermic step" is related to the topotactic transformation that gives the vanadyl pyrophosphate. The consequence is that in the PI the decomposition and transformation of the precursor occur at 350°C whereas in the PP (in which the resistance of the oven provides the necessary heat) at 425°C. This causes difference in the crystallinity and, of course, in the catalytic performance.

For this reason, some experiment varying the heating ramp were performed, in other word the "endothermic step" was forced adding an isotherm at 350°C, in order to understand its effect on the formation of an active and selective catalyst.

The atmosphere used for the tests were the same used in the industrial, i.e. 70%mol of water and the remaining 30%mol was air (the same used for the obtainment of L70) and the different heating ramp were schematized in Figure 62:

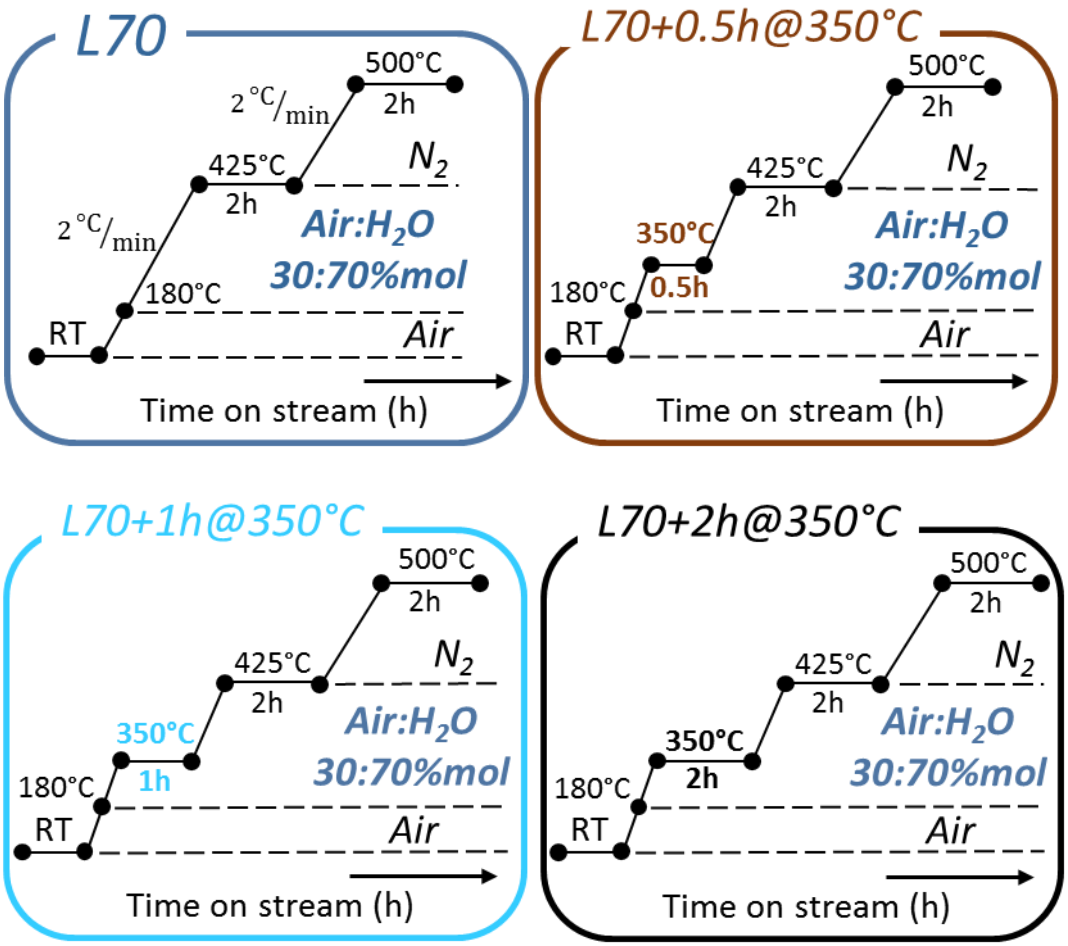

Figure 62. Heating ramp performed to study the effect of adding an isothermal step at 350°C of 0h (blue), 0.5h (brown), 1h (light blue) and 2hours (black).

4.7.1. Synthesis and characterization of VPP catalysts

First of all the four catalysts were synthetized in a lab scale reactor and the outlet stream was analysed by using an online micro GC; the water was condensed and separated before entering in the GC analyser, avoiding damages in the separation columns, for this reason in Figure 63 are compared the molar ratio of oxygen consumed and only the CO_2 formed as a function of time on stream.

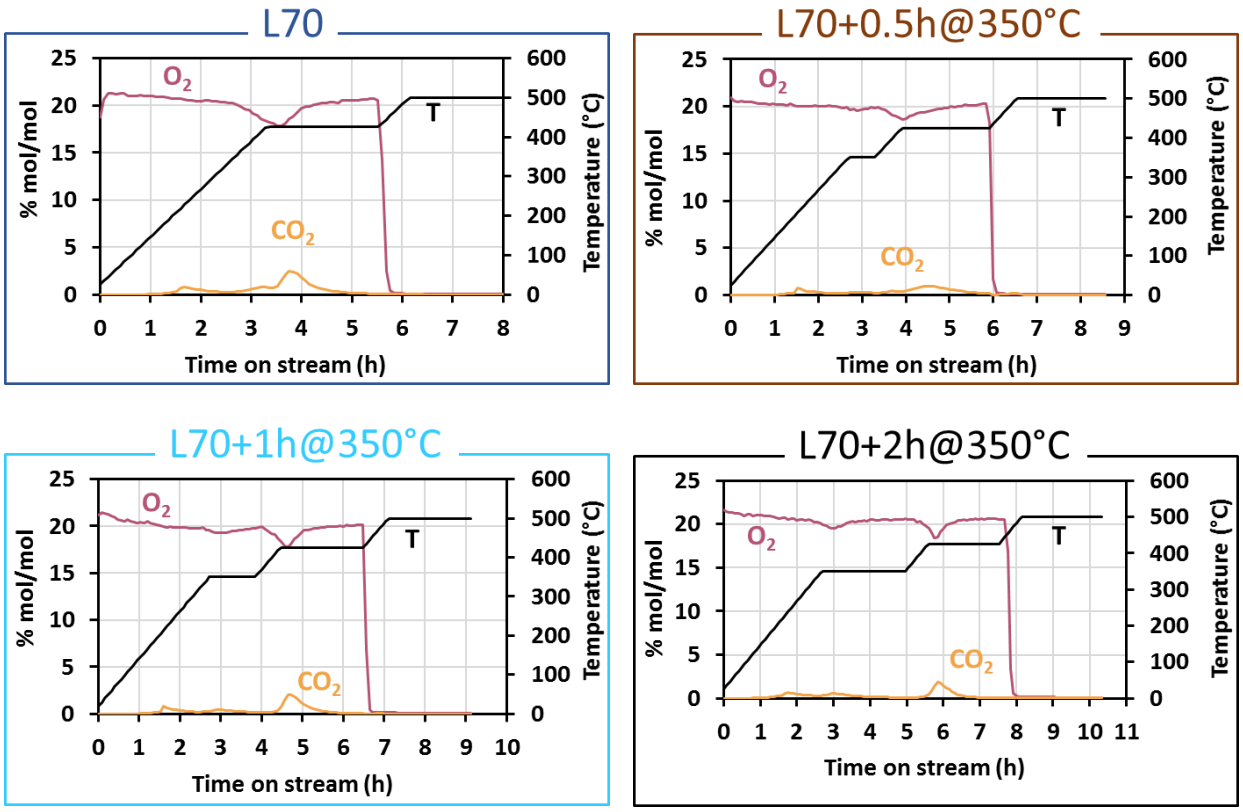

Figure 63. Consumption of oxygen (pink) and formation of CO_2 (orange) during the calcination of L70 (top, left), L70+0.5h 350°C (top, right), L70+1h 350°C (bottom, left) and L70+2h 350°C (bottom, right).

Increasing the time on stream (and as a consequence the temperature) a consumption of oxygen was observed: in particular, when no isotherm was added (L70, blue line), the maximum of the consumption was located at the temperature of 425°C, but when the heating ramp was modified (adding 0.5, 1 or 2h at 350°C) two decreasing in oxygen molar ratio were detected: the first one at 350°C and the second at 425°C. Same trends were observed for the carbon dioxide formed: when the oxygen was consumed, the combustion product was formed. Important to note is that the major formation of CO_2 is at 425°C: this temperature is necessary to complete the combustions and achieve the transformation of VHP to VPP, regardless the duration of isothermal step at 350°C.

Figure 64 shows the room-temperature XRD patterns of the samples obtained after calcination: in all the four catalysts, besides the reflections of VPP (●), also those attributable to V(V) phosphate were presents. In particular, in L70 pattern, reflections are attributable to ω-$VOPO_4$; when the isothermal step was added, signals characteristics of the δ-$VOPO_4$ were also presents. A further consideration concerns the crystallinity: increasing the duration of isothermal step from 0h (blue sample), 0.5h (brown) and 1h (light blue) an increase in crystallinity is observed. Surprisingly, 2h at 350°C (black line) causes a decrease in crystallinity.

Also in the industrially calcination a similar behaviour is observed: adding the isothermal step at 350°C, increasing in crystallinity, specific surface area and catalytic performances are observed, but if this step is too long it became detrimental.

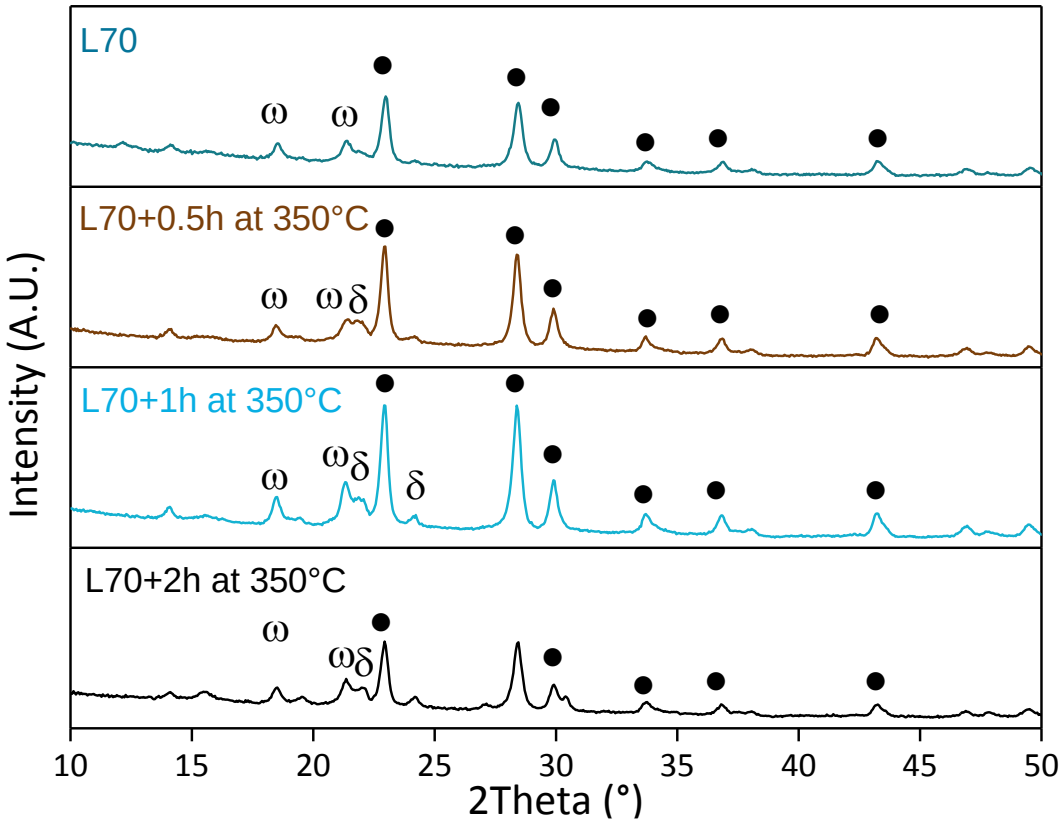

Figure 64. XRD diffractograms of fresh catalysts L70 (blue), L70+0.5h 350°C (brown), L70+1h 350°C (light blue), L70+2h 350°C (black). Symbols: ω = ω-$VOPO_4$; δ =δ-$VOPO_4$; ●=VPP.

4.7.2. Reactivity and characterization of used catalysts

To completely understand the role of the isothermal step at 350°C, it has been decided to compare the catalytic behaviour of L70 (30:70%mol air:H_2O without isothermal step) and L70+1h at 350°C (30:70%mol air:H_2O with 1h at 350°C) catalysts, because the latter presents the higher crystallinity and, together with VPP, also δ-$VOPO_4$ phase is detected that is the selective one for the reaction.

In Figure 65 are reported the conversion of *n*-butane and the selectivity in maleic anhydride and COx, at the constant temperature of 400°C, for L70 (blue, empty bars) and L70+1h at 350°C (light blue, full circle).

Before reactivity at various temperatures, an equilibration under reaction conditions was performed, leading to crystallization of amorphous phase if any were presents in the fresh catalyst, reduction of

bulk $VOPO_4$ to VPP and increase in the crystallinity of VPP; all these transformations results in stable catalytic performance.

The catalysts present very similar conversion of *n*-butane (within experimental error, equal to 3% due to the analytical system) equal to 20%mol at 400°C but differ in the selectivity: just adding a short isotherm a higher selectivity in the desire product MA was observed (55% without isotherm and 75% with 1h at 350°C). Thus encouraging the total combustion reaction when L70 was used as a catalyst for the oxidation of *n*-butane: the selectivity in COx, in fact, is 26% for the catalyst obtained with the additional step at 350°C and 41%mol for L70.

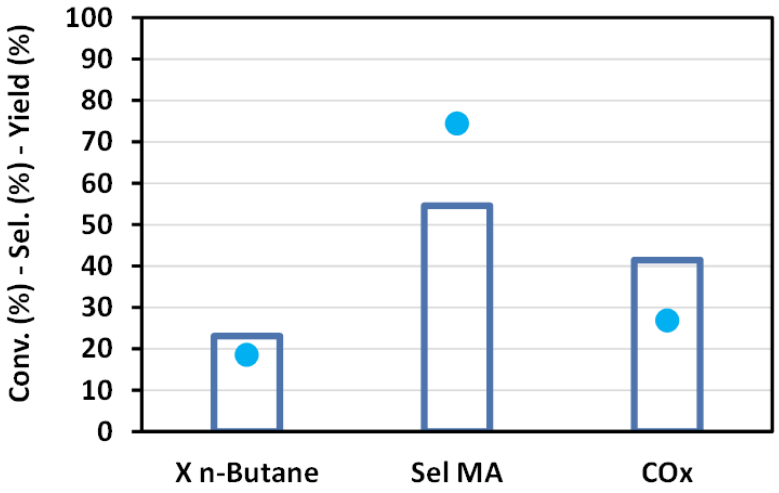

Figure 65. Catalytic behaviour for the catalysts obtained without isothermal step (blue empty bars) and adding 1h at 350°C (light blue full circle) with 70% H_2O and 30% air.
Conditions: T=400°C, W/F=1.33g*s/mL, *n*-butane:O_2:inert 1.7%:17%:remain.

The reason for this difference is attributable to the species that characterize the active layers in the two catalysts: comparing the Raman spectra of the fresh catalysts after calcination (Figure 66), L70 presents bands of VPP (●) and dihydrate V^{5+} phosphate ($VOPO_4 \cdot 2H_2O$, #) as a main phases; ω- and δ-$VOPO_4$ has been found only in two spectra, i.e. only two points between all those analysed are composed of these selective phosphates. On the contrary, just adding a short isotherm the presence of ω- and δ-$VOPO_4$ (together with VPP) in each spot analysed may be the reason for the greater selectivity at the lower temperature investigated (400°C) with respect to L70.

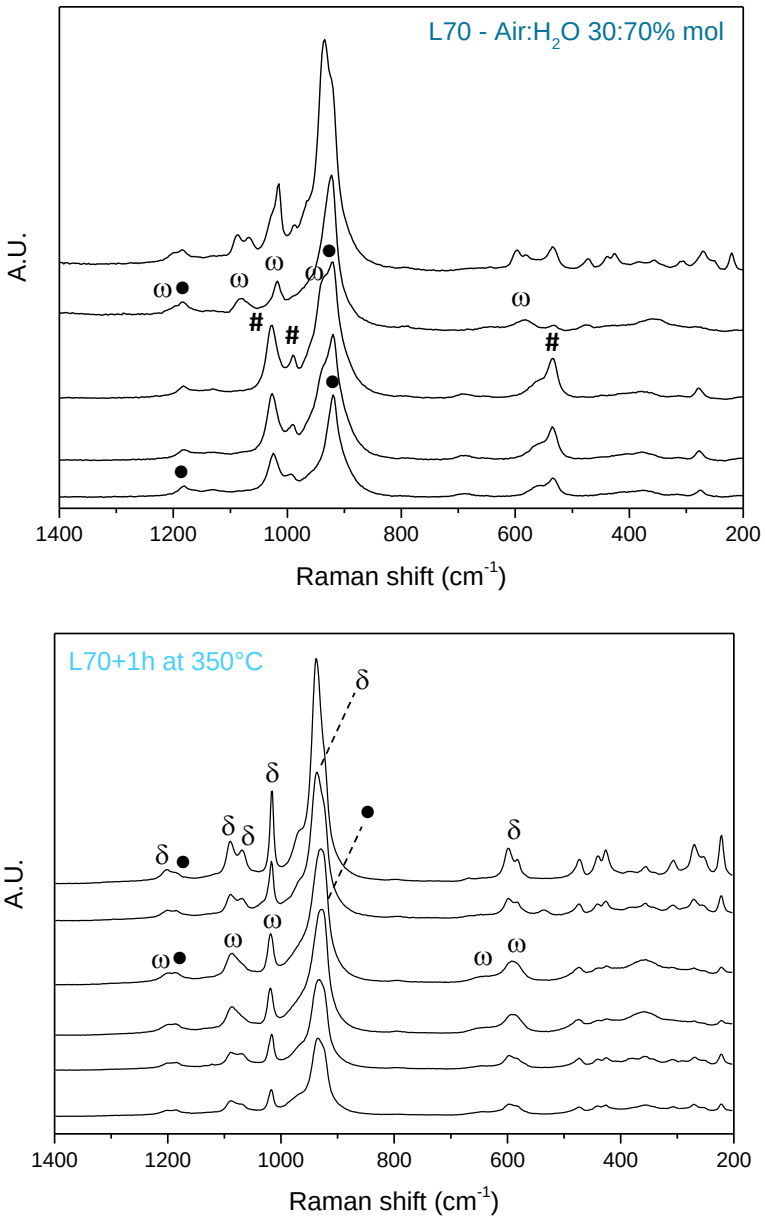

Figure 66. Raman spectra of fresh catalysts (after calcination in wet air, with 70%mol of water). Top: L70, bottom: L70 with an addition isothermal step at 350°C for 1 hour. Symbols: ω = ω-$VOPO_4$; δ =δ-$VOPO_4$; # = $VOPO_4 \cdot 2H_2O$; ●=VPP.

In Figure 67 are reported the catalytic behaviour in the entire temperature range investigated (400-440°C), in terms of conversion (♦), yield in MA (full ■) and COx (●) and, finally, selectivity in MA (empty □) for the two samples: in blue are reported the results of L70 and in light blue those of L70+1h at 350°C. Increasing temperature improves the activity of both catalysts, due to the kinetics, and L70 has slightly higher values, especially at higher temperature. The yield in MA presents the same values at all temperatures but differences in COx yield were observed: L70 leads to the preferential formation of combustion products. This means that the higher conversions of L70 are

related to un-desired reactions, and thus the selectivity in MA has higher value when an isothermal step at 350°C was added during the calcination (light blue line in Figure 67). Increasing temperature, causes a slight decrease in MA because of the combustion reaction is the favoured.

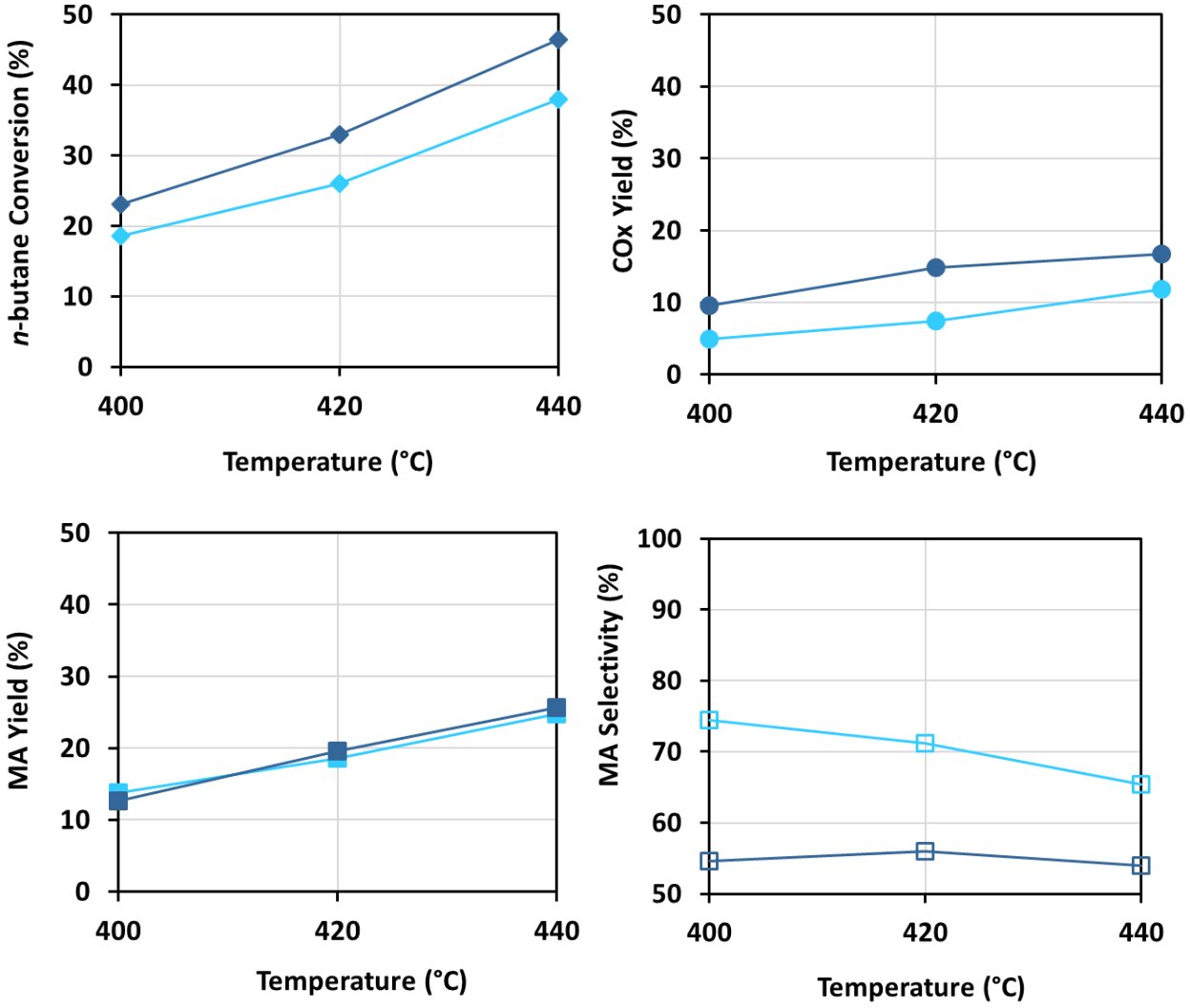

Figure 67. *n*-butane conversion (top, left), yield in COx (top, right), maleic anhydride yield (bottom, left) and selectivity (bottom, right) for L70 (blue) and L70+1h at 350°C (light blue) as a function of temperature. Feed: *n*-butane:O_2:Inert 1.7%:17%:remain; W/F: 1.33 g·s/mL.

Finally, analysing the characterization results reported in Figure 68 it is possible to assume that:

- L70, thanks to the poorly oxidizing atmosphere (30%mol of air, which correspond 6.3%mol O_2) after the calcination is mainly formed of VPP and of V^{5+} phosphate, namely the ω-$VOPO_4$ and the dihydrate form. During reaction, being in the absence of water VPP tends to oxidize, leading to the formation of α_I-$VOPO_4$; increasing the reaction temperature until 440°C in the presence of air, α_I- is transformed into another allotropic form of $VOPO_4$, the δ- which is

known to be the selective for the reaction. For this reason the selectivity of L70 does not change with the temperature, because the decreasing due to the temperature (which favours the total combustion reaction) is compensated by the *in-situ* formation of the selective δ-$VOPO_4$, so the mean value is constant. At the end of reaction, when the temperature was decreased again, δ- transformed back again to α_I-$VOPO_4$, as demontrated by the Raman spectra reported in Figure 68 (top, left). Therefore, the two V(V) phosphate interconvert and the nature of the dominant compound is a function of temperature. The redox cycle descripted above is in accordance to *in-situ* study previously made by Cavani and co-workers[45].

- L70+1h at 350°C presents δ-$VOPO_4$ as a main phase, instead of the dihydrate form: it is as if $VOPO_4 \cdot 2H_2O$ was an intermediate phase formed during the calcination, when more time is left to oxidize the organic species remained from the synthesis and reorganize the structure, the dihydrate transforms into the δ-$VOPO_4$ that is considered to be more stable than its dihydrate form, enhancing the performance of this catalyst. During reaction probably more δ- is formed *in-situ* in form of "patches" over the VPP structure. As in the previous case, after reaction, the catalyst presents the same bands as observed for L70 and attributable to α_I-$VOPO_4$, because they interconvert as a function of the temperature.

The X-ray diffractograms, instead, do not show any difference in the two used catalysts: they are both formed of crystalline VPP (●).

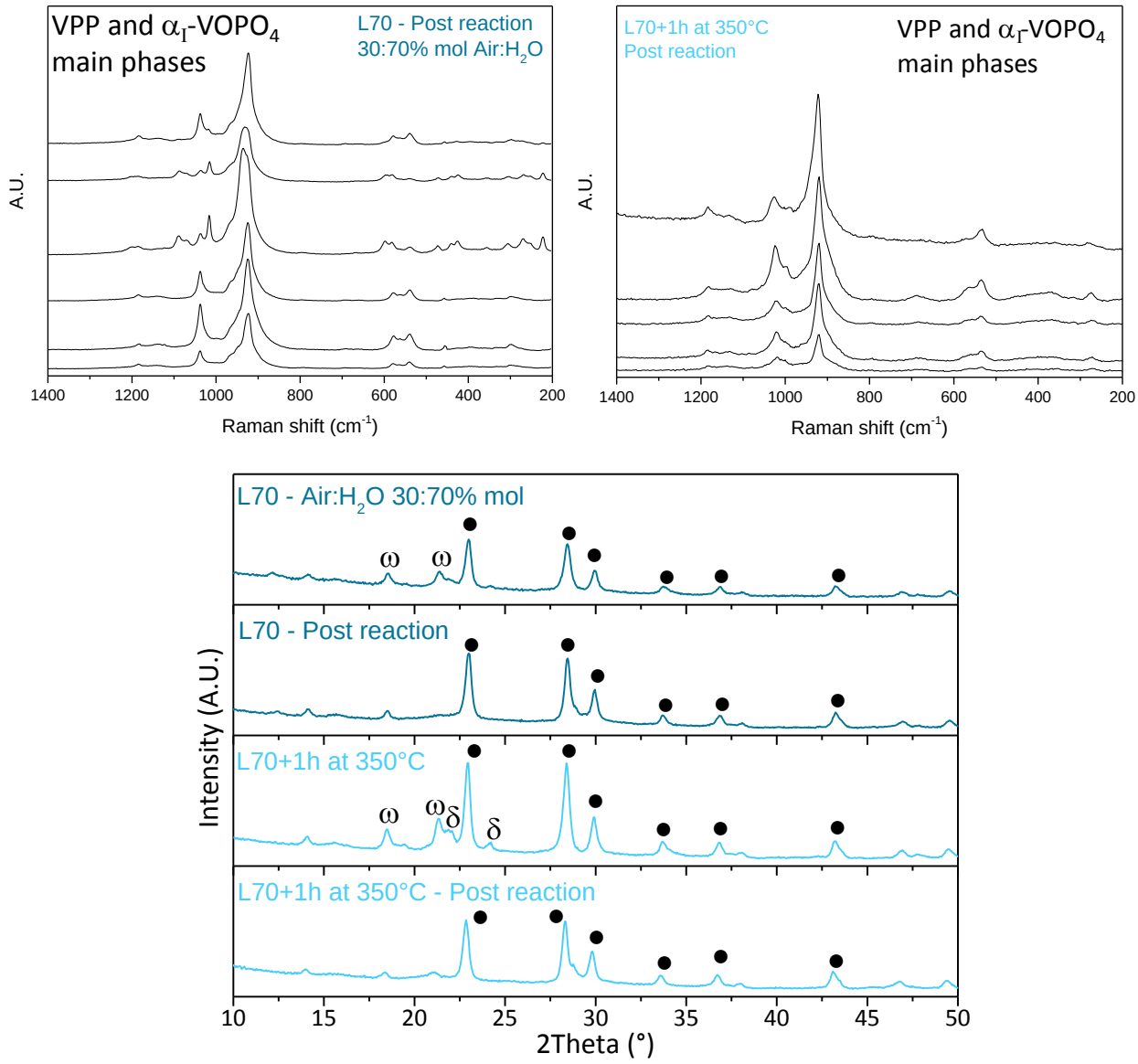

Figure 68. Top: Raman spectra of used catalysts. L70 in blue (left) and L70+1h at 350°C in light blue (right). Bottom: X-ray diffractogram of fresh and used catalysts. L70 (blue) and L70+1h at 350°C (light blue). Symbol: ω = ω-$VOPO_4$; δ =δ-$VOPO_4$; ●=VPP.

In conclusion, catalytic tests and the characterization, show the importance and the direct influence that the mechanism of transformation of the precursor has on the chemical-physical properties of the final catalyst and, as a consequence, the catalytic performance. In particular, promoting the transformation of VHP at 350°C instead of 425°C leads to the formation of an highly performing material, but, at the same time, the duration of treatment at 350°C is fundamental: when the isotherm is too long, the catalyst presents an higher vanadium oxidation state, lower surface area and lower crystallinity of all reflections, causing the decreasing of catalytic properties (tested/verified internally by Polynt).

4.8. Effect of the precursor type

Since the ultimate purpose of this work is to develop a versatile and reproducible calcination method, regardless of the precursor characteristics, a different industrially-made VHP (renamed M16) was treated in the same conditions as used for the previous M17 precursor.

The main differences of the two precursors are in the vanadium oxidation state, P/V atomic ratio and the content of carbonaceous species remained from the synthesis, in particular:

- M17, the first precursor employed for the study, presents lower amount of V^{5+} species: 0.006% compared to 0.040% for M16.
- The P/V ratio for M17 was 1.15, while 1.20 was the value for M16.
- M17 presents higher quantities of C (renamed Cin): 9490ppm compared to 6344 for M16.

Also the specific surface area has been measured by the BET method: for M17 it was 12 m^2/g, while for M16 was 17 m^2/g. Considering that the error associated at these measures is about 7% on values over 3 m^2/g, the two surface area could be considered different, even if they are still very low values. The differences related to the SSA values are consistent to the crystallinity of the two precursors and reported in the X-ray diffractograms in Figure 18: M16 which presents the higher surface area, presents an higher disorder, clearly visible along the (202) plane.

4.8.1. TGA analysis

Considering the different amount of carbonaceous species remained trapped in M16 and M17, first of all thermogravimetric analyses were performed also for the new precursor (M16) in the three different environment: using air in the first step (until the end of the isothermal step at 425°C) and then nitrogen from 425°C to the end of isotherm at 500°C (case a), in the second case (case b) only nitrogen was used as a carrier gas for the entire thermal treatment and the last calcination was performed using only air in the inlet stream (case c).

The heating ramp used are schematized in Figure 69:

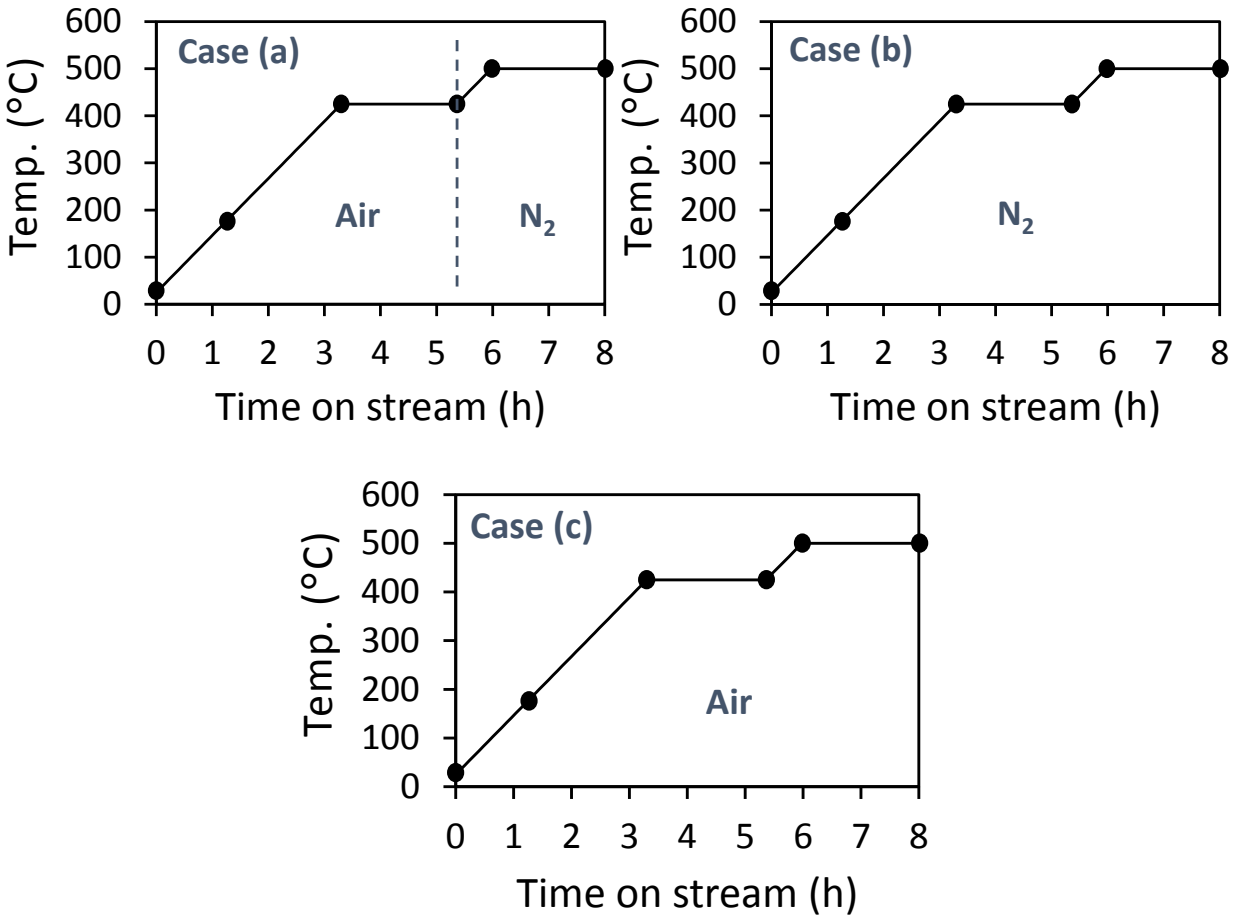

Figure 69. Heating ramp employed during TG analysis. Case (a)-top left: first step in air and the second in nitrogen, case (b)-top right: only nitrogen was fed and case (c)-bottom: only air was used as a carrier gas.

The aim of these preliminary experiment was to evaluate the loss in weight that characterized the two precursors as a function of the carbonaceous content and, if possible, the nature of the carbonaceous species formed.

In Figure 70 are reported the derivative weight loss that characterized M16 (top) compared to the analysis previously made on M17 (bottom) in the same conditions.

The first big difference that it is possible to observe comparing the two series of thermograms is that, regardless the atmosphere performed, M16 presents a single weight loss in the range of time on stream between 120 and 180 mins, while for M17 three main peaks where observed: the first after one hour, the second correspond to the loss in weight observed for M16 and the third observed when the temperature reaches 425°C (it occurs at higher temperature, this means that is related to organic species strongly linked to lattice oxygen).

The single peak of loss in weight registered for M16 occurs at a lower time on stream, and consequently, at lower temperature; this could be related to:

1) The slightly higher surface area (and disordered structure) that facilitate the combustion reactions and increases the rate of dehydration of VHP to give VPP.
2) Different organic species trapped between the layers: both the precursors were synthetized in an organic medium, following the same procedure, but the alcohol used as a solvent and as a reducing agent is not always fresh, in fact, it undergoes distillation and then it was recycled. Industrial evidences demonstrate that, even though the distillation, as a function of the number of uses, the alcohol is enriched with by-products deriving from oxidation of the alcohol itself; this is the cause of the different trends of loss in weigh in the two cases.

Noteworthy, the weight loss in non-oxidizing condition (case b) for M16 is considerably higher compared to the one observed for M17 treated in the same condition. Thus confirming the Mars-Van Krevelen mechanism responsible for the combustion of carbon residues: M16 contains slight higher amount of V^{5+} which acts as oxidizing agent towards carbon residues, causing a decreases in weight, anyway without oxygen replacement the process is slower (signal detected with the TGA wider than cases where air is fed) and cannot be completed.

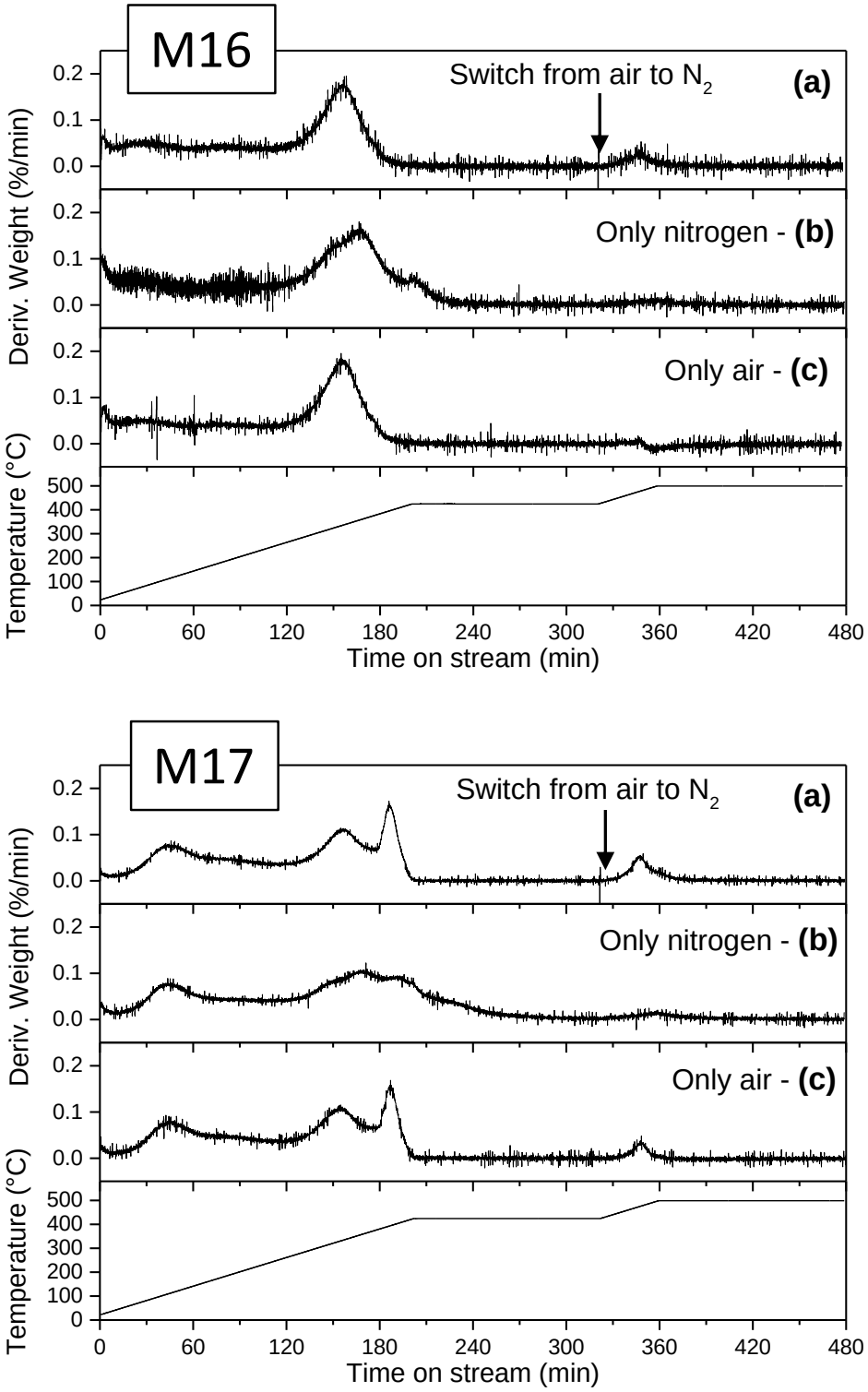

Figure 70. Derivatives of the weight and temperature ramp as a function of time when air/nitrogen (a), only nitrogen (b) and only air (c) used as a carrier gas, for M16 (top) and M17 (bottom) precursor.

Regardless the type of organic materials remained after the synthesis and, as a consequence the profile registered with the TG analysis, the total weight loss observed for M16 and for M17 was consistent with the carbonaceous species-content before the thermal treatments: the higher the Cin, the higher the loss in weight, when the same conditions were used for the treatments (the results are reported in Table 10). Again, the small difference observed when the thermal treatment was performed in nitrogen stream with M16 or M17 precursor, is due to the higher amount of vanadium in the 5+ oxidation state, that promotes the oxidation of organics, resulting in high loss in weight.

Table 10. Comparison of loss in weight for the two precursors.

Precursor	**Cin**	**Weight loss (%)**		
		Case a: air/N_2	Case b: only N_2	Case c: only air
M16	6344	11.0	14.3	10.5
M17	9490	12.3	14.5	11.2

It is possible to assume that the lower carbon content that has to be eliminated during heat treatment causes less distortion to the structure; this, together with the shorter time required for complete combustion, leave more time to the catalysts to reorganize the structure in a more efficient way.

4.8.2. The addition of water during thermal treatment

Synthesis and characterization

First of all it was investigated the role of water added during the calcination on the new precursor M16.

It was used the same heating ramp and the same gaseous mixture as for M17, as reported in Figure 71:

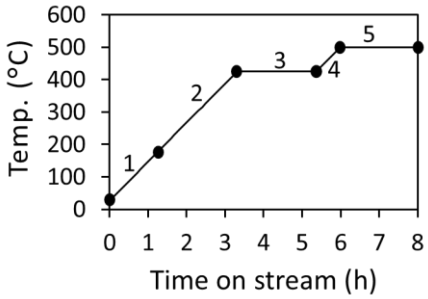

Step	Temp. (°C)	Atmosphere condition (%mol)			
		Sample name			
		L0	L10	L40	L70
1	RT→180	Air	Air	Air	Air
2	180-425	Air	$Air:H_2O$ 90:10	$Air:H_2O$ 60:40	$Air:H_2O$ 30:70
3	Isot. 2h @ 425	Air	$Air:H_2O$ 90:10	$Air:H_2O$ 60:40	$Air:H_2O$ 30:70
4	425→500	N_2	N_2	N_2	N_2
5	Isot. 2h @ 500	N_2	N_2	N_2	N_2

Figure 71. Heating ramp and calcination atmosphere used for the thermal treatment of M16 precursor changing water amount.

During the thermal treatments the combustion products and the oxygen consumed were monitored with an online micro-GC, connected to the outlet stream of the lab-scale plant used for the calcination. In Figure 72 are compared the CO_2 evolution as a function of molar ratio of water (or, on the other hand, the remaining air) for the two precursors.

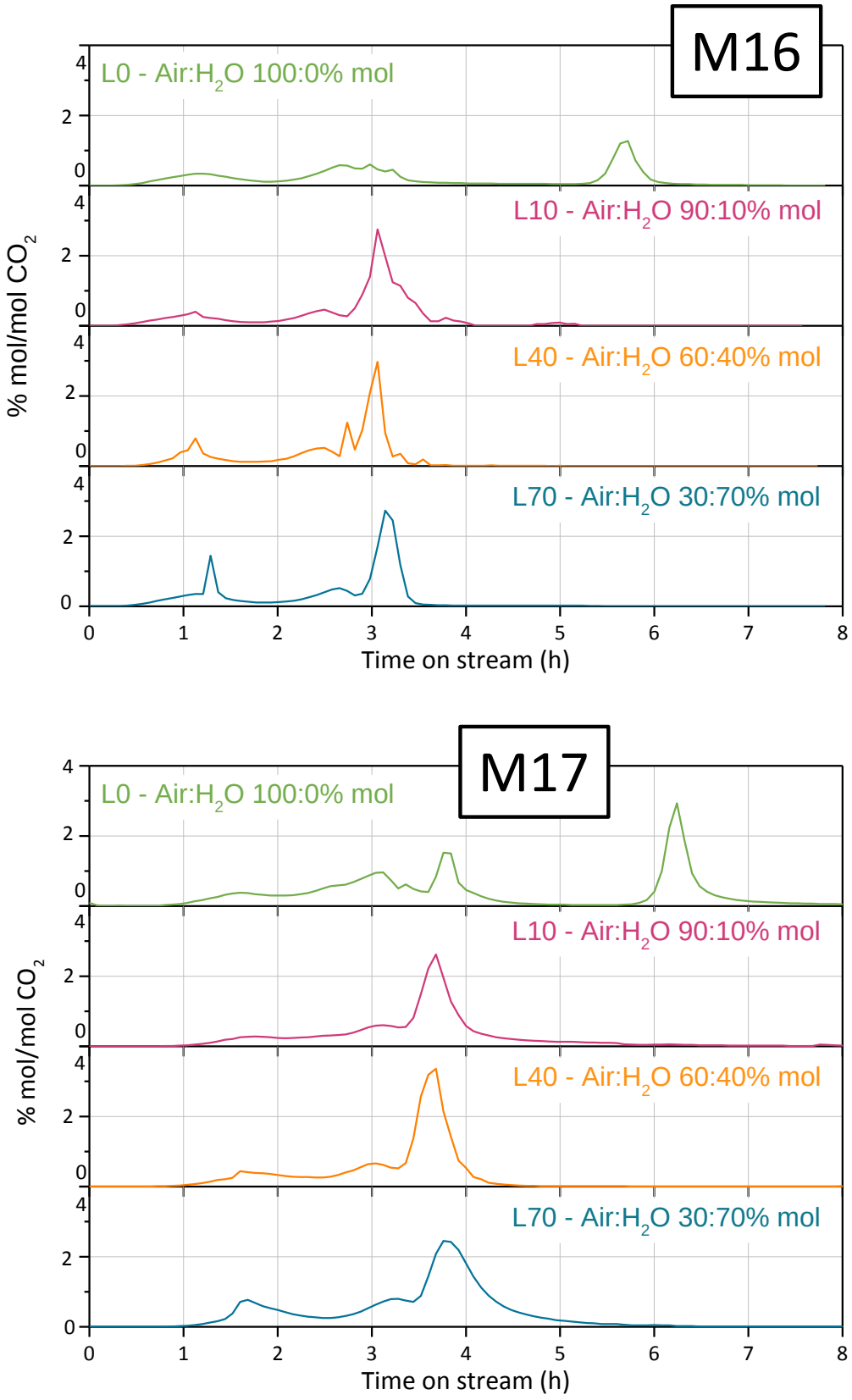

Figure 72. Carbon dioxide formed during the calcination of M16 (top) and M17 (bottom) in anhydrous condition (L0, green), with 10%mol (L10, pink), 40%mol (L40, orange) and 70% mol (L70, blue) of water and the remaining part was air.

To parity of composition of the inlet mixture, it is possible to observe that:

- L0, obtained without water in the inlet stream, shows a slow and gradual release of CO_2 when air was fed (from zero to five hours of time on stream, which correspond to the end of the isothermal step at 425°C); moreover, when the carrier gas was switched from air to nitrogen, another formation of carbon dioxide was observed. This occurs for both the precursors, the difference is in the amount of it: in the case of M16 lower quantity of CO_2 formed was registered, as compared to the one in M17. This phenomenon is easily explained by observing the amount of C that characterized the two precursors and the loss in weight registered by TG analysis because there is a direct match between them: the lower is the Cin (M16), the lower is the amount of carbonaceous species burnt during the calcination and monitored by micro GC and the lower is the weight loss.
- When water was added in the stream and co-fed in a mixture with air (L10, L40 and L70) a more marked formation of CO_2 occurs 3 hours after starting treatment and no further combustion occurs at 500°C in nitrogen atmosphere (after about 5.5 hours) as in the case of L0. This demonstrates that, as descripted in the previous paragraph for M17, also with the new precursor water is necessary to speed-up the combustion of organics and the transformation of VHP to give the final catalyst, because it favours the formation of more easily oxidizable molecules.

After the thermal treatment, the catalysts were characterized by means of X-Ray diffraction analysis and Raman spectroscopy with the aim to evaluate the phases that composed each catalyst; vanadium oxidation state and specific surface were also determined.

The diffractograms are reported in Figure 73: the catalyst obtained without the co-feeding of steam, renamed L0 (green), presents the typical pattern attributable to V^{5+}-phosphate, both in anhydrous (ω) and hydrated (#) state; VPP (●) has been found only in traces.

Increasing the partial pressure of water co-fed with air, or rather, decreasing the percentage of oxygen (pink, orange and blue catalysts respectively), an increase in VPP phase is observed; the other patterns are attributable to the same ω-$VOPO_4$ and $VOPO_4 \cdot 2H_2O$ as in the first diffractogram. The only difference is related to the L70 sample: in the bulk it does not shows the presence of the dihydrate phase, probably because the lower oxygen content in the feeding mixture limits the formation of oxidized phases.

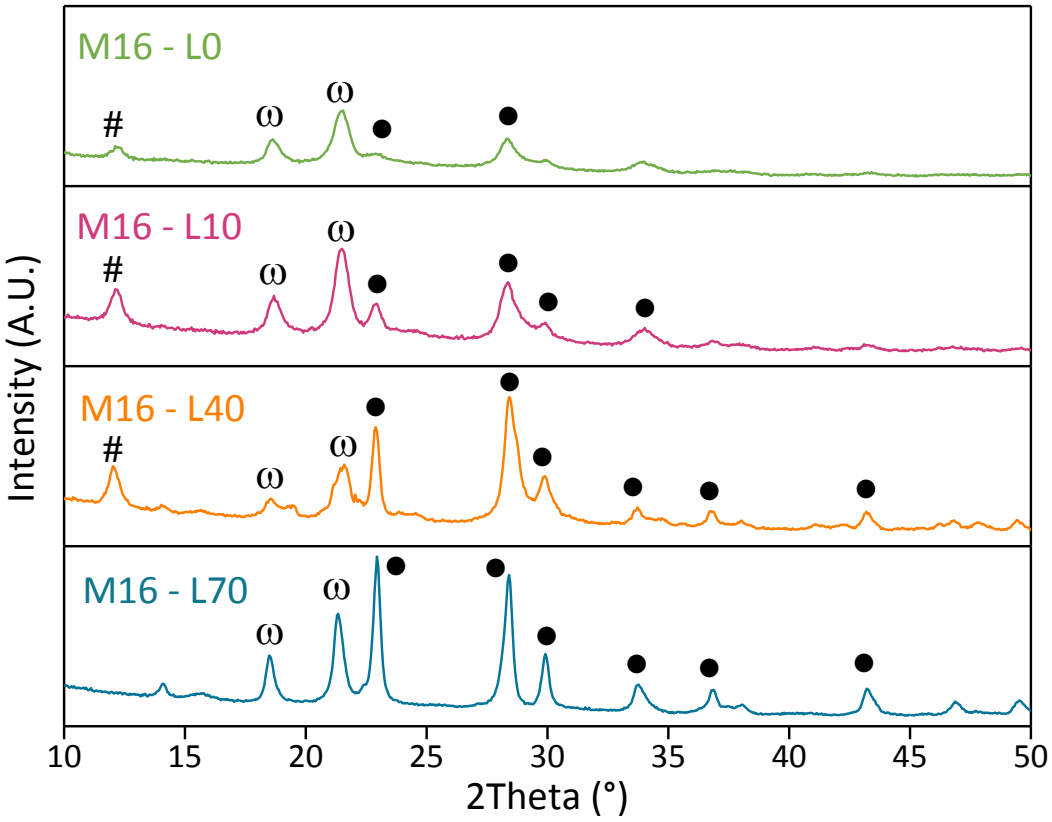

Figure 73. XRD diffractograms of catalysts obtained calcinating M16 without water (green), with 10% H_2O (pink), 40% H_2O (orange) and 70% H_2O (blue); the remain is air.

Symbols: ω = ω-$VOPO_4$; # = $VOPO_4 \cdot 2H_2O$; ● = VPP.

The identification of the type of orthophosphate was possible thanks to the Raman spectra collected in different spots of the samples: as mentioned in the previous paragraph, the latter technique provides more information about these type of catalysts, succeeding in differentiate the allotropic forms of $VOPO_4$; they are all reported in Figure 74.

L0 shows the typical bands of ω-$VOPO_4$, except for the first spectra that presents also α_I -$VOPO_4$. The spectra collected over the catalyst renamed L10 (calcined with 10%mol of water and the remaining 90% was air) presents the same pattern as found in L0, the only difference is in the identification of $VOPO_4 \cdot 2H_2O$ phase (#) in traces (just in the first spectrum).

Increasing the amount of water from 10 to 40% leads to the formation of $VOPO_4 \cdot 2H_2O$ (#) as a main phase on the catalytic surface, together with VPP in traces (●).

Finally, the Raman characterization of L70 showed the presence of $VOPO_4 \cdot 2H_2O$ (#) even if it was not found in the X-ray diffractogram (Figure 73); moreover the VPP is present in each spectrum registered and its signal is well distinguishable. The mean vanadium oxidation state determined by titration, in fact, shows the lower value with respect to the previous three catalysts (listed in Table 11).

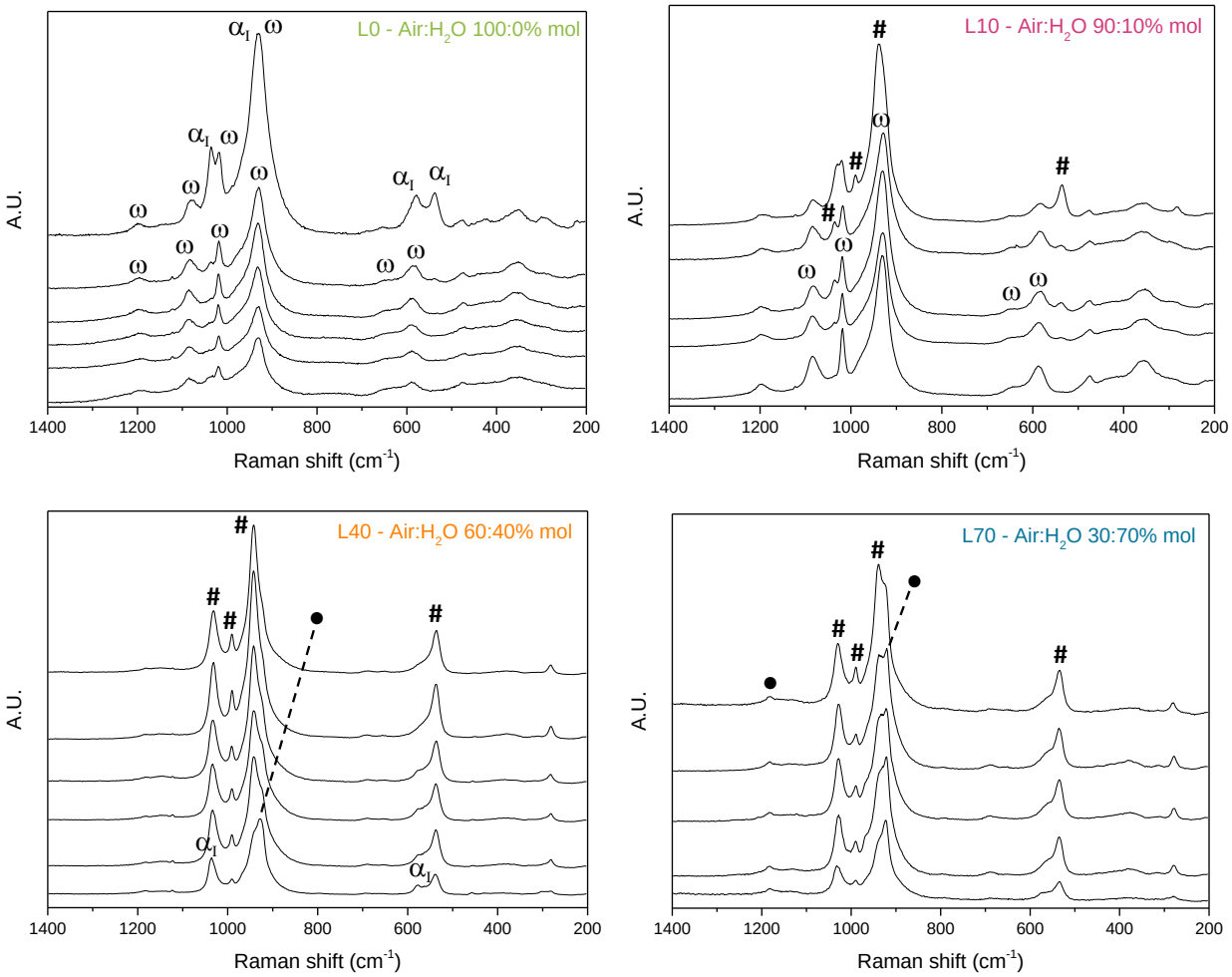

Figure 74. Raman spectra of L0 (top, left), L10 (top, right), L40 (bottom, left) and L70 (bottom, right) catalysts derived from M16.

Symbols: ω = ω-$VOPO_4$; α_I = α_I -$VOPO_4$; # = $VOPO_4 \cdot 2H_2O$; ● = VPP.

Table 11. Surface area (BET) and Vanadium oxidation state for L0, L10, L40 and L70 catalyst derived from the precursor M16 (top) and M17 (bottom).

	Catalyst	SSA (m^2/g)	Vox
M16-derived	**L0**	13	4.58
	L10	9	4.60
	L40	7	4.51
	L70	17	4.27
M17-derived	**L0**	9	4.52
	L10	12	4.53
	L40	11	4.41
	L70	7	4.21

These results obtained with the characterization of M16-derived catalysts, compared with the M17 previously reported means that:

1. Same qualitative trend was observed both for M16 and M17 treated in the same conditions. Regardless the precursor type and characteristics, the water favours the combustion at lower temperature (and time on stream) and, as a consequence, the transformation of the hemihydrate structure to the final catalyst, completing it before the carrier gas was switched to N_2.
2. The lower organics trapped in the precursor in the case of M16 react with oxygen in shorter time, as demonstrated by the micro GC analyses and the TGA (Figure 70) and when the combustion is over the catalysts has time to reorganize the structure in a more efficient way. This is demonstrated by the generally higher crystallinity for all the samples obtained starting from the M16 precursor, compared to the M17-derived catalyst calcined in the same condition (Figure 32).
3. Increasing the water fed (i.e. decreasing the oxygen molar ratio): (i) increases the VPP crystallinity, (ii) the Raman spectroscopy shows in L40 and L70 greater number of spectra characterized by the bands of VPP and (iii) the vanadium oxidation state decreases its value; this means that water not only favours the crystallinity, but there is a concomitant effect of oxygen that avoids over-oxidation of catalysts.
4. In contrast to the M17-derived catalysts, in the case of M16 also a dihydrate phase of $VOPO_4$ was detected in the diffractogram: this could be an important point to deepen because, in the reaction temperatures range, the dihydrate phase may convert to the more selective δ-$VOPO_4$.[42]
5. Under the same calcination atmosphere, the catalysts obtained from M16 presents an higher Vox; this is attributable to the lower carbon content (Cin), because when no more organic species are available for the combustion, the gaseous oxygen fed starts to oxidize the vanadium. In addition, M16 presents a higher amount of V^{5+} species in the precursor (0.04%, compared to 0.006% in M17), this could be the second reason for the higher vanadium oxidation state found in the M16-derived catalysts.

Reactivity test and characterization of used catalysts

By performing the selective oxidation of *n*-butane in the same conditions used for M17-derived catalysts, has been obtained the results reported in Figure 75, in terms of *n*-butane conversion (blue

rhombus) and selectivity in MA (red square) and CO+CO_2 (COx) (orange circle) plotted as a function of temperature. Other products (not reported) are acetic acid, acrylic acid.

Catalytic tests were carried out in a continuous-flow fixed bed glass reactor. Catalysts are used in form of pellets sized in 30-40 mesh and the reactor was filled with steatite. The feed composition was: 1.7%mol of hydrocarbon, 17% of O_2 and the remain was inert. The products formed and the reagents not reacted are quantify using an online gas chromatograph equipped with two columns and two detectors, one TCD and one FID.

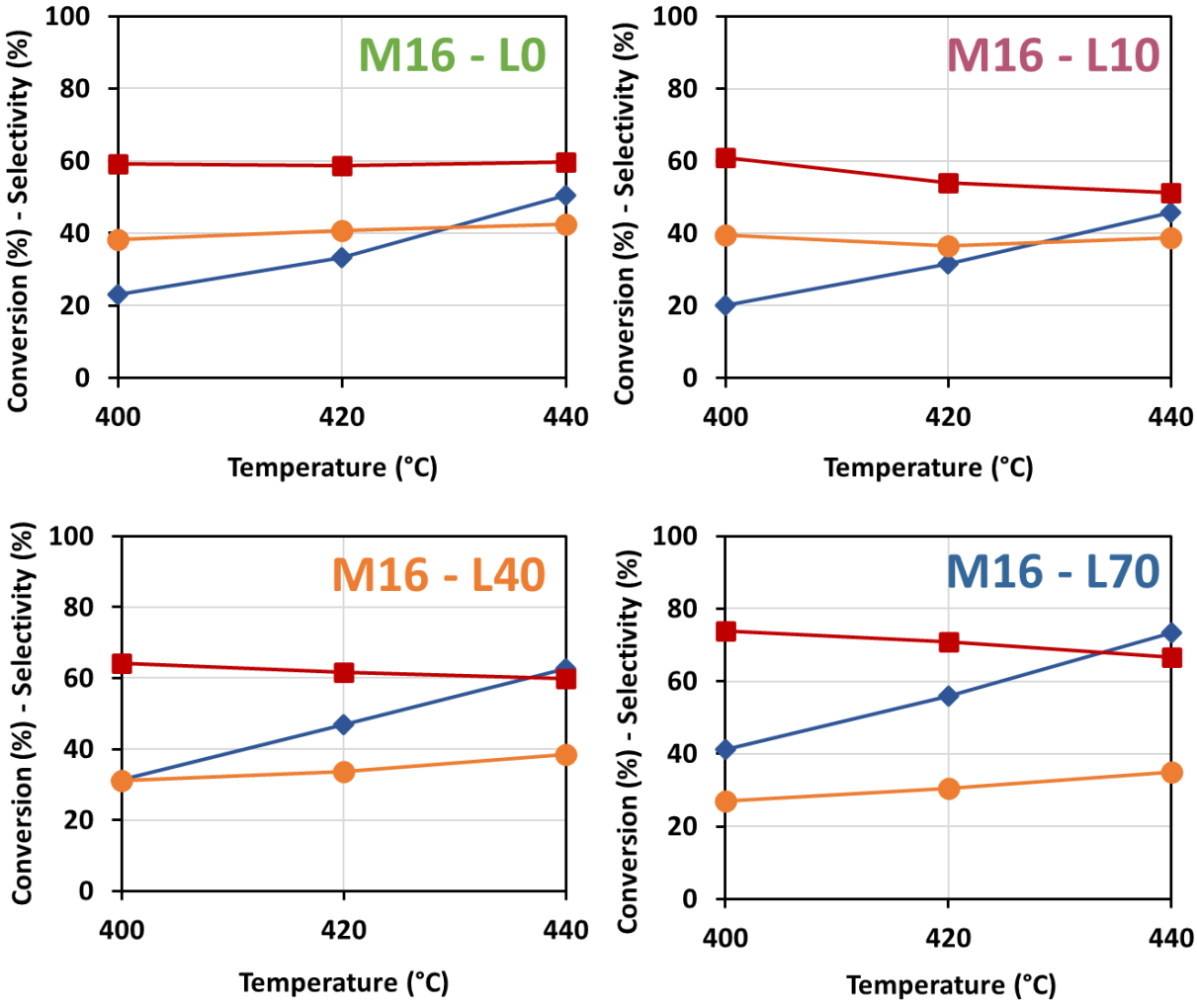

Figure 75. *n*-butane conversion (♦), MA (■) and COx (●) selectivities for the catalysts obtained calcinating M16 in different condition: L0 (100:0%mol Air:H_2O), L10 (90:10%mol Air:H_2O), L40 (60:40%mol Air:H_2O) and L70 (30:70%mol Air:H_2O).

Conditions: 1.7% *n*-butane, 17% O_2, W/F=1.33 g·s·mL^{-1}.

The key point of this work is in the correlation between the catalytic performance of the catalysts as a function of the precursor characteristics; to clarify this effect has been compared the results when

the two VHP were treated in the same water amount conditions, respectively Figure 76-top for the new one, M16, and Figure 76-bottom for the catalysts obtained starting from the first precursor studied, namely M17.

Regarding the reactivity of M16-derived catalysts, increasing the amount of water, from 0% used for the calcination of L0 (green) to 70% mol used in a mixture with air for the obtainment of L70 (blue), a gradually increasing in the conversion of *n*-butane occurs, due to the increases of vanadyl pyrophosphate as a main phase constituting the samples, as observed both in the XRD and Raman spectra. At the same time, it was also observed the increasing in MA selectivity: this results it is due to the lower over-oxidation that characterize the catalysts, because higher catalytic performance are achieved when the active layer is composed of VPP with patches of oxidized phase, well dispersed on the catalytic surface and in low amount.

Comparing the results obtained treating the two VHP in the same condition during the calcination:

- In general, catalysts obtained starting from the precursor M16 presents greater catalytic performance, in terms of conversion and yield/selectivity towards maleic anhydride, when the same calcination atmosphere were performed: for example, L0 obtained from M16 presents a conversion value equal to 23% with a selectivity in the desired product of 60%, rather than 12% and 19% respectively for L0 obtained treating M17 in anhydrous conditions. Same trends were observed for all the four catalysts. In both cases the catalysts that shown the best results are those obtained treating the precursor with a mixture of air and water with the molar ratio equal to 30:70%mol respectively (L70), even if the M16-derived one leads to the greater results: *n*-butane conversion was 41% and the selectivity to MA was 74%, at 400°C.
- For M16 increasing in conversion and MA selectivity were observed when the water fed during the calcination was increased; regarding the selectivity, it presents value higher than 60% for all the catalysts. M17-derived catalysts, on the other hand, presents very low activities and the selectivity increases its value with the increasing of water; for these latter the increasing in selectivity towards MA is much more marked with respect to the M16-derived catalysts, which correspond also the same (but opposite) trend in the selectivity of combustion products. The different trends in the selectivity observed for the two cases are probably caused by a different species that composed the active layer of VPP: it has been hypothesized that with M16-derived samples the same phases were presents in the surface layer, leading to the same selectivity; in the case of M17 it was found that the difference in selectivity were due to the different amount of α_I-$VOPO_4$ content found in the used catalysts.

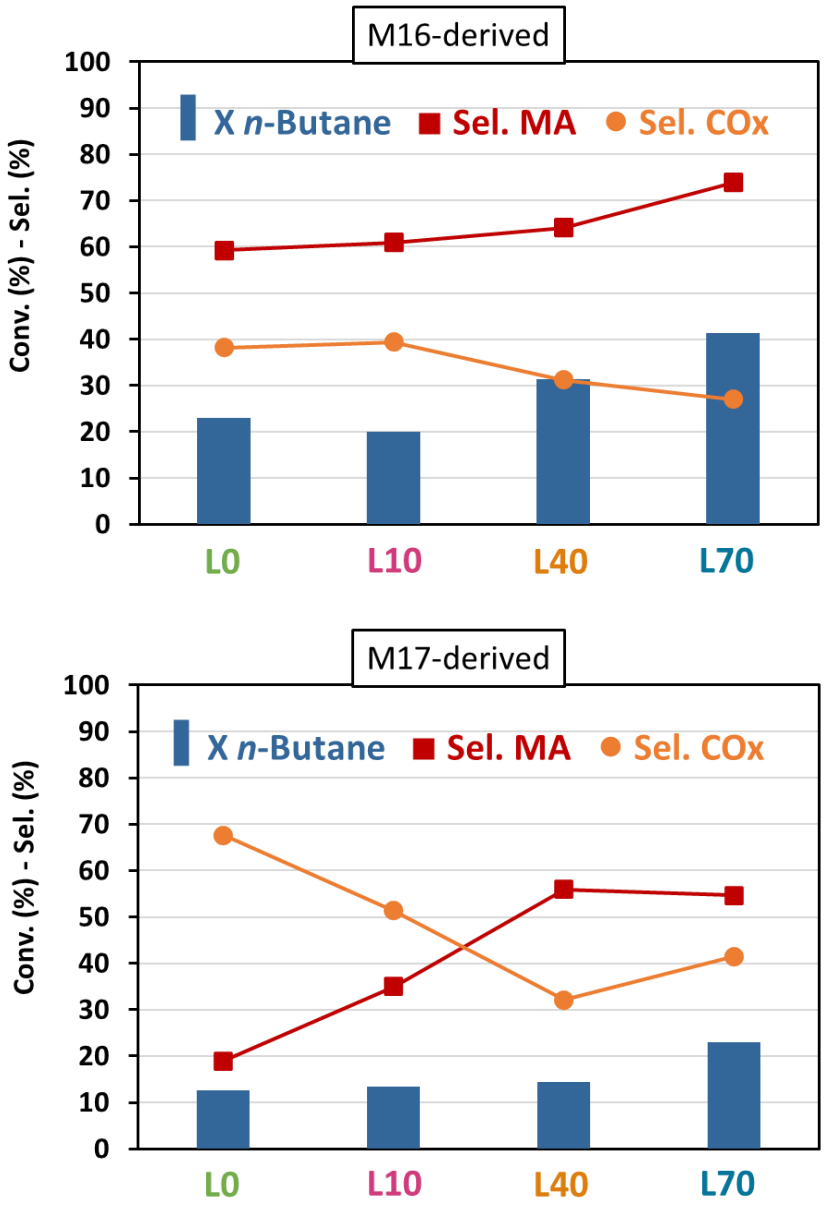

Figure 76. Catalytic behaviour for the catalysts obtained calcinating M16 (top) and M17 (bottom) in different environments. T=400°C, W/F=1.33 g*s/mL, *n*-butane:O_2:inert 1.7:17:remaining (%mol).

XRD pattern of used M16-derived catalysts, compared to the fresh, are shown in Figure 77.

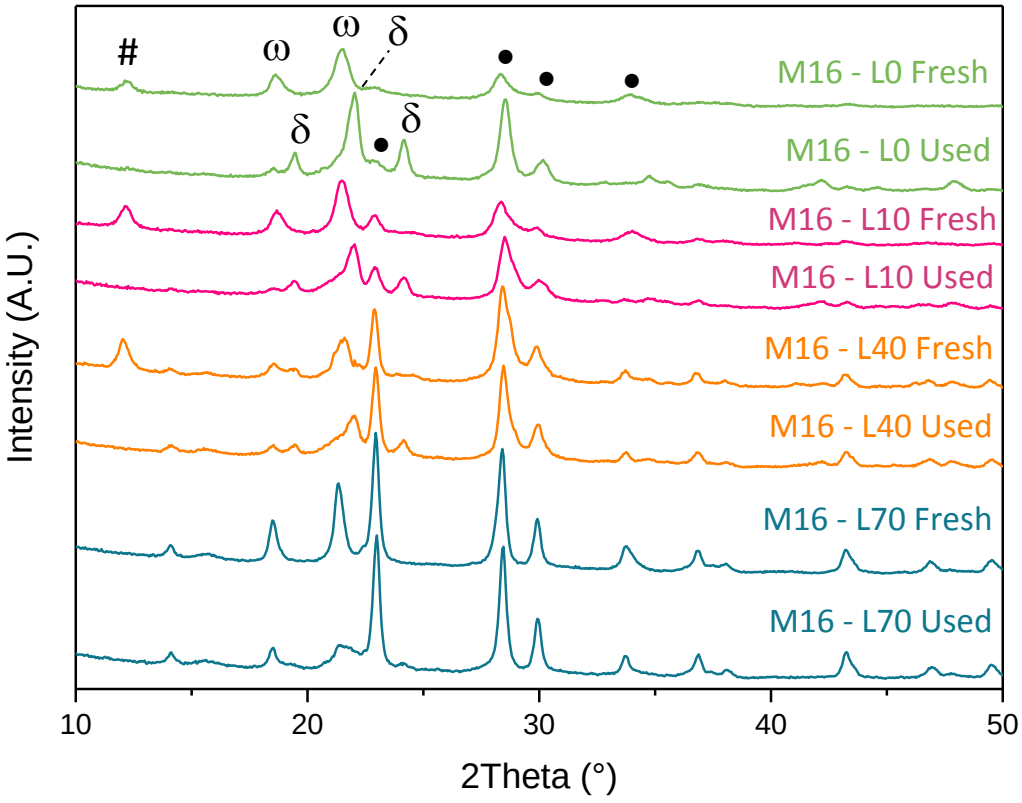

Figure 77. X-ray pattern of fresh and used L0, L10, L40 and L70 derived from the calcination of M16-VHP. Symbols: ω = ω-$VOPO_4$; δ = δ -$VOPO_4$; # = $VOPO_4 \cdot 2H_2O$; ● = VPP.

The XRD patterns of calcined and used sample contain the reflection of VPP (●) and also lines attributable to V(V) phosphates (identified by the symbols #, ω and δ).

In the fresh L0, L10 and L40 pattern, reflections are attributable to ω-$VOPO_4$ (main peaks at 18.6° and 21.4°) and to a hydrated oxidized V/P/O, namely $VOPO_4 \cdot 2H_2O$ identified by the lines at 2θ=12.1°, 18,6° and 28.2° (very strong, strong and medium respectively). The differences is the crystallinity (and also the amount, due to the decreasing in Vox previously determined) of the VPP phase.

In the used catalysts the phase detected are slightly different:

- No more dihydrate phase (#) was found at 12.1°.
- The main $VOPO_4$ phase was not the ω (as attributed in the fresh) but the δ, identified by the shift at higher angle relative to the most intense peaks at 19.4° and 22° (in the ω they were centred at 18.6° and 21.4°), and it was also observed the formation of a new reflection at 24.1°.

In the case of the catalyst L70, instead, no dihydrate oxidized phase was detected in the fresh catalyst, it presents only pattern related to VPP (●) and ω-$VOPO_4$. After reaction the it presents VPP and ω as well, and traces in δ-$VOPO_4$ was also found (even if with very poor crystallinity).

The characterization of the most superficial phases was performed as usual using the Raman spectroscopy because it is more sensitive to the "surface" (ca. 1μm depth) than XRD. The Raman analyses of used catalysts are shown in Figure 78-Figure 81.

Catalyst L0 and L10 showed the presence of δ-$VOPO_4$ and $VOPO_4 \cdot 2H_2O$; sample L40, in addition to the previous two phases, permits the identification of the most important band related to the VPP (centred at 927 cm^{-1}) partially overlapped with the one of δ-$VOPO_4$ at 936 cm^{-1}. Finally, sample L70 shows the presence of VPP as a major compound, but also bands due to the presence of δ-$VOPO_4$ were also been identified, even if the latter was not clearly presents in the XRD, meaning that this phase is present in form of dispersed patches over the VPP: from the literature is already known that this features is related to an highly active and selective catalyst, in fact it is the one with the best performance compared to the other samples obtained calcinating both M16 and M17 precursors in different environments[72,81,82].

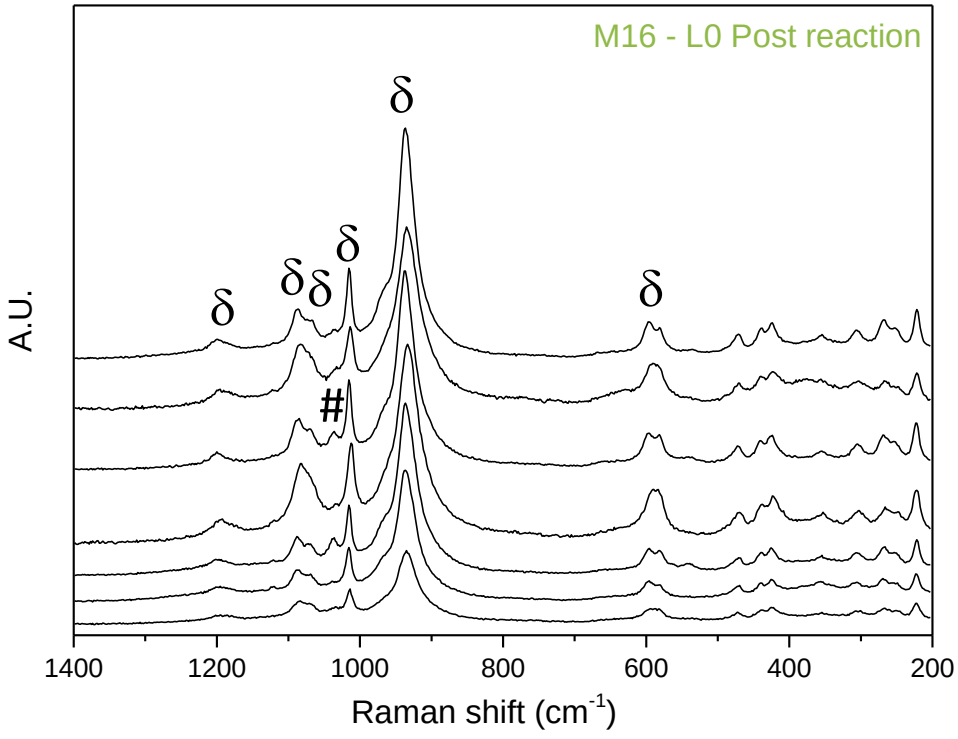

Figure 78. Raman spectra taken at different spots for used L0. Symbols: δ = δ -$VOPO_4$; # = $VOPO_4 \cdot 2H_2O$.

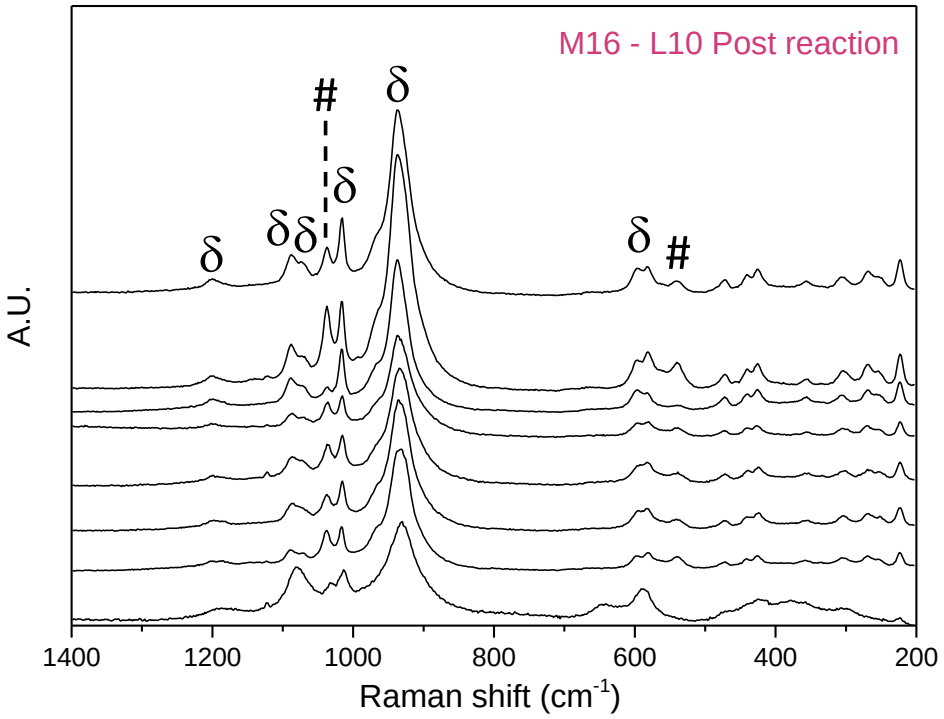

Figure 79. Raman spectra taken at different spots for used L10.

Symbols: δ = δ -$VOPO_4$; # = $VOPO_4 \cdot 2H_2O$.

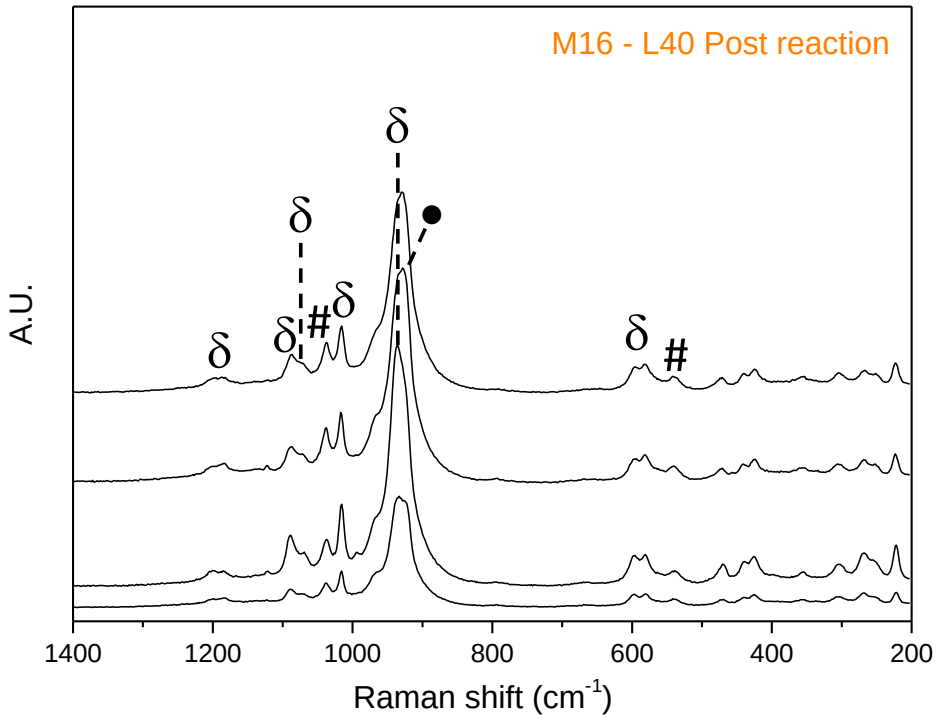

Figure 80. Raman spectra taken at different spots for used L40.

Symbols: δ = δ -$VOPO_4$; # = $VOPO_4 \cdot 2H_2O$; ● = VPP.

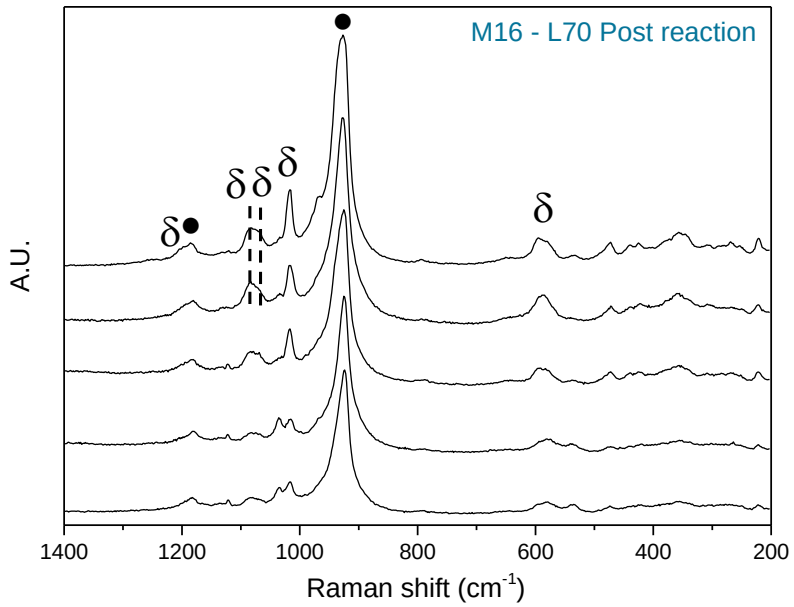

Figure 81. Raman spectra taken at different spots for used L70. Symbols: δ = δ -$VOPO_4$; ● = VPP.

In conclusion, the analysis of spent catalyst confirms the hypothesis of a change in orthophosphate phase composing the catalysts from the ω- to its allotropic form, namely δ-$VOPO_4$. This feature was reported in the literature to occurs when air or inert gas was fed at 400°C in a mixture with *n*-butane, in our case 1.7%mol of hydrocarbon with air[38].

4.8.3. Relationship between structure and catalytic performance

In order to explain and better understand the difference in catalytic performance related to the different morphologic characteristics of the precursor tested, a resume of the textural properties, with particular attention to the phases that compose each catalysts, are reported in Table 12.

It should be noted that in brackets are indicated the phases present in considerably lower amount or in traces.

Table 12. Resuming table of the catalysts tested for the selective oxidation of *n*-butane, after calcination (fresh) and after reaction (used).

Symbols: VPP=$(VO)_2P_2O_7$; $2H_2O$=$VOPO_4 \cdot 2H_2O$; δ = δ -$VOPO_4$; ω = ω-$VOPO_4$; α_I = α_I -$VOPO_4$.

VHP	Name	Phase in fresh catalyst		Phase in used catalyst	
		XRD	*Raman*	*XRD*	*Raman*
M16	**L0**	$2H_2O$; ω	ω; (α_I)	δ	δ; ($2H_2O$)
	L10	$2H_2O$; ω; (VPP)	$2H_2O$; ω	δ; (VPP)	δ; ($2H_2O$)
	L40	$2H_2O$; ω; VPP	$2H_2O$; VPP	δ; VPP	δ; VPP; ($2H_2O$)
	L70	ω; VPP	VPP; $2H_2O$	VPP; (ω; δ)	VPP; δ
M17	**L0**	ω	$2H_2O$; α_I; (VPP;ω)	α_I; (VPP; ω)	α_I
	L10	ω; (VPP)	$2H_2O$; ω; VPP	ω; VPP; α_I	α_I
	L40	ω; VPP	ω; VPP; $2H_2O$	VPP; α_I; (ω)	α_I; (VPP; δ)
	L70	VPP; (ω)	ω; VPP; $2H_2O$	VPP; (ω)	α_I; VPP; δ

Comparing the phases found in the fresh catalysts obtained from M16 and M17, the main difference is in the presence of vanadyl orthophosphate dihydrate ($2H_2O$) both in the bulk and in the most superficial layers, in the catalysts obtained starting from M16-VHP in different conditions. This represents one of the main phases constituting the samples after calcination. In the case of M17-VHP, the catalysts obtained using different amount of water have shown the presence of ω and VPP (in different amount, as discussed in the previous chapter) as principal phases, together with $VOPO_4 \cdot 2H_2O$, even if it was found not in all the samples and just only in the Raman spectra.

After the reaction an interesting change in phase composition occurred: M16 leads to the formation of δ-$VOPO_4$, whereas M17 shows the presence of α_I-$VOPO_4$ as the main V(V) phosphates.

Experimental evidence reports that small difference in P/V atomic ratio have relevant effects on the surface composition, more importantly affecting the catalytic performance[42,45,83]. We assumed that the different behaviour observed with our catalysts could be caused by the slightly differences in P/V atomic ratio, which characterized the two precursors used: 1.15 for M17 and 1.20 for M16.

Both the precursors has been calcined in the same conditions (0, 10, 40 and 70%mol of water, the remaining part was air), but both in the fresh and used catalyst they leads to the formation of different phases. In the case of lower P/V atomic ratio (M17), during reaction, the α_I-$VOPO_4$ phase was formed by the topotactic dehydration of $VOPO_4 \cdot 2H_2O$; if this phase constitutes the active layer and it is dispersed on the surface of VPP, is considered to be an active but not selective (in MA) phase, leading

to the worst performance. Our experimental results shown, in fact, a relevant formation of COx (with selectivity higher than MA); the very low conversion is due to the fact that α_I-$VOPO_4$ was not presents only as a dispersed phase on VPP surface, but it constitutes also the core of the catalyst. A decreasing in this phase, observed in the diffractograms, leads to the formation of VPP and, as a consequence, a highly active catalyst. On the other hand, when the precursor is characterized by an higher P/V atomic ratio (M16), the behaviour was different: the active layer was made up of δ-$VOPO_4$ and an improvement in MA selectivity can be obtained. Moreover, this phase is formed, in our catalyst, by two processes that occur simultaneously:

1. The first one is related to the not reversible dehydration of $VOPO_4 \cdot 2H_2O$ occurring in the reaction temperature range. The dihydrate phase was formed in wet air conditions when the P/V was equal or higher than 1.20. The great presence of this phase and the highly amount of water formed due to its in-situ dehydration to form δ-$VOPO_4$, could have a positive effect: Cavani et al. demonstrate that water prevents the non-reactive irreversible adsorption of *n*-butane and favours the desorption of products.[42,45]
2. The second formation of the selective δ- phase was due to the rapid transformation that undergoes the ω-$VOPO_4$ under our experimental conditions (400°C, 1.7% *n*-butane in air).[38]

In the characterization of L70 derived from M16, no dihydrate was observed by XRD and lower amount of vanadyl orthophosphate in the δ-form was observed: this means that the selective phase was formed only with the second route (i.e. starting from the ω). This sample shows the best catalytic behaviour because containing the lower fraction of V^{5+}: we confirm that the main peculiarity of the VPP with the best performance is the one that generate in-situ domains of δ-$VOPO_4$ dispersed on the vanadyl pyrophosphate surface. Moreover it has been demonstrated that also the intrinsic properties of precursors used are crucial: a lower carbonium content and/or the higher P/V atomic ratio affect the phases formed both during the calcination and the reaction, improving the catalytic performance.

4.8.4. The role of the diluting agent

Ascertained the important effect of a slight excess of phosphorous found when the vanadyl hydrogenphosphate hemihydrate (VHP) was calcined in different atmosphere and, even more, considering that the best results has been found when only 30%mol of air was used as a carrier gas during the thermal treatments, it has been decided to change the diluting agent from 70% of water to 70% of nitrogen and a mixture of water and nitrogen respectively 10:60%mol. The same feeding

mixture were previously performed also with the M17 precursor, leading to the best performing catalysts.

In Figure 82 are reported the heating ramp and the conditions in the inlet stream; as for M17, the catalysts obtained with the three conditions were renamed L70 (in which 70%mol of water was used and the remaining 30% was air), L70-N means that the 70%mol was nitrogen (and the remain air), finally L10:60 was obtained after calcination with a mixture of air:water:nitrogen equal to 30:10:60%mol.

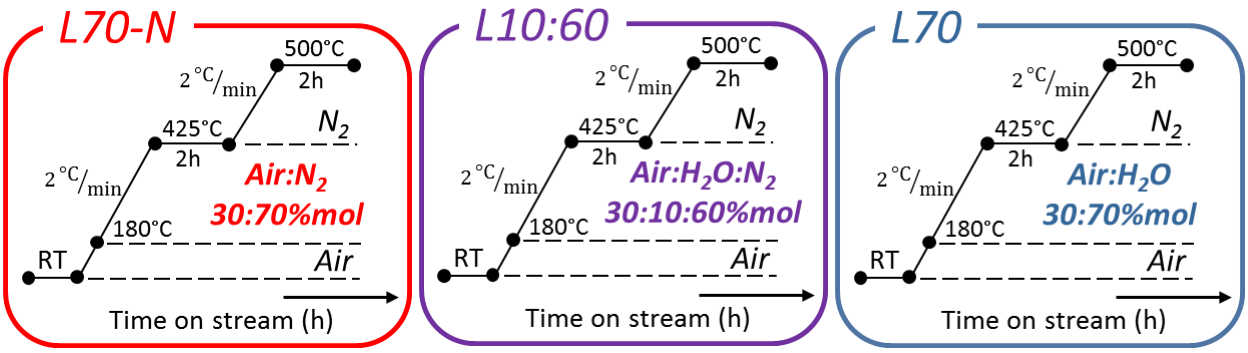

Figure 82. Heating ramp and feeding gas used for the obtainment of L70-N, L10:60 and L70 from M16-VHP.

The catalysts were obtained calcinating M16 in a lab-scale reactor and the outlet stream was analysed for the entire thermal treatment, with the aim of identify and quantify the reagents consumed and the products formed due to the oxidation of the carbonaceous species and the dehydration of VHP structure to obtain the VPP. The trend of oxygen consumption and CO_2 formed, reported in Figure 83, are consistent with all the previous discussions: in anhydrous conditions, leading to the formation of L70-N, the combustion is slowed down by the absence of water. In fact, in the temperature range in which has been proven to occurs the dehydration of VHP and the burning of organic molecules (350-425°C) the maximum molar ratio of CO_2 registered by the micro GC was about 1%mol/mol. The remaining part of the carbonaceous species are then released when the temperature reaches 500°C, even if the carrier gas was nitrogen (i.e. inert). The latter release could be caused by a further combustion due to the high temperature or, alternatively, the CO_2 previously formed, when also oxygen was fed, remain trapped inside the structure and the high temperature favours its desorption. Just adding 10%mol of water, that probably penetrates inside the structure favouring the release of water and carbon dioxide (Figure 83-middle), the combustion is completed during the isotherm at 425°C; same trend was observed also with 70%mol of water (Figure 83-bottom), meaning that also with a different precursor, a small amount of water is enough to complete the combustion within 425°C and obtain a well-crystallized catalyst.

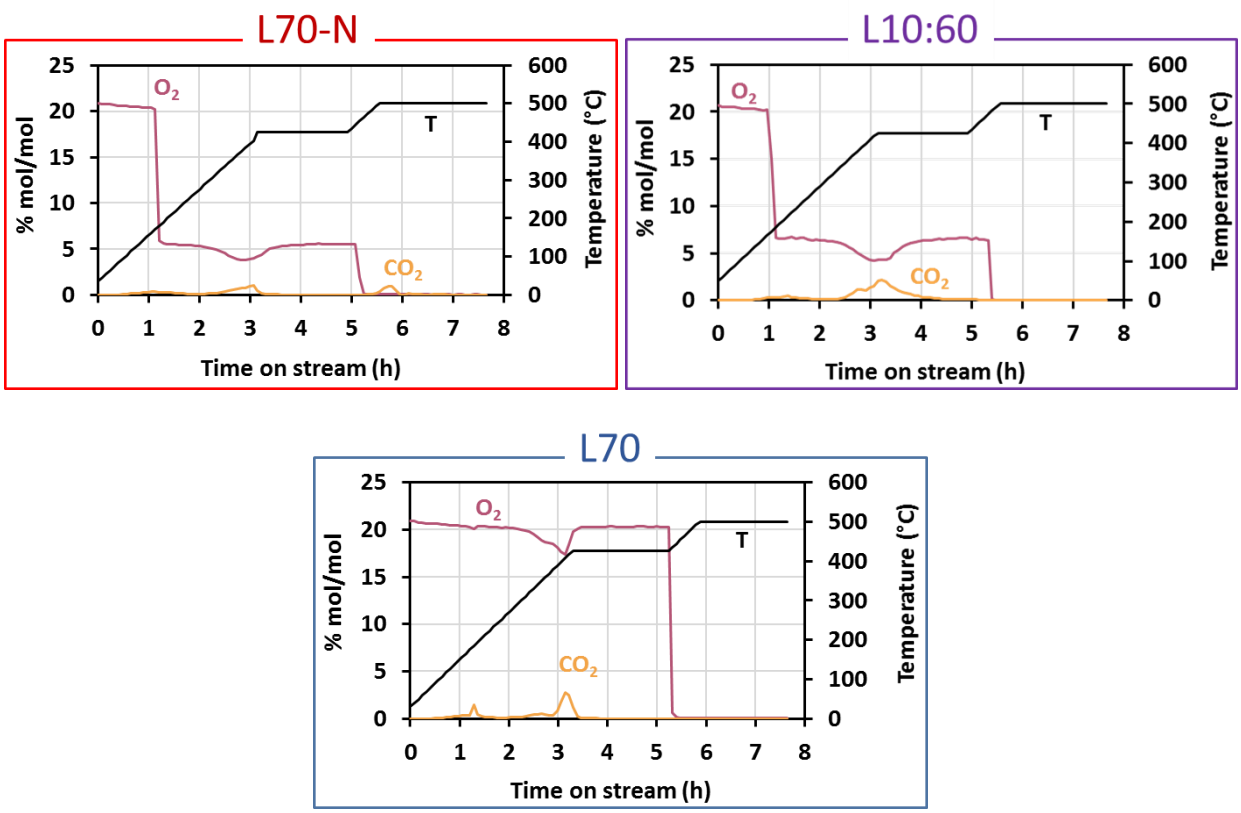

Figure 83. Oxygen consumption (pink) and carbon dioxide formed (orange) during the formation of L70-N (top, left), L10:60 (top, right) and L70 (bottom).

Comparing the X-ray diffractograms and the mean vanadium oxidation state determined by titration (Figure 84 and Table 13), the fresh catalysts results to be mainly constituted of VPP (●), and also characteristic reflections attributable to ω-$VOPO_4$ (ω) has been found. All the three samples present the same crystalline phase, meaning that, surprisingly, the water is not involved in the formation of the active phase (vanadyl pyrophosphate). The absence of dihydrate phase in the bulk was due to the poorly oxidant conditions used for the obtainment of these catalysts: this condition disadvantages the over-oxidation, as mentioned in the previous paragraph for L70, so the VPP is partially oxidized to form only the ω- phase.

The Vox are the same in the three cases, considering the experimental error, thus demonstrating that all the catalysts are composed of the same phase, in the same amount, the only difference is due to the crystallinity related to the quantity of steam fed during the calcination: increasing the molar ratio of water, causing an increases also of the crystallinity.

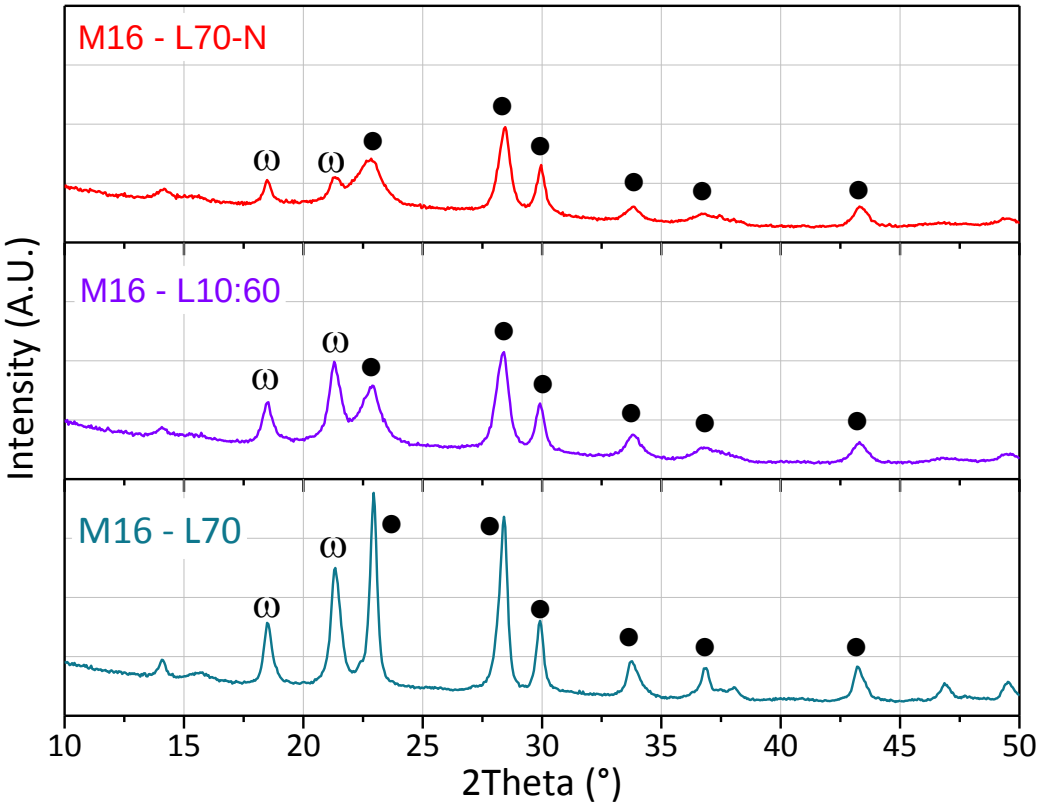

Figure 84. X-ray pattern of the samples after calcination changing the diluting agent. L70-N (red) 30:70%mol Air:N_2; L10:60 (purple) 30:10:60%mol Air:H_2O:N_2; L70 (blue) 30:70%mol Air:H_2O.

Table 13. Surface area (BET) and vanadium oxidation state for the catalyst obtained calcinating M16 and M17 with 30%mol of air.

	Catalyst	SSA (m^2/g)	Vox
M16-derived	**L70-N**	16	4.21
	L10:60	19	4.33
	L70	17	4.27
M17-derived	**L70-N**	14	4.25
	L10:60	11	4.19
	L70	7	4.21

After calcination, butane/air mixture was fed and catalytic tests were performed. The temperature range investigated was from 400 to 440°C, the feed composition was: 1.7%mol *n*-butane, 17% O_2 and W/F=1.33g·s·mL^{-1}. In Figure 85 are plotted the conversion of hydrocarbon (♦), the selectivity in MA (■) and in COx (●) in function of temperature for each catalyst.

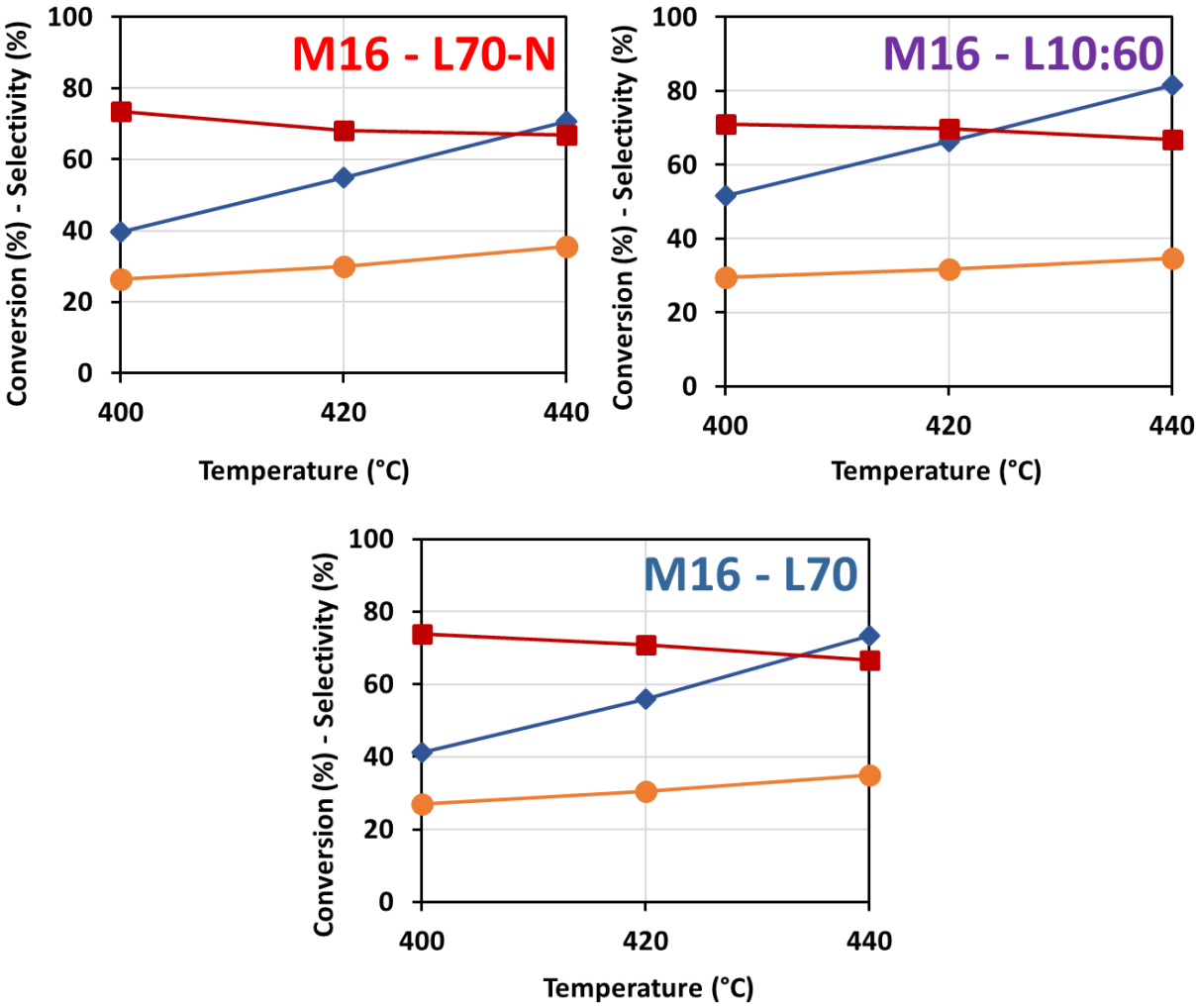

Figure 85. *n*-butane conversion (♦), MA (■) and COx (●) selectivities for the catalysts obtained calcinating with 30%mol of air and 70%mol N_2 (L70-N, red), 10:60%mol H_2O:N_2 (L10:60, purple) and 70%mol H_2O (L70, blue). Conditions: 1.7% *n*-butane, 17% O_2, W/F=1.33 g·s·mL^{-1}.

The catalysts show very high performance, reaching 70% of selectivity in the desired product in all the three cases. In particular:

- L70-N and L70 presents the same trend both in terms of *n*-butane conversion and selectivity in maleic anhydride and carbon oxides: the conversion increases with temperature from 40% to 70% at the maximum temperature investigated; at the same time a small increases in COx was observed, but it is important to note that the selectivity in MA remains constant throughout experiments. This means that during the equilibration period, carried out before each reactivity test at 400°C in reactive mixture, the phases formed over the catalytic surface are stable and do not undergo changes during the reaction. Analysing the Raman spectra of the fresh (left) and used (right) catalysts (Figure 87), they presents VPP (●) as a main phase but small differences in the V(V) phosphates also presents of the superficial layers has been

found: L70-N presents only δ-$VOPO_4$ (δ) while L70 presents the $VOPO_4 \cdot 2H_2O$ (#), probably because the large amount of water used during the calcination promote the formation of V^{5+} species in the hydrate form. During reaction the latter dehydrate leading to the formation of superficial δ- as well and consequently the two catalysts presents the same reactivity. The different conversion expected due to the different disorder along (200) plane (2θ=23°) in the VPP pattern (XRD of fresh and used catalysts reported in Figure 86) is probably compensated by the very high crystallinity that characterize all the reflections of L70, compared to the L70-N which presents general lower crystallinity, probably due to amorphous compound, since the characteristic bands at 1185, 1135 and 927 cm^{-1} were quite broad and of low intensity.

- L10:60 instead presents in the fresh catalyst VPP, ω-$VOPO_4$ and just one spot presents pattern attributable to α_I-$VOPO_4$, the latter phase it is known to enhance the activity of the catalyst when it is presents on the surface layer in very small amount and well dispersed; it does not influence the selectivity, in fact it presents the same value as for the previously descripted L70 and L70-N.

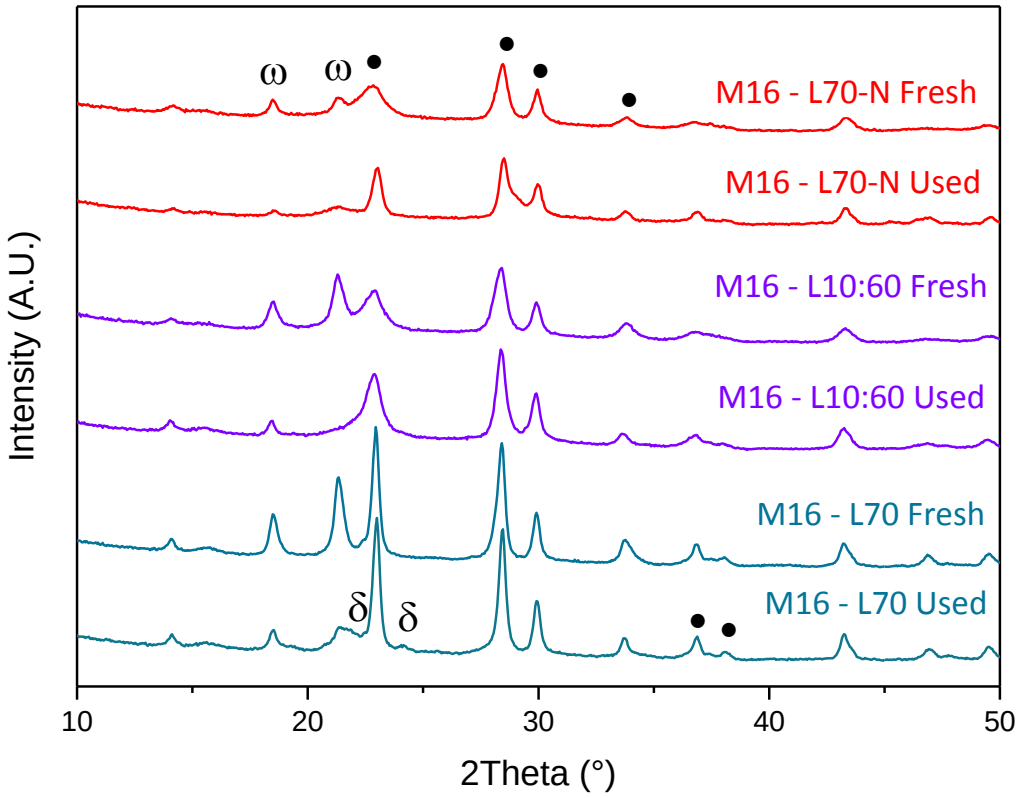

Figure 86. X-ray diffraction pattern of fresh and used L70-N, L10:60 and L70 derived from the calcination of M16-VHP. Symbols: ω = ω-$VOPO_4$; δ = δ -$VOPO_4$; ● = VPP.

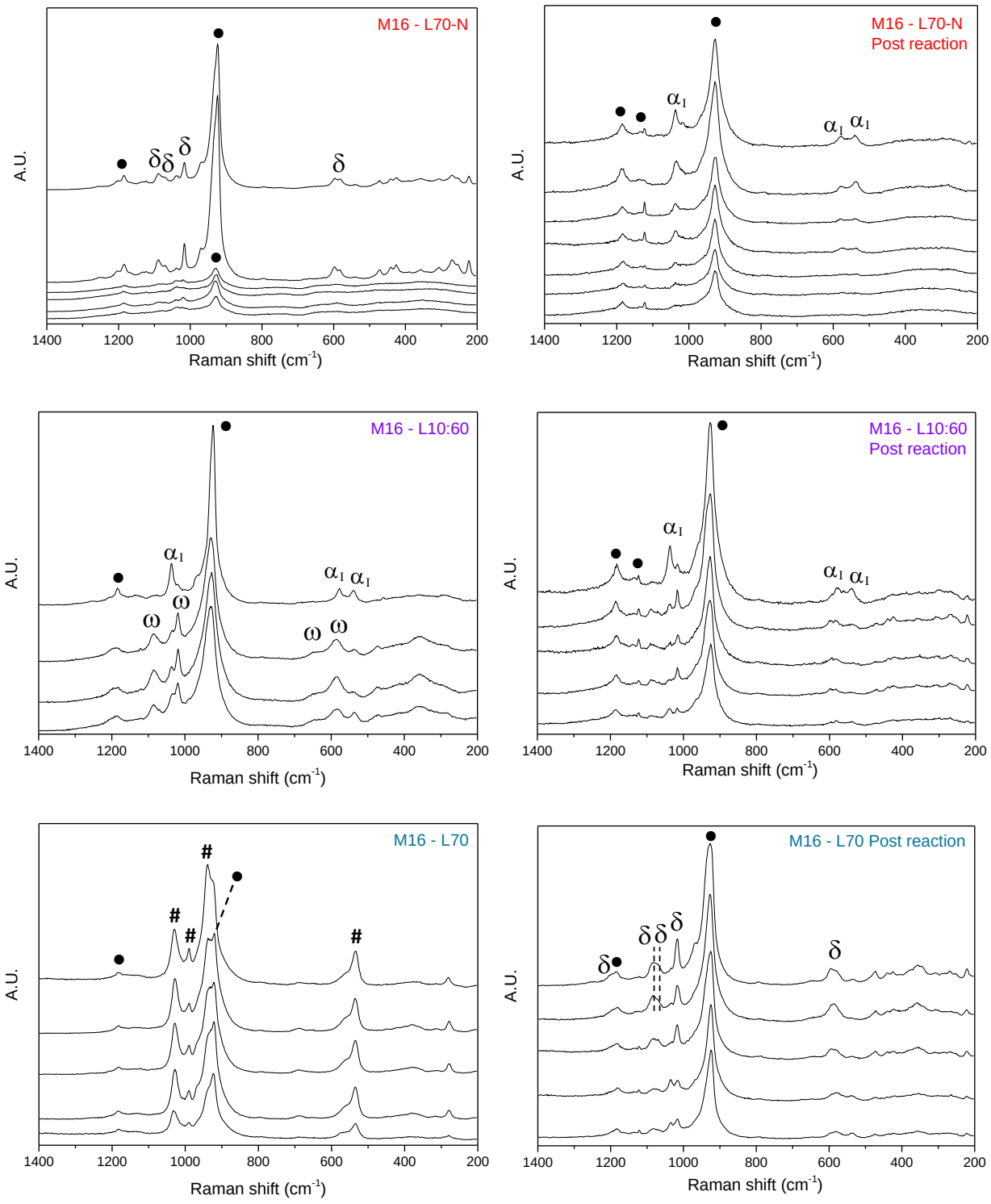

Figure 87. Raman spectra of L70-N (red), L10:60 (purple) and L70 (blue) after calcination (left) and after reaction (right). Symbols: δ = δ -$VOPO_4$; # = $VOPO_4 \cdot 2H_2O$; ● = VPP ; ω = ω -$VOPO_4$; α_I = α_I -$VOPO_4$.

Since the final aim is to find out the difference in terms of catalytic performance exhibited by different types of precursor, characterized by different chemical and physical properties, Figure 88 compares the catalytic performance of the samples obtained with 30%mol of air starting from the precursor

M16 (left) and M17 (right), at the constant temperature of 400°C, as previously used for all the comparison.

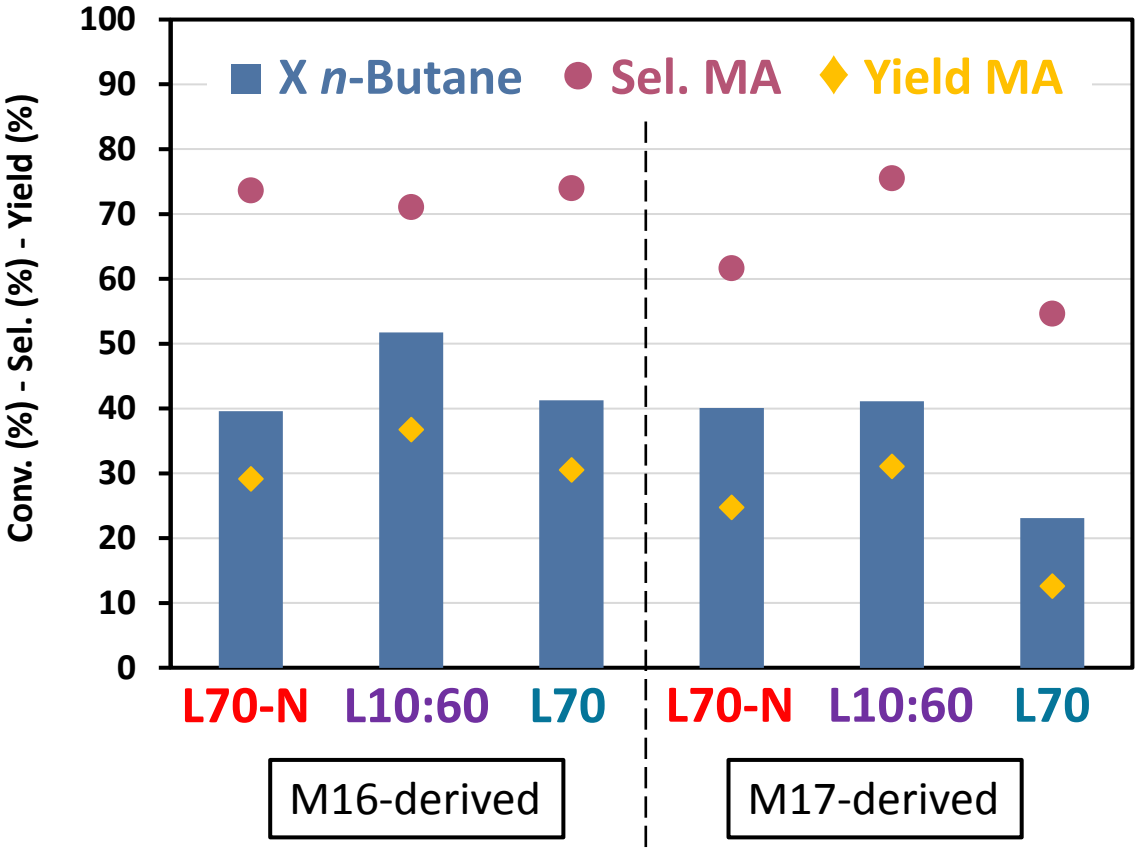

Figure 88. Conversion of *n*-butane (blue bar), selectivity in MA (pink circle) and yield in MA (yellow rhombus) for the catalysts obtained starting from the M16-VHP (left) and M17-VHP (right). Reaction conditions: T=400°C, W/F=1.33 g*s/mL, *n*-butane:O_2:inert 1.7:17:remaining (%mol).

The M16-derived catalysts present very high selectivity in the product of interest, with a value just over 70% (pink circle) in all the cases. In particular, the higher conversion of *n*-butane observed for the M16-L10:60 (52% at 400°C) makes it the best catalyst compared to the other tested so far, with a yield in MA at 400°C equal to 37%mol.

Regarding the conversions: during the discussion of L70-N, L10:60 and L70 obtained starting from M17 it was assumed that the higher activity of the first two catalysts was due to the increased disorder observed in the X-ray diffractograms along (200) plane of VPP. In the case of M16-derived catalysts the higher conversion which was expected for L70-N, due to the highly disorder along (200) planes of VPP is compensated by the very high crystallinity observed in X-ray diffractogram of L70. L10:60

probably has the best compromise between disorder which favours the activity of the catalyst and the crystallinity due to low amount of amorphous species.

Analysing the results, it can be concluded that regardless the type of precursor, its chemical-physical characteristics and its morphology, calcinating with poorly oxidant condition (30%mol of air) allows to obtain, in all the cases, the highly performing catalysts, reducing the difference in terms of activity and selectivity obtained when equal heat treatments was applied to different precursor (unlike previously observed for the two precursors treated with different amount of oxygen, reported in Figure 76).

Moreover, in both cases studied (M16 and M17), the catalyst which leads to the best performance is the one obtained with the ternary mixture composed of 30:10:60%mol respectively of Air:H_2O:N_2, meaning that the simultaneous activities of air and water in a specific ratio are the key parameters for an efficient calcination.

To demonstrate the relationship between air and water and the catalytic performance, in Figure 89 has been reported the catalytic performance for the samples obtained treating M16 (full symbols) and M17 (open symbols) with different amount of water and air during the calcination step.

In particular, Figure 89-top reports the molar ratio of oxygen and water (red and blue bars respectively) and the conversion of *n*-butane (rhombus, black lines); on the other hand bottom of Figure 89 shows the molar ratio of oxygen and water (red and blue bars respectively) and the yield in maleic anhydride (square, black lines).

The comparison has been made up considering the five catalysts in which air, water or a mixture of the two were fed. The atmosphere performed are resumed in Table 14 and the heating ramp used was the same for all the catalyst (Figure 71).

Table 14. Data used for the construction of volcano plot.

	H_2O	O_2	X *n*-butane		Yield MA	
Catalyst	**(%mol)**	**(%mol)**	*M16*	*M17*	*M16*	*M17*
L10	10	18.9	20	13	12	5
L10:30	10	12.6	26	10	17	6
L40	40	12.6	31	14	20	8
L10:60	10	6.3	52	41	37	31
L70	70	6.3	41	23	30	13

Note that the catalyst L10:30 has been obtained calcinating the precursors with a ternary mixture

composed of air:H_2O:N_2 in 60:10:30%mol, thus using the same molar ratio of air as for L40 and the same amount of water used for the synthesis of L10. The characterization (not reported) shows the same phases as in L40 (in fact they have been treated in the same oxidizing conditions), but with lower crystallinity, due to the lower amount of water used.

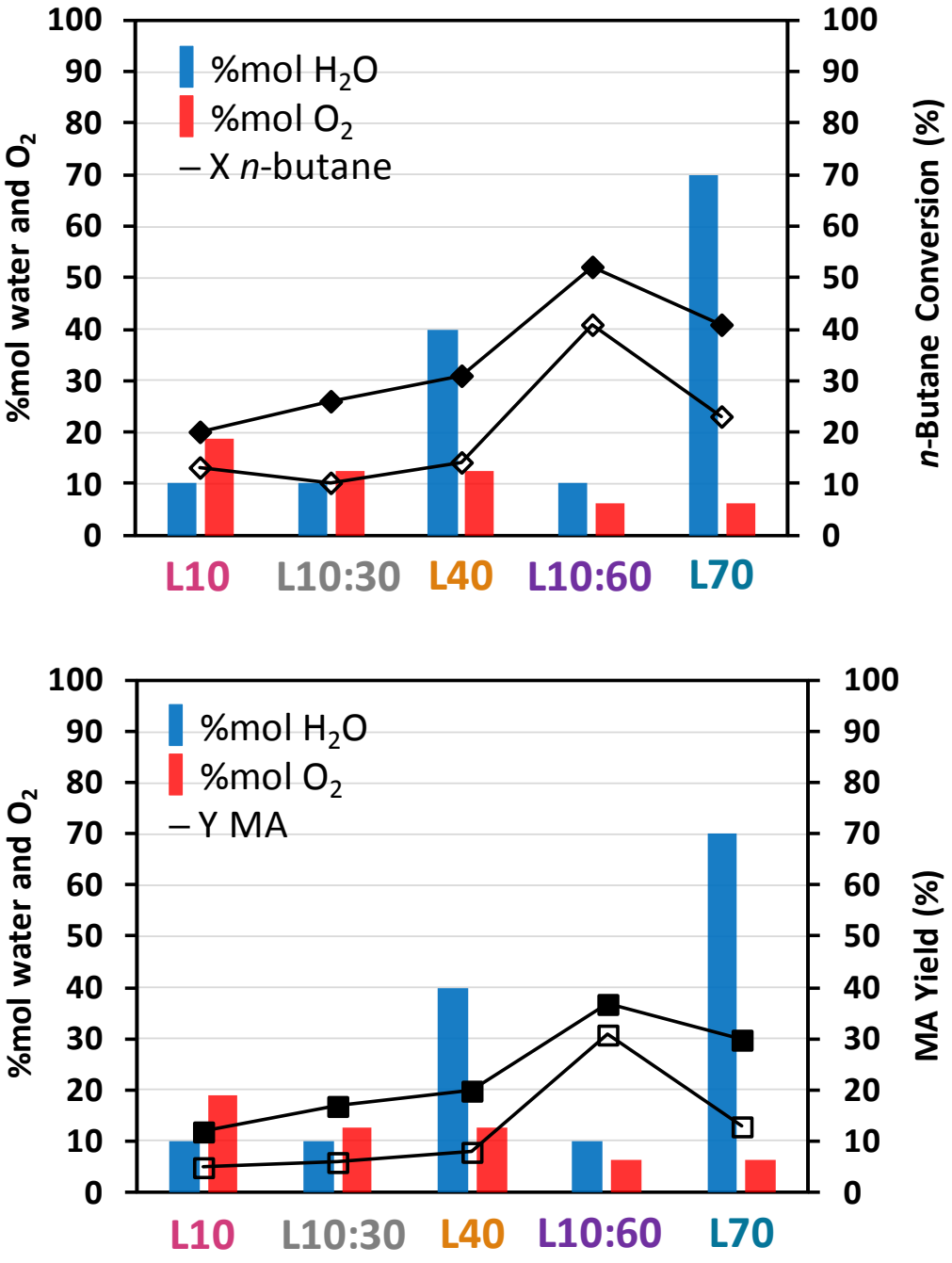

Figure 89. ***n*-butane conversion (top, ♦ ◊) and MA yield (bottom, ■ □) as a function of O_2 (red bars) and H_2O (blue bars) molar content in the calcination atmosphere for M16 (full symbol) and M17 (open symbol). Data are ordered with decreasing amount of oxygen from left to right.**
Reaction conditions: T=400°C, W/F=1.33 g*s/mL, *n*-butane:O_2:inert 1.7:17:remaining (%mol).

Both the M16- and M17-derived catalysts show the same trend, in the case of M17 (full symbol) it's shifted to lower conversion and yield values due to the worse performances registered, to the parity of calcination condition with M16-obtained catalysts, depending on the different species formed in the active layer. Such plots can be assimilated to a "volcano plot" because of their shape passing through a maximum referred to the results of L10:60. Moreover, the same trend was observed both in terms of activity and plotting the yield in the desired product maleic anhydride.

Thus demonstrating that the type of precursor influences the phases formed during reaction and, as a consequence, the related catalytic performance but, regardless the intrinsic characteristics of VHP, performing the calcination with the mixture 30:10:60%mol air:water:nitrogen leads to obtain the best catalytic results.

5. Conclusions

Several topics has been investigated and discussed in this thesis, with the focus on the study of the calcination process and the parameters that affect this sensitive procedure. The final aim is to find out a reproducible method, regardless the precursor characteristics, to improve the catalytic behaviour of vanadyl pyrophosphate (VPP) in *n*-butane oxidation into maleic anhydride (MA).

All the work has been possible thanks to the financial and scientific support of Polynt S.p.A.

The results obtained pointed out the role of both water and oxygen during the calcination step in order to obtain an active and selective V/P/O catalyst.

From the combination of XRD and Raman characterization of the materials we were able to correlate the conditions used in the heat treatment to the phases formed and, last but not least, to the catalytic activity.

In particular, by increasing the percentage of steam, and as a consequence decreasing the molar ratio of oxygen fed during the calcination, a greater crystallinity and an increased amount of the active phase, VPP, with respect to $VOPO_4$, has been observed. As a consequence, materials with both an enhanced catalytic activity and selectivity toward maleic anhydride has been obtained.

In particular, we found that only limited amount of water is necessary in order to promote the crystallinity of the obtained phases, while the amount of oxygen can also be effectively limited by co-feeding an inert diluent (e.g. nitrogen), finally decreasing the costs associated with the generation of huge amount of steam in the case of industrial applications.

Using the calcination conditions optimized according to the above observations, we were able to get a highly active and selective catalyst, with a hydrocarbon conversion of 40% and MA selectivity of 75% also at the lower temperature investigated (400°C). This material renamed L10:60, was obtained by treating the M17 precursor with a ternary mixture of air, H_2O and N_2 in the molar ratio equal to 30:10:60% respectively.

Also the heating ramp used is important. Indeed, just by adding 1h of isotherm at the temperature of 350°C the selectivity toward MA increases of 25 percentage points compared to the “standard” temperature ramp. This could be probably be ascribable to an increased efficiency in the crystallization and reorganization of the structure during the conversion of VHP to VPP, thanks to the extended time.

Ascertained the importance of the atmosphere used for the calcination, also the intrinsic properties of precursors used are crucial: comparing M17 and M16 derived catalysts when treated in the same conditions, the latter presents enhanced catalytic performances. The first reason could be in the P/V atomic ratio: it is well known from the literature that lower P content led to the formation of un-

selective species, in fact the catalysts obtained calcinating M17 (which presents lower P/V with respect to M16) in the characterization post-reaction presents α_I-$VOPO_4$ phase. On the other hand, high P/V in M16, causes the formation of $VOPO_4 \cdot 2H_2O$ that, during reaction is dehydrated and give the selective phase δ-$VOPO_4$. The second point is the C content: probably the lower value for M16 (6344 ppm compared to 9490 for M17) permits its combustion during the thermal treatment in a shorter time; when the combustion is over the catalysts has time to reorganize the structure in a more efficient way.

In conclusion, the key parameter to obtain the highly performing catalyst is to be sought in the air and water specific amount: the design of L10:60, obtained treating the hemihydrate precursor with a mixture of air:H_2O:N_2 for both precursors, allowed to get the best catalytic performances, compared to the other tested in the same condition; this is possible thanks to the possibility to generate the right active sites on the catalytic surface, helping to drive the transformation of the hydrocarbon to the desired product.

In the light of the results obtained, future works regarding the modulation of calcination condition foreseeing the catalytic properties as a function of precursor characteristics will be performed also in the industrial scale, with the aim to generate a new catalyst generation with greater productivity.

Bibliography

(1) Maleic Anhydride - Chemical Economics Handbook https://ihsmarkit.com/products/maleic-anyhydride-chemical-economics-handbook.html.

(2) Felthouse, T. R.; Burnett, J. C.; Horrell, B.; Mummey, M. J.; Kuo, Y.-J. Maleic Anhydride, Maleic Acid, and Fumaric Acid. *Kirk-Othmer Encycl. Chem. Technol.* **2001**, No. 10.

(3) ECHA - https://echa.europa.eu/it/substance-information/-/substanceinfo/100.003.247.

(4) Hood, D. K.; Musa, O. M. *Handbook of Maleic Anhydride Based Materials*; 2016.

(5) www.polynt.com.

(6) European Environmental Agency. *EEA Report No 12/2018*; 2018; Vol. 12.

(7) For Italy: Decreto Ministeriale n°60, 2nd April 2002. For Italy: Decreto Ministeriale N°60, 2nd April 2002.

(8) Arpentier, P.; Cavani, F.; Trifirò, F. *The Technology of Catalytic Oxidation*, Technip.; 2001.

(9) Bither, T. A. J. Catalyst for Vapor Phase Oxidation of N-Butane to Maleic Anhydride. US Patent 4442226, 1984.

(10) Pavarelli, G.; Velasquez Ochoa, J.; Caldarelli, A.; Puzzo, F.; Cavani, F.; Dubois, J. L. A New Process for Maleic Anhydride Synthesis from a Renewable Building Block: The Gas-Phase Oxidehydration of Bio-1-Butanol. *ChemSusChem* **2015**, *8* (13), 2250–2259.

(11) Hernandez, R. A.; Ozkan, U. S. Structural Specificity of Molybdenum Trioxide in C4Hydrocarbon Oxidation. *Ind. Eng. Chem. Res.* **1990**, *29* (7), 1454–1459.

(12) Ozkan, U.; Schrader, G. L. NiMoO4 Selective Oxidation Catalysts Containing Excess MoO3 for the Conversion of C4 Hydrocarbons to Maleic Anhydride. II. Selective Oxidation of 1-Butene. *J. Catal.* **1985**, *95* (1), 137–146.

(13) McMurry, J. *Chimica Organica*; Piccin, E., Ed.; 2009.

(14) Cavani, F.; Trifirb, F. Some Innovative Aspects in the Production of Monomers via Catalyzed Oxidation Processes *. **1992**, (*88)*, 115–135.

(15) Centi, G.; Trifirò, F.; Ebner, J. R.; Franchetti, V. M. Mechanistic Aspects of Maleic Anhydride Synthesis from C4 Hydrocarbons Over Phosphorus Vanadium Oxide. *Chem. Rev.* **1988**, *88* (1), 55–80.

(16) Contractor, R. M.; Sleight, A. W. Selective Oxidation in Riser Reactor. *Catal. Today* **1988**, *3* (2–3), 175–184.

(17) Dummer, N. F.; Bartley, J. K.; Hutchings, G. J. *Vanadium Phosphate Materials as Selective Oxidation Catalysts*, 1st ed.; Elsevier Inc., **2011**; Vol. 54.

(18) Cavani, F.; Colombo, A.; Giuntoli, F.; Gobbi, E.; Trifirò, F.; Vazquez, P. Role of Surface

Properties of the Vanadyl Pyrophosphate in the Formation of Maleic and Phthalic Anhydrides by N-Pentane Oxidation. *Catal. Today* **1996**, *32* (1–4), 125–132.

(19) Johnson, J. W.; Johnston, D. C.; Jacobson, A. J.; Brody, J. F. Preparation and Characterization of VO(HPO4)•0.5H2O and Its Topotactic Transformation to (VO)2P2O7. *J. Am. Chem. Soc.* **1984**, *106* (26), 8123–8128.

(20) Cornaglia, L. M.; Caspani, C.; Lombardo, E. A. Physicochemical Characterization and Catalytic Behavior of VPO Formulations. *Appl. Catal.* **1991**, *74* (1), 15–27.

(21) Contractor, R. M.; Ebner, J. R.; Mummey, M. J. Butane Oxidation in A Transport Bed Reactor – Redox Characteristics of The Vanadium Phosphorus Oxide Catalyst. In *New Developments in Selective Oxidations*; Centi, G., Trifirò, F., Eds.; Elsevier Science, **1990**; p 553.

(22) Horowitz, H. S.; Blackstone, C. M.; Sleight, A. W.; Teufer, G. VPO Catalysts for Oxidation of Butane to Maleic Anhydride. Influence of (VO)2H4P2O9 Precursor Morphology on Catalytic Properties. *Appl. Catal.* **1988**, *38* (2), 193–210.

(23) Okuhara, T.; Misono, M. Key Reaction Steps and Active Surface Phase of Vanadyl Pyrophosphate for Selective Oxidation of Butane. *Catal. Today* **1993**, *16* (1), 61–67.

(24) Contractor, R. M.; Bergna, H. E.; Horowitz, H. S.; Blackstone, C. M.; Malone, B.; Torardi, C. C.; Griffiths, B.; Chowdhry, U.; Sleight, A. W. Butane Oxidation to Maleic Anhydride over Vanadium Phosphate Catalysts. *Catal. Today* **1987**, *1* (1–2), 49–58.

(25) Leonowicz, M. E.; Johnson, J. W.; Brody, J. F.; Shannon, H. F.; Newsam, J. M. Vanadyl Hydrogenphosphate Hydrates: VO(HPO4) · 4H2O and VO(HPO4) · 0.5H2O. *J. Solid State Chem.* **1985**, *56* (3), 370–378.

(26) Zhang, Y.; Sneeden, R. P. A.; Volta, J. C. On the Nature of the Active Sites of the VPO Catalysts for N-Butane Oxidation to Maleic Anhydride. *Catal. Today* **1993**, *16* (1), 39–49.

(27) Albonetti, S.; Cavani, F.; Trifirò, F.; Venturoli, P.; Calestani, G.; López Granados, M.; Fierro, J. L. G. A Comparison of the Reactivity of "Nonequilibrated" and "Equilibrated" V-P-O Catalysts: Structural Evolution, Surface Characterization, and Reactivity in the Selective Oxidation of n-Butane and n-Pentane. *J. Catal.* **1996**, *160* (1), 52–64.

(28) Albonetti, S.; Budi, F.; Cavani, F.; Ligi, S.; Mazzoni, G.; Pierelli, F.; Trifirb, F. ALMAX Catalyst for the Selective Oxidation of N-Butane to Maleic Anhydride : A Highly Efficient V / P / O System for Fluidized-Bed Reactors. **2001**, 141–146.

(29) Hodnett, B. K.; Delmon, B. Influence of the Phosphorus/Vanadium Ratio on the Solid State Chemistry and Redox Properties of Vanadium Phosphate-Based Catalysts. *J. Catal.* **1984**, *88* (1), 43–53.

(30) Caldarelli, A.; Bañares, M. A.; Cortelli, C.; Luciani, S.; Cavani, F. An Investigation on Surface Reactivity of Nb-Doped Vanadyl Pyrophosphate Catalysts by Reactivity Experiments and in Situ Raman Spectroscopy. *Catal. Sci. Technol.* **2014**, *4* (2), 419–427.

(31) Bordes, E.; Courtine, P. New Phases in V-P-O Catalysts and Their Role in Oxidation of Butane to Maleic Anhydride. *J. Chem. Soc. Chem. Commun.* **1985**, No. 5, 294–296.

(32) Bordes, E. Nature of the Active and Selective Sites in Vanadyl Pyrophosphate, Catalyst of Oxidation of n-Butane, Butene and Pentane to Maleic Anhydride. *Catal. Today* **1993**, *16* (1), 27–38.

(33) Matsuura, I.; Yamazaki, M. REACTIVITY AND STRUCTURE OF VANADYL PYROPHOSPHATE AS A BUTANE OXIDATION CATALYST. *Stud. Surf. Sci. Catal.* **1990**, (*55)*, 563.

(34) Matsuura, I. Vanadyl Pyrophosphate as an Acidic and Oxidic Catalyst. *Catal. Today* **1993**, *16* (1), 123–129.

(35) Bordes, E.; Courtine, P. Some Selectivity Criteria in Mild Oxidation Catalysis. VPO Phases in Butene Oxidation to Maleic Anhydride. *J. Catal.* **1979**, *57* (2), 236–252.

(36) Jordan, B.; Calvo, C. Crystal Structure of A-VPO5. *Can. J. Chem.* **1973**, (*51)*, 2621.

(37) Ballutaud, D.; Bordes, E.; Courtine, P. An E.S.R. Study of Paramagnetic Centers in α-VOPO4 and α-VOPO4,2H2O. *Mater. Res. Bull.* **1982**, *17* (4), 519–526.

(38) Conte, M.; Budroni, G.; Bartley, J. K.; Taylor, S. H.; Carley, A. F.; Schmidt, A.; Murphy, D. M.; Girgsdies, F.; Ressler, T.; Schlo, R. Chemically Induced Fast Solid-State. **2006**, *313* (September), 1270–1274.

(39) Bastians, P. R. P.; Caussin, L.; Reuse, R.; Daza, L.; Acosta, D. New Aspects of the Cooperation between Phases in Vanadium Phosphate Catalysts. **1993**, (*16)*, 99–111.

(40) Garbassi, F.; Bart, J. C. J.; Montino, F.; Petrini, G. Preparation and Characterization of Vanadium-Phosphorus Oxidation Catalysts. *Appl. Catal.* **1985**, *16* (3), 271–287.

(41) Cavani, F.; Centl, G.; Manenti, I.; Trlflro, F. Catalytic Conversion of C4 Hydrocarbons on Vanadium-Phosphorus Oxides: Factors Influencing the Selectivity of 1-Butene Oxidation. *Ind. Eng. Chem. Prod. Res. Dev.* **1985**, *24* (2), 221–226.

(42) Cavani, F.; De Santi, D.; Luciani, S.; Löfberg, A.; Bordes-Richard, E.; Cortelli, C.; Leanza, R. Transient Reactivity of Vanadyl Pyrophosphate, the Catalyst for n-Butane Oxidation to Maleic Anhydride, in Response to in-Situ Treatments. *Appl. Catal. A Gen.* **2010**, *376* (1), 66–75.

(43) Cavani, F.; Trifirò, F. Catalyzing Butane Oxidation to Make Maleic Anhydride. *Chemtech* **1994**, (*24)*, 18–25.

(44) V, E. S. P. B. Vanadyl Pyrophosphate - A Critical Overview. **1993**, (*16)*, 5–26.

(45) Cavani, F.; Luciani, S.; Esposti, E. D.; Cortelli, C.; Leanza, R. Surface Dynamics of a Vanadyl Pyrophosphate Catalyst for N-Butane Oxidation to Maleic Anhydride: An in Situ Raman and Reactivity Study of the Effect of the P/V Atomic Ratio. *Chem. - A Eur. J.* **2010**, *16* (5), 1646–1655.

(46) Mars, P.; Krevelen, D. W. Van. Oxidations Carried out by Means of Vanadium Oxide Catalysts. *Chem. Eng. Sci.* 1954, *3*, 41–59.

(47) Mallada, R.; Sajip, S.; Kiely, C. J.; Menéndez, M.; Santamaría, J. Influence of the Reaction Atmosphere on the Characteristics and Performance of VPO Catalysts. *J. Catal.* **2000**, *196* (1), 1–7.

(48) Mota, S.; Abon, M.; Volta, J. C.; Dalmon, J. A. Selective Oxidation of N-Butane on a V-P-O Catalyst: Study under Fuel-Rich Conditions. *J. Catal.* **2000**, *193* (2), 308–318.

(49) Hutchings, G. J.; Chomelt, A. D.; Ollert, R.; Voltat, B. J. Catalyst to Its Active State. **1994**, *368* (March), 41–45.

(50) Abon, M.; Bere, K. E.; Tuel, A.; Delichere, P. Evolution of a VPO Catalyst in N-Butane Oxidation Reaction during the Activation Time. *Journal of Catalysis*. 1995, pp 28–36.

(51) Cavani, F.; Ligi, S.; Monti, T.; Pierelli, F.; Trifirò, F.; Albonetti, S.; Mazzoni, G. Relationship between Structural/Surface Characteristics and Reactivity in n-Butane Oxidation to Maleic Anhydride. The Role of V3+species. *Catal. Today* **2000**, *61* (1), 203–210.

(52) Centi, G.; Golinelli, G.; Busca, G. Modification of the Surface Pathways in Alkane Oxidation by Selective Doping of Brønsted Acid Sites of Vanadyl Pyrophosphate. *J. Phys. Chem.* **1990**, *94* (17), 6813–6819.

(53) Bertola, A.; S, C.; Nsunda, K. Process for the Preparation of Improved Vanadium-Phosphorus Catalysts and Use Thereof for the Production of Maleic Anhydride. US 6174833 B1, 2001.

(54) Abon, M.; Herrmann, J. M.; Volta, J. C. Correlation with the Redox V 5 + / V 4 + Ratio in Vanadium Phosphorus Oxide Catalysts for Mild Oxidation of n -Butane to Maleic Anhydride. **2001**, *71*, 121–128.

(55) Mota, S.; Volta, J. C.; Vorbeck, G.; Dalmon, J. A. Selective Oxidation of N-Butane on a V-P-O Catalyst: Improvement of the Catalytic Performance under Fuel-Rich Conditions by Doping. *J. Catal.* **2000**, *193* (2), 319–329.

(56) Sajip, S.; Bartley, J. K.; Burrows, A.; Rhodes, C.; Volta, J. C.; Kiely, C. J.; Hutchings, G. J. Structural Transformation Sequence Occurring during the Activation under N-Butane Air of a Cobalt-Doped Vanadium Phosphate Hemihydrate Precursor for Mild Oxidation to Maleic

Anhydride. *Phys. Chem. Chem. Phys.* **2001**, *3* (11), 2143–2147.

(57) Sajip, S.; Bartley, J. K.; Burrows, A.; Sananés-Schulz, M. T.; Tuel, A.; Volta, J. C.; Kiely, C. J.; Hutchings, G. J. Structure-Activity Relationships for Co- and Fe-Promoted Vanadium Phosphorus Oxide Catalysts. *New J. Chem.* **2001**, *25* (1), 125–130.

(58) Cornaglia, L.; Irusta, S.; Lombardo, E. A.; Durupty, M. C.; Volta, J. C. The Beneficial Effect of Cobalt on VPO Catalysts. *Catal. Today* **2003**, *78* (1–4 SPEC.), 291–301.

(59) Cornaglia, L. M.; Carrara, C. R.; Petunchi, J. O.; Lombardo, E. A. Characterization of Cobalt-Impregnated VPO Catalysts. *Catal. Today* **2000**, *57* (3–4), 313–322.

(60) Carrara, C.; Irusta, S.; Lombardo, E.; Cornaglia, L. Study of the Co-VPO Interaction in Promoted n-Butane Oxidation Catalysts. *Appl. Catal. A Gen.* **2001**, *217* (1–2), 275–286.

(61) Taufiq-Yap, Y. H.; Tan, K. P.; Waugh, K. C.; Hussein, M. Z.; Ramli, I.; Abdul Rahman, M. B. Bismuth-Modified Vanadyl Pyrophosphate Catalysts. *Catal. Letters* **2003**, *89* (1–2), 87–93.

(62) Matsuura, I.; Ishimura, T.; Hayakawa, S.; Kimura, N. Promotional Effect of Niobium Phosphate for Vanadyl Pyrophosphate Catalyst on Selective Oxidation of Butane to Maleic Anhydride. *Catal. Today* **1996**, *28* (1–2), 133–138.

(63) Duarte de Farias, A. M.; De Gonzalez, W. A.; Pries de Oliveira, P. G.; Eon, J. G.; Herrmann, J. M.; Aouine, M.; Loridant, S.; Volta, J. C. Vanadium Phosphorus Oxide Catalyst Modified by Niobium Doping for Mild Oxidation of N-Butane to Maleic Anhydride. *J. Catal.* **2002**, *208* (1), 238–246.

(64) Oliveira, P. G. P. De; Eon, J. G.; Chavant, M.; Riché, A. S.; Martin, V. Modification of Vanadium Phosphorus Oxides Used for n -Butane Oxidation to Maleic Anhydride by Interaction with Niobium Phosphate. **2000**, *57*, 177–186.

(65) Overbeek, R. A.; Pekelharing, A. R. C. J.; Dillen, A. J. Van; Geus, J. W. Preparation , Characterization and Testing of Newly Developed Silica-Supported V-P-O Catalysts. **1996**, *135*, 231–248.

(66) Nakamura, M.; Kawai, K.; Fujiwara, Y. The Structure and the Activity of Vanadyl Phosphate Catalysts. *J. Catal.* **1974**, *34* (3), 345–355.

(67) Kuo, P. S.; Yang, B. L. AlPO4 as a Support Material for VPO Catalysts. *J. Catal.* **1989**, *117* (2), 301–310.

(68) Sartoni, L.; Bartley, J. K.; Wells, R. P. K.; Delimitis, A.; Burrows, A.; Kiely, C. J.; Volta, J. C.; Hutchings, G. J. Unexpected Enhanced Activity Catalysts for Butane Oxidation Using Mixtures Derived from VOHPO4·0.5H2O and AlPO4. *J. Mater. Chem.* **2005**, *15* (40), 4295–4297.

(69) Ziòlotkowski, J.; Bordes, E.; Courtine, P. Dynamic Description of the Oxidation of N-Butane on Various Faces of (VO)2P2O7 in Terms of the Crystallochemical Model of Active Sites. *J. Mol. Catal. A Chem.* **1993**, *84*, 307–326.

(70) Cornaglia, L. M.; Caspani, C.; Lombardo, E. A. Physicochemical Characterization of VP0 Formulations and Catalytic Behavior. **1991**, *74*, 15–27.

(71) Busca, G. Nature and Mechanism of Formation of Vanadyl Pyrophosphate : Active Phase in n-Butane Selective Oxidation. **1986**, *414*, 400–414.

(72) Zhanglin, Y.; Forissier, M.; Sneeden, R. P.; Vedrine, J. C.; Volta, J. C. On the Mechanism of N-Butane Oxidation to Maleic Anhydride on VPO Catalysts. *Journal of Catalysis*. 1994, pp 256–266.

(73) Vidano, R.; Fischbach, D. B. New Lines in the Raman Spectra of Carbons and Graphite. *J. Am. Ceram. Soc.* **1978**, *61*, 13–17.

(74) Angoni, K. A Study of Highly Ordered Carbons by Use of Macroscopic and Microscopic Raman Spectroscopy. *J. Mater. Sci.* **1998**, *33*, 3693–3698.

(75) Ben Abdelouahab, F.; Olier, R.; Guilhaume, N.; Lefebvre, F.; Volta, J. C. A Study by in Situ Laser Raman Spectroscopy of VPO Catalysts for N-Butane Oxidation to Maleic Anhydride I. Preparation and Characterization of Pure Reference Phases. *J. Catal.* **1992**, *134* (1), 151–167.

(76) Cavani, F.; Centi, G.; Trifiro, F. Structure Sensitivity of the Catalytic Oxidation of N-Butane to Maleic Anhydride. *J. Chem. Soc. Chem. Commun.* **1985**, No. 8, 492–494.

(77) Ebner, J. R.; Thompson, M. R. An Active Site Hypothesis for Well-Crystallized Vanadium Phosphorus Oxide Catalyst Systems. *Catal. Today* **1993**, *16* (1), 51–60.

(78) Koyano, G.; Yamaguchi, F.; Okuhara, T.; Misono, M. Anisotropic Oxidation of Crystallites of Vanadyl Pyrophosphate. *Catal. Letters* **1996**, *41* (3–4), 149–152.

(79) Bordes, E.; Courtine, P.; Johnson, J. W. On the Topotactic Dehydration of VOHPO4 · 0.5 H2O into Vanadyl Pyrophosphate. *J. Solid State Chem.* **1984**, *55* (3), 270–279.

(80) Nguyen, P. T.; Sleight, A. W.; Roberts, N.; Warren, W. W. Modeling of Extended Defects in the Vanadium Phosphate Catalyst for Butane Oxidation, (VO)2P2O7. *J. Solid State Chem.* **1996**, *122* (2), 259–265.

(81) Batis, N. H.; Batis, H.; Ghorbel, A.; Vedrine, J. C.; Volta, J. C. Synthesis and Characterization of New VPO Catalysts for Partial N-Butane Oxidation to Maleic Anhydride. *J. Catal.* **1991**, *128* (1), 248–263.

(82) Kiely, C. J.; Sajip, S.; Ellison, I. J.; Sananes, M. T.; Hutchings, G. J.; Volta, J. C. Electron Microscopy Studies of Vanadium Phosphorus Oxide Catalysts Derived from VOPO4·2H2O.

Catal. Letters **1995**, *33* (3–4), 357–368.

(83) Ballarini, N.; Cavani, F.; Cortelli, C.; Ricotta, M.; Rodeghiero, F.; Trifirò, F.; Fumagalli, C.; Mazzoni, G. Non-Steady Catalytic Performance as a Tool for the Identification of the Active Surface in VPO, Catalyst for n-Butane Oxidation to Maleic Anhydride. *Catal. Today* **2006**, *117* (1–3), 174–179.

(84) Torardi, C. C.; Calabrese, J. C. Ambient-and Low-Temperature Crystal Structure of Vanadyl Hydrogen Phosphate, (VO)2H4P2O9. *Inorg. Chem.* **1984**, *23* (10), 1308–1310.